UNIVERSITY OF NOVI SAD

**FACULTY OF TECHNICAL SCIENCES
NOVI SAD**

DESIGN, FABRICATION AND CHARACTERISATION OF HUMIDITY AND FORCE SENSORS BASED ON CARBON NANOMATERIALS

PhD thesis

Candidate: Advisor:

Dragana Vasiljević, MSc   Prof. Goran Stojanović, PhD

Novi Sad, 2018

UNIVERSITY OF NOVI SAD ●FACULTY OF TECHNICAL SCIENCES
21000 NOVI SAD, Trg Dositeja Obradovića 6

KEY WORDS DOCUMENTATION

Редни број, **РБР**:	
Идентификациони број, **ИБР**:	
Тип документације, **ТД**:	Монографска документација
Тип записа, **ТЗ**:	Текстуални штампани материјал
Врста рада, **ВР**:	Докторска дисертација
Аутор, **АУ**:	Драгана Васиљевић
Ментор, **МН**:	Проф. др Горан Стојановић
Наслов рада, **НР**:	Пројектовање, фабрикација и карактеризација сензора влаге и силе на бази угљеничних наноматеријала
Језик публикације, **ЈП**:	енглески
Језик извода, **ЈИ**:	српски/енглески
Земља публиковања, **ЗП**:	Србија
Уже географско подручје, **УГП**:	
Година, **ГО**:	2018
Издавач, **ИЗ**:	Ауторски репринт
Место и адреса, **МА**:	
Физички опис рада, **ФО**: (поглавља/страна/ цитата/табела/слика/графика/прилога)	6 поглавља/91 страна/131 референцу/5 табела/69 слика
Научна област, **НО**:	Електротехничко и рачунарско инжењерство
Научна дисциплина, **НД**:	Електроника
Предметна одредница/Кдучне речи, **ПО**:	Сензори силе, сензори влаге, угљенични наноматеријали
УДК	Монографска документација
Чува се, **ЧУ**:	Библиотека Факултета техничких наука, Универзитет у Новом Саду
Важна напомена, **ВН**:	

| Извод, **ИЗ**: | Детекција и контрола влажности су од суштинског значаја у нашем свакодневном животу. Сензори влаге се користе у многим областима, као што су метеорологија, заштита животне средине, медицина, прехрамбена индустрија, пољопривреда, итд. За дизајн сензора влаге углавном се користе капацитивне, резистивне, акустичне, механичке или оптичке структуре. У посљедње двије деценије све више се користе наноструктурни угљенични материјали, посебно графен. Поред графена велику пажњу у многим областима од електронике до сензора је привукао графен-оксид (*Graphene-oxide - GO*). Штампана електроника све више постаје водећа технологија у изради сензора. Поред јефтине израде и адитивних процеса са смањеном инфраструктуром, предности штампане технологије су компоненте мале масе, савитљиве, транспарентне, танке, компоненте које се могу уградити у/на гардеробу и носити, као и производња великог броја компоненти. У последњих неколико година роботи се све више укључују у људски живот, што је довело до потребе за усавршавањем у области роботике. Људи са окружењем комуницирају помоћу четири чула: додира, слуха, вида и укуса. Чуло додира људима омогућава да дохвате различите предмете, подигну их, обављају различите задатке, итд. Из тог разлога је развој сензора додира, односно сензора који би се уградили у роботске прсте, од веома великог значаја. Као једна врста таквих сензора су отпорнички сензори силе (Force Sensing Resistors - FSR). Код ових сензора долази до промјене отпорности уколико се на сензор дјелује одређеном силом. |

Датум прихватања теме, **ДП**:	05. Октобар 2017. године	
Датум одбране, **ДО**:		
Чланови комисије, **КО**:	Председник:	Проф. др Јован Бајић	
	Члан:	Проф. др Роман Шорђан	
	Члан:	Проф. др Далибор Секулић	Потпис ментора
	Члан:	Проф. др Владимир Срдић	
	Члан, ментор:	Проф. др Горан Стојановић	

Accession number, **ANO**:	
Identification number, **INO**:	
Document type, **DT**:	Monograph documentation
Type of record, **TR**:	Textual printed material
Contents code, **CC**:	PhD thesis
Author, **AU**:	Dragana Vasiljević
Mentor, **MN**:	Goran Stojanović, PhD
Title, **TI**:	Design, fabrication and characterisation of humidity and force sensors based on carbon nanomaterials
Language of text, **LT**:	English
Language of abstract, **LA**:	Serbian/English
Country of publication, **CP**:	Serbia
Locality of publication, **LP**:	
Publication year, **PY**:	2018
Publisher, **PB**:	Author reprint
Publication place, **PP**:	
Physical description, **PD**: (chapters/pages/ref./tables/pictures/graphs/appendixes)	6 chapters/91 pages/131 references/5 tables/69 figures
Scientific field, **SF**:	Electrical and Computer Engineering
Scientific discipline, **SD**:	Electronics
Subject/Key words, **S**/**KW**:	Humidity sensors, Force sensors, Carbon nanomaterials
UC	
Holding data, **HD**:	Library of the Faculty of Technical Sciences, University of Novi Sad
Note, **N**:	

KEY WORDS DOCUMENTATION

| Abstract, **AB**: | Detection and control of humidity is very important in our everyday life. Humidity sensors are used in many areas, such as meteorology, environmental protection, medicine, food industry, agriculture, etc. Various transduction techniques, such as capacitive, resistive, acoustic, optical and mechanical, have been adopted for the design of humidity sensors. In the last two decades, carbon nanomaterials materials, especially graphene, are taking their place in the production of humidity sensors. In addition to graphene, graphene oxide (Graphene-oxide-GO) is involved in many areas from electronics to sensors. Printed electronics increasingly becomes the leading technology in the fabrication of sensors. In addition to inexpensive manufacturing and additive processes with reduced infrastructure, the benefits of printed technology are low-power components, flexible, transparent, thin, components that can be embedded in/on clothes, as well as the production of a large number of components. In the last few years, robots are more involved in human's life, which has led to the need for advanced research in the field of robotics. People communicate with the environment using four senses: touch, hearing, sight and taste. The sense of touch allows people to grab various objects, lift them, perform various tasks, etc. For this reason, it is very important to develop touch sensors, that is, the sensors that will be incorporated into robotic fingers. As one type of such sensor, Force Sensing Resistors (FSR) are used. In these sensors, there is a change in resistance if the sensor is affected by a certain force. |

Obrazac **Q2.HA.06-05**- Izdanje 1

PROŠIRENI IZVOD NA SRPSKOM JEZIKU

"Projektovanje, fabrikacija i karakterizacija senzora vlage i sile na bazi
ugljeničnih nanomaterijala"

Uvod

Detekcija i kontrola vlažnosti su od suštinskog značaja u našem svakodnevnom životu. Senzori vlage se koriste u mnogim oblastima, kao što su meteorologija, zaštita životne sredine, medicina, prehrambena industrija, poljoprivreda, itd. Poslednjih godina je uloženo mnogo napora u razvoj senzora vlage visokih performansi (velike osjetljivosti, brzog vremena odziva i oporavaka, malog histerezisa, itd.). Za dizajn senzora vlage uglavnom se koriste kapacitivne, rezistivne, akustične, mehaničke ili optičke strukture. U posljednje dvije decenije sve više se koriste nanostrukturni ugljenični materijali, kao što su 1-dimenzionalne ugljenične nanotube (*Engl. Carbon Nano Tube – CNT*) i 0-dimenzionalni fulereni (C_{60}). U poređenju sa polimernim materijalima ugljenični nanomaterijali nude mnogo prednosti, kao što su bolja mehanička čvrstoća, veći odnos površine i zapremine i bolja stabilnost. Kao dvodimenzionalni ugljenični nanomaterijal, grafen (ugljenična struktura debljine 1 atoma) je privukao mnogo pažnje zbog svojih izvanrednih električnih, termičkih i mehaničkih osobina. Pored grafena veliku pažnju u mnogim oblastima od elektronike do senzora je privukao grafen-oksid (*Engl. Graphene oxide - GO*). Objavljeni su mnogi radovi o izvanrednim strukturnim i mehaničkim osobinama grafen oksida u prisustvu vlage iz atmosfere. Pokazalo se da zbog postojanja kiseoničnih grupa, prikazanih na Slici 1, atomi vode mogu lako da prodru u međuslojeve ugljenika i formiraju H-veze između molekula i listova grafen-oksida.
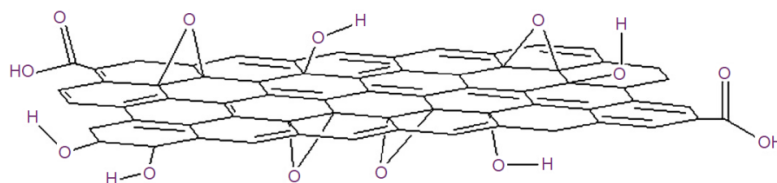
*Slika 1 – Prikaz hemijske strukture grafen-oksida.*

Poslednjih nekoliko decenija uložen je veliki napor u razvoj i implementaciju elektronskih komponenti na fleksibilnim i elastičnim supstratima za mnoge aplikacije, kao što su senzorske aplikacije u kojima ova tehnologija omogućava nove pogodnosti, kao što su smanjena cijena prozvodnje senzora, njihova savitljivost, providnost, itd. Praćenje parametara životne sredine je od interesa u mnogim poljima, za komfor, zdravlje, sigurnost i druge potrebe. Mnogo truda je uloženo u „pametne" senzore i bežične senzorske mreže bazirane na tehnologiji silicijuma, ciljajući na taj način različite tipove aplikacija. Međutim, štampana elektronika sve više postaje vodeća tehnologija u izradi senzora. Pored jeftine izrade i aditivnih procesa sa smanjenom infrastrukturom, prednosti štampane tehnologije su komponente male mase, savitljive,

transparentne, tanke, komponente koje se mogu ugraditi u/na garderobu i nositi, kao i proizvodnja velikog broja komponenti.

U poslednjih nekoliko godina roboti se sve više uključuju u ljudski život, što je dovelo do potrebe za usavršavanjem u oblasti robotike. Takva usavršavanja su posebno značajna u cilju unapređenja znanja u oblasti robotike kako bi roboti što preciznije i sigurnije stupali u kontakt sa okruženjem. U ovom smislu, veoma je važno prostudirati načine na koje roboti komuniciraju sa okruženjem. Ljudi sa okruženjem komuniciraju pomoću četiri čula: dodira, sluha, vida i ukusa. Čulo dodira ljudima omogućava da dohvate različite predmete, podignu ih, obavljaju različite zadatke, itd. Iz tog razloga je razvoj senzora dodira, odnosno senzora koji bi se ugradili u robotske prste, od veoma velikog značaja. Kao jedna vrsta takvih senzora su otpornički senzori sile (*Engl. Force Sensing Resistors - FSR*). Kod ovih senzora dolazi do promjene otpornosti (*R*) ukoliko se na senzor djeluje određenom silom (F). Upotreba senzora sile, pored robotike, sve više nalazi primjenu u mnogim drugim oblastima poput medicine, stomatologije, rehabilitacione medicine, itd.

Fabrikacija senzora vlage i sile na bazi ugljeničnih nanomaterijala

Fabrikacija senzora vlage je rađena dijelom na Fakultetu tehničkih nauka, Univerziteta u Novom Sadu, a dijelom u Grupi za nanoelektronske uređaje u Komu, Univerziteta *Politecnico di Milano,* Italija. Senzori sile su u potpunosti fabrikovani na Fakultetu tehničkih nauka, Univerziteta u Novom Sadu. Korišćena podloga pri izradi senzora je *GTS* poliimidni film debljine 75 µm. Za izradu elektroda tehnologijom ink-džet štampe korišćeno je *SunChemical* nanočestično srebrno mastilo sa 20 %wt udjela nanočestica srebra, dok se kao aktivni sloj senzora sile koristio *Graphenea* vodeni rastvor grafen-oksida, koji je nanošen spinerom (*Engl. spin coating*), a kao aktivni sloj senzora sile ugljenično mastilo nanošeno sitoštampom. Prikaz dizajniranih senzora se može vidjeti na Slici 2.


(a) *(b)*
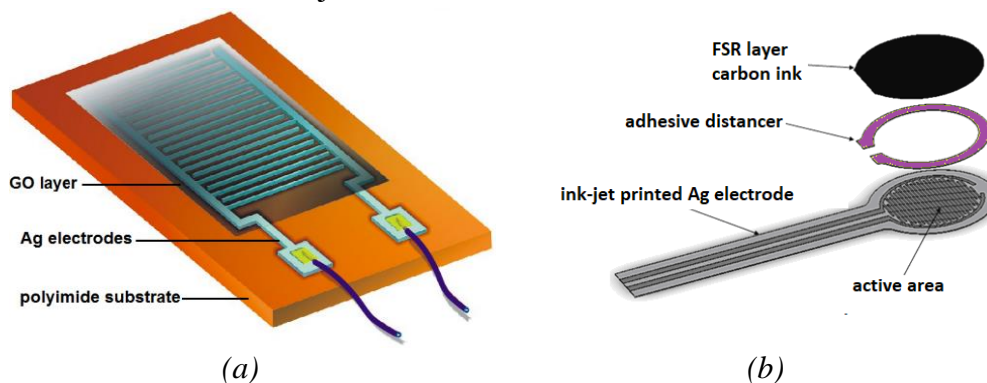
*Slika 2 -Šematski prikaz senzora (a) vlage i (b) sile.*

Proces štampe na *Dimatix* štampaču *DMP 3000* (*Engl. Deposition Material Printer*), prikazanom na Slici 3, je optimizovan kako bi se ostvario stabilan tok kapljica iz kertirdža prema podlozi, bez takozvanih "satelita", kapljica koje se formiraju nakon osnovne kapljice i koje uzrokuju kratko spajanje štampanih elektroda i "repa" kapljice koji najčešće dovodi do "neuredne" i neuspješne štampe struktura, Slika 4a, i da bi se dobile ujednačene kapljice iste brzine bez satelita i "repova", Slika 4b. Selektovani parametri ink-džet štampe su: 21 V amplituda aktuacionog napona na piezoelementu; 1 kHz brzina štampe; 3 inchH$_2$O pritisak meniskusa i 1 mm rastojanje od kertridža do supstrata.

Slika 3 – Izgled Dimatix DMP 3000 ink-jet štampača.
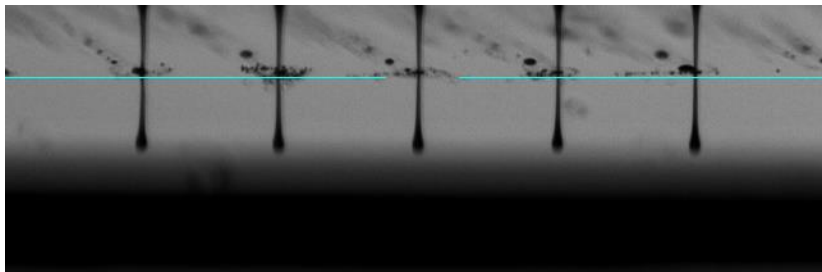
(a)
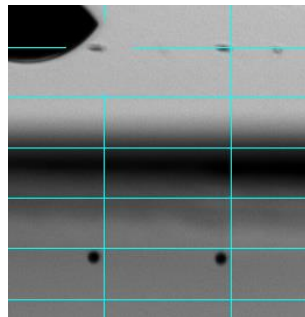
(b)

Slika 4 - Izgled kapljica pri izlasku iz DMP kertridža a) nepodešene kapljice sa "repovima" i b) izgled podešenih kapljica spremnih za štampu.

Elektrode senzora, prikazane na Slikama 5 i 6. Dizajnirane su tri različite geometrije elektroda senzora vlage i četiri različite geometrije elektroda senzora sile.

(a)   (b)   (c)
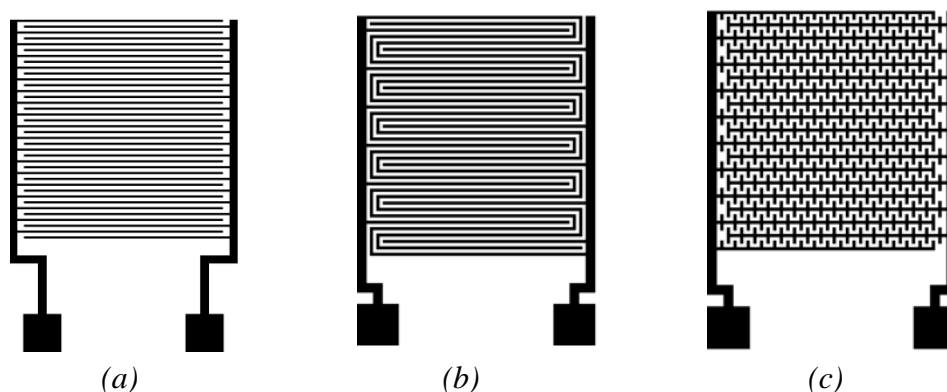
Slika 5 -Dizajn elektroda senzora vlage: (a) interdigitalni, (b) serpentine i (c) nazubljeni oblik elektroda.

(a)   (b)

(c)   (d)
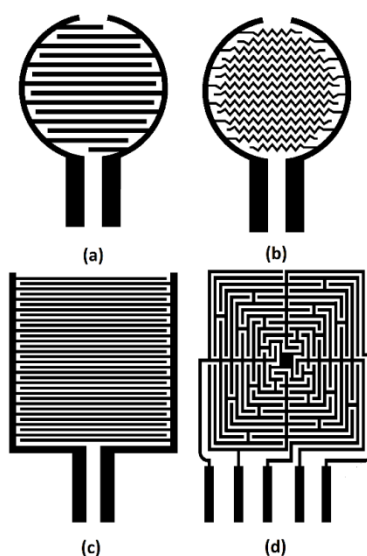
Slika 6 - Dizajn elektroda senzora sile: (a) okrugle interdigitalne, (b) okrugle nazubljene, (c) kvadratne interdigitalne i (d) elektrode sa 4 zone djelovanja.

Rezolucija štampe je 18 μm od centra do centra kapljice koja je izračunata na osnovu mjerenja prečnika jedne kapljice srebrnog mastila na podlozi koja je iznosila ~38 μm. Na Slici 6(a) prikazan je izgled elektroda nakon štampe na kome se takođe vidi da su štampane elektrode istih dimenzija kao što je i dizajnirano. Nakon procesa štampe slijedi sinterovanje na 270 ˚C u trajanju od 30 min. Do temperature (*T*) od 270 ˚C se došlo prethodnim testiranjem slojeva srebra sinterovanim na različitim temperaturama u opsegu od 180 ˚C do 300 ˚C, pri čemu se pokazalo da srebrni sloj ima željenu provodljivost, bez narušavanja njegove mehaničke fleksibilnosti, ukoliko se sinteruje na 270 ˚C. Tokom procesa sinterovanja dolazi do isparavanja

rastvarača i organskih faza mastila, nakon čega dobijamo sloj čistog srebra. Zbog isparavanja rastvarača i organske faze mastila dolazi do skupljanja štampanih elektroda, a samim tim i do smanjenja njihove širine, što se može vidjeti na Slici 6, gdje se jasno vidi da je širina elektroda nakon štampe 83,7 µm, a razmak između njih 117 µm.


(a)   (b)
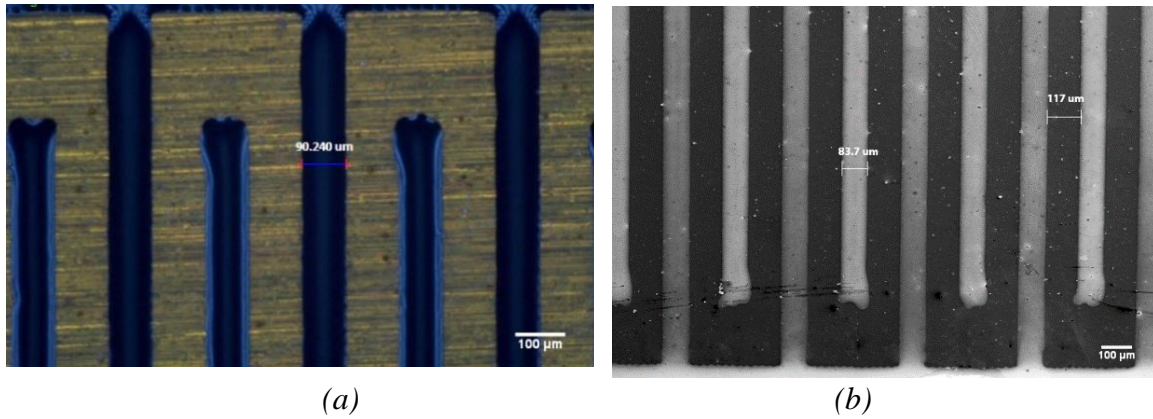
Slika 6 – Izgled elektroda a) prije sinterovanja i b) nakon sinterovanja.

Konačan izgled elektroda senzora vlage i sile nakon sinterovanja prikazan je na Slici 8(a) i 8(b), respektivno.

(a)   (b)
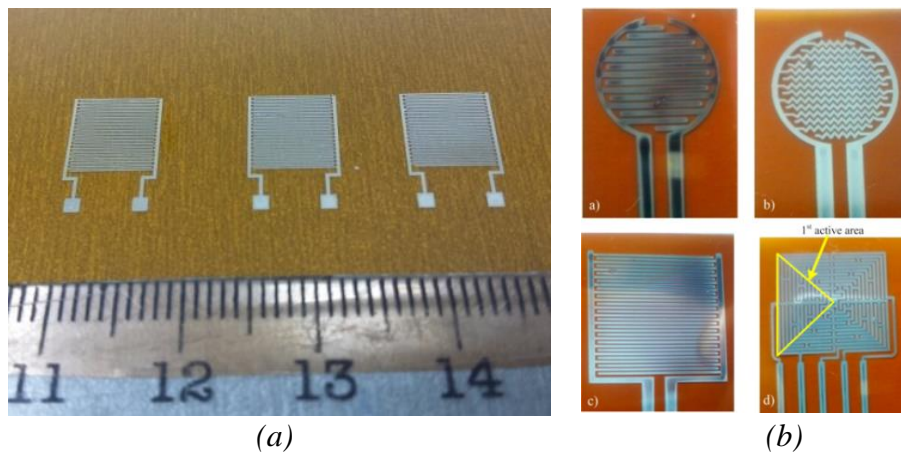
Slika 8 - Izgled sinterovanih elektroda (a) senzora vlage i (b) senzora sile.

Drugi sloj senzora vlage fabrikovan je nanošenjen grafen oksida spinerom, dok je za *FSR* ugljenično mastilo nanošeno fleksoštampom na fleksibilni supstrat debljine 0,5 µm. Nakon izrade slojevi se spajaju dvokomponentnim ljepilom koji se nanosi po ivicama štampanih elektroda. Nakon spajanja slojeva izvlače se kontakti provodnom žicom i srebrnom pastom koji će olakšati postupak karakterizacije. Izgled gotovih struktura je prikazan na Slici 9.
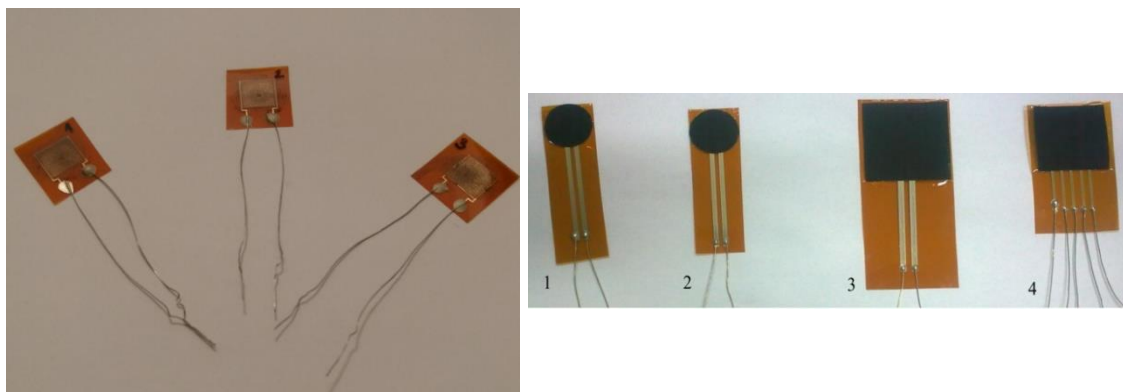
(a) *(b)*

Slika 9 - Izgled gotovih struktura senzora (a) vlage i (b) sile.

Rezultati i diskusija

U slučaju senzora vlage na bazi grafen oksida mjerenja su izvršena korišćenjem laboratorijski postavljenog mjernog sistema, prikazanog na Slici 10. Sistem se sastojao od komore i izvora vlage. Kapacitivnost i otpornost senzora su mjereni pomoću Agilent 4284A LCR metra. Za potrebe kalibracije i kao referentni senzor za mjerenje koncentracije vlage unutar komore korišćen je *Omega* senzor vlage i temperature.
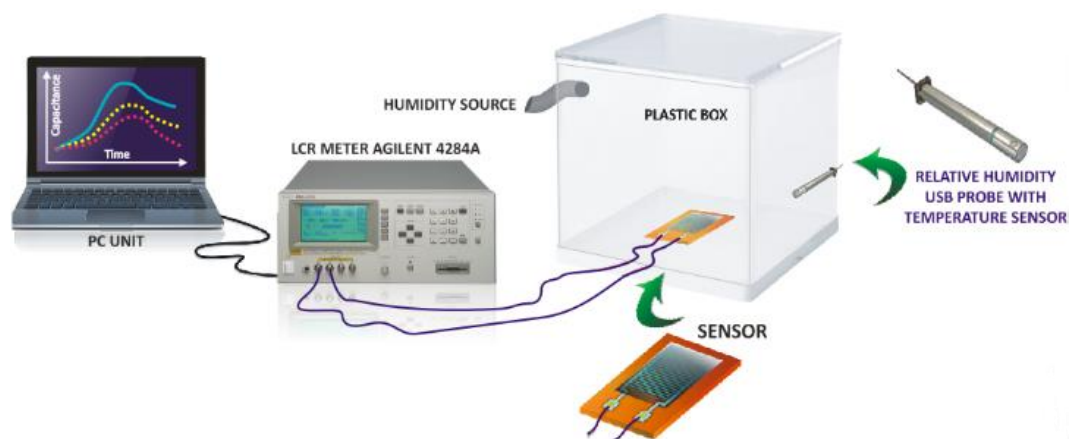
Slika 10 - Laboratorijski razvijena mjerna postavka za testiranje senzora vlage na bazi grafen oksida.

Mjerenja kapacitivnosti i otpornosti u zavisnosti od vremena i koncentracije relativne vlažnosti (*Engl. Relative humidity - RH)* unutar komore su izvršena za 3 fabrikovana senzora iste geometrije. Prvo su urađenja mjerenja na senzorima bez aktivnog sloja od grafen oksida da bi se utvrdile početne vrijednosti kapacitivnosti i otpornosti. Na Slici 11(a) se mogu vidjeti

rezultati dobijeni mjerenjima za interdigitalne senzore bez GO gdje se vidi da se kapacitivnost povećala ~10 puta u opsegu vlage od 55 do 95 %RH ali nije prešla 120 pF. Međutim, u mjerenjima urađenim na interdigitalnim senzorima sa slojem GO kapacitivnost se povećala za 4 reda veličine, sa 430 pF na 1,6 μF za isti opseg koncentracije vlage, što se može vidjeti na Slici 11(b). Za vrijeme mjerenja senzora sa GO senzor je postavljen u komoru pod laboratorijskom atmosferom nakon čega je uključen izvor vlage koji je bio uključen 9 min dok koncentracija od 95 %RH nije dostignuta. Nakon što je dostignuta konstantna koncentracija od 95 %RH izvor vlage je isključen i senzor je ponovo izložen laboratorijskoj atmosferi.

(a)   *(b)*
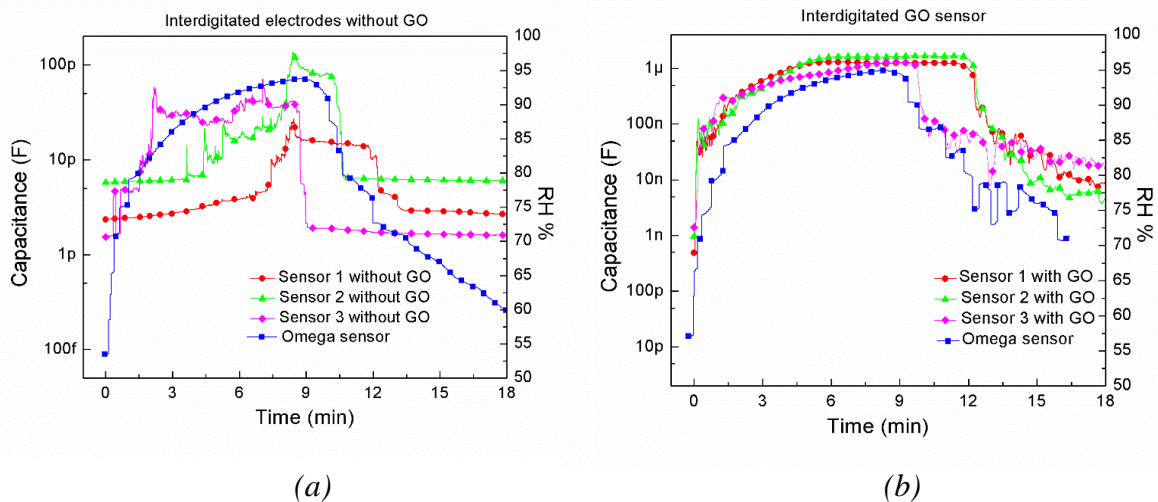
Slika 11 - Kapacitivnost 3 fabrikovana interdigitalna senzora kao funkcija vremena za senzore (a) bez sloja GO i (b) sa slojem GO.

Slika 12 prikazuje vremensku zavisnost otpornosti 3 fabrikovana senzora sa slojem GO snimljenu u isto vrijeme kao i kapacitivnost prikazana na Slici 11(b). Otpornost senzora pokazuje obrnuto ponašanje od kapacitivnosti. Kao što je već poznato GO se ponaša kao p-tip poluprovodnika, što znači da se transport vrši preko šupljina, dok je voda poznata kao donor elektrona. Interakcija između GO i vode se javlja usled prisustva kiseoničnih grupa unutar sloja GO. Mnoga istraživanja su pokušala da objasne zavisnost mehanizma detekcije vlage grafen-oksida od nivoa koncentracije vlage. Na niskim koncentracijama RH molekuli vode su adsorbovani na GO preko vodoničnih veza za hidrofilne grupe. Protoni mogu da „skaču" sa kiseoničnih grupa na molekule vode (gustina nosilaca naelektrisanja unutar GO se smanjuje dovodeći do povećanja njegove otpornosti) i stvore hidronijum jone. Sa povećanjem RH formira se uniforman sloj vode, koji omogućava hidronijum jonima da se slobodno kreću i dovode do jonske provodnosti. Ova pojava bi trebala da dovede do povećanja pozitivnih

nosilaca naelektrisanja u sloju GO i smanjenju otpornosti. Promjena otpornosti za iste koncentracije vlage kao u mjerenjima kapacitivnosti je bila sa 2,5 MΩ na 5 kΩ.
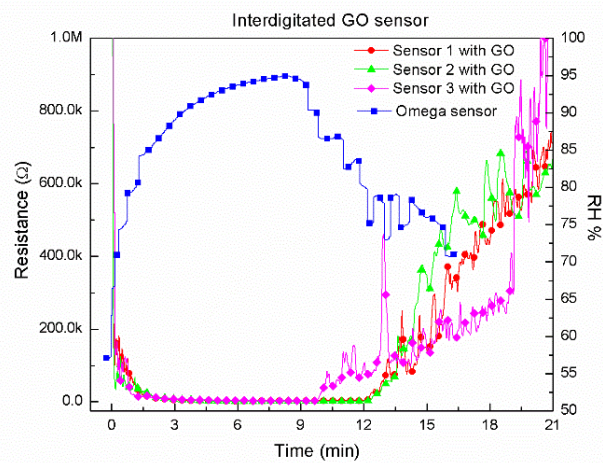
Slika 12 - Otpornost fabrikovanih interdigitalnih senzora kao funkcija vremena za senzore sa slojem GO.

Urađeno je ispitivanje uticaja fleksibilnosti senzora na njegov odziv, što je prikazano na Slici 13. Sa slike se može vidjeti da fleksibilnost ne utiče na promjenu odziva senzora što je veoma važno jer se u tom slučaju senzor može postaviti i na nepristupačne i neravne površine, a da to ne utiče na njegov odziv.
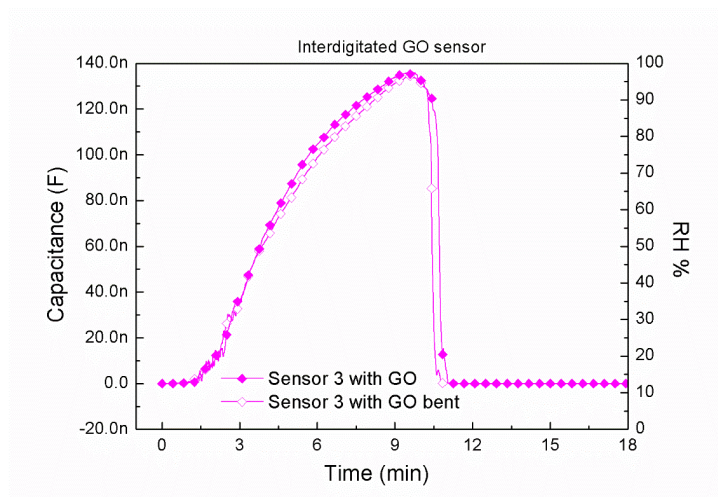
Slika 13 - Uticaj fleksibilnosti na odziv interdigitalnog senzora vlage na bazi grafen oksida.

Za potrebe testiranja FSR-ova napravljena je laboratorijska mjerna postavka koja je prikazana na Slici 14. Oprema se sastoji od čvrstog nosača, linernog aktuatora sa mogućnošću povratne sprege, referentnog senzora sile, kao i digitalne elektronske kontrole sistema i operatorske kontrole softvera, prikazanih na Slici 15. Elektronska kontrola sistema i operatorska kontrola softvera omogućavaju promjenu pozicije i promjenu primijenjene sile. Multimetrom su

mjerene otpornost i napon (*V*) realizovanih senzora. U sklopu mjerne postavke korišćen je i naponski izvor.
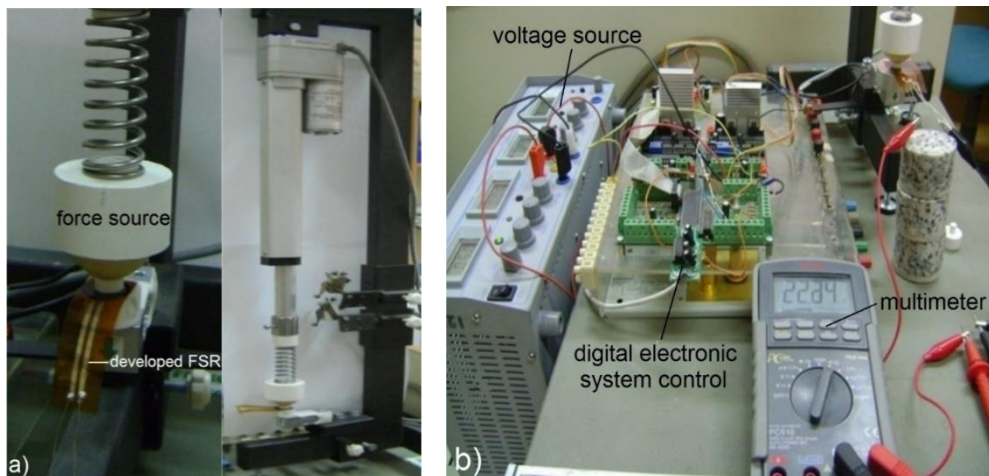

Slika 14 - Laboratorijski razvijena mjerna postavka za testiranje otporničkih senzora sile.
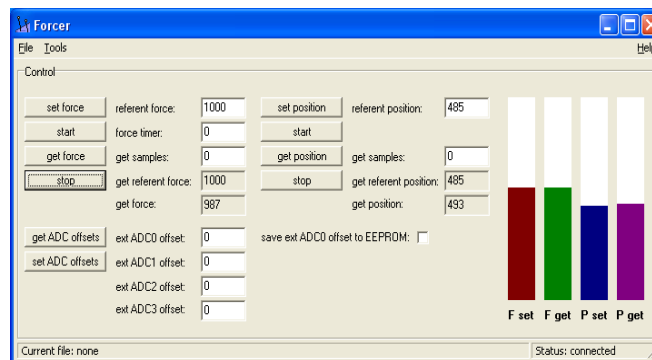
Slika 15 - Softverska kontrola uređaja za testiranje.

Testirane su sve četiri komponente, i za svaku su prikazani grafici zavisnosti otpornosti od sile i temperature, kao i napona od sile. U slučaju prve zavisnosti korišćena je opisana mjerna postavka, dok je u slučaju druge dodatno korišćen i naponski razdjelnik, prikazan na Slici 16, u koji je bio priključen fabrikovani FSR.
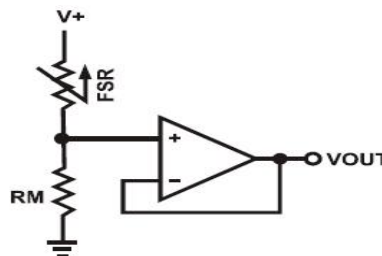
Slika 16- Naponski razdjelnik.

U slučaju treće zavisnosti korišćen je fen sa mogućnošću podešavanja temperature da bi se postigla određena temperatura kao i infracrvena kamera kojom je kontrolisana preciznost

postignute temperature. Rezultati mjerenja su prikazani na tri posebna grafika, R u funkciji od F, V u funkciji od F, i R u funkciji od T.

Na Slici 17 prikazana je promjena otpornosti pri promjeni za sva 4 realizovana FSR-a i jasno se vidi da se pri povećanju sile dolazi do smanjenja otpornosti FSR-ova.
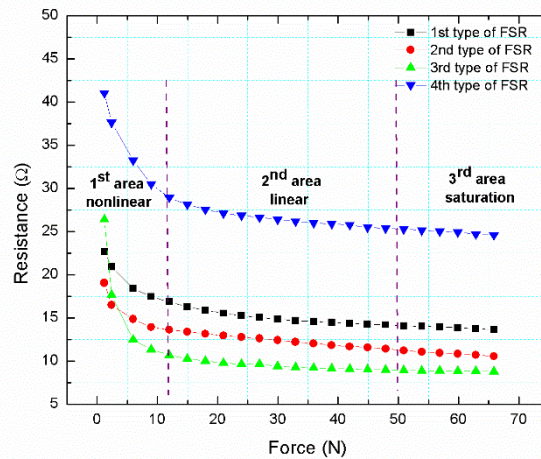

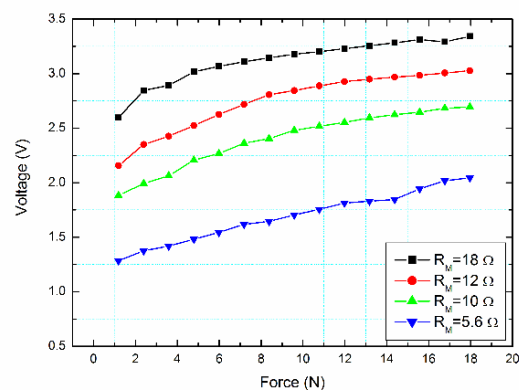*Slika 17 - Zavisnost otpornosti od sile za sva 4 FSR-a.*

Tabela 1. Opseg otpornosti pri promjeni sile sa Slike 17.

|	1. FSR	2. FSR	3. FSR	4. FSR
R_{FSRmax}	22,65 Ω	19,07Ω	26,43 Ω	41,05 Ω
R_{FSRmin}	13,67 Ω	10,57 Ω	8,81 Ω	24,81 Ω

Za sva 4 FSR-a je korišćen isti opseg sile 1.19 - 65,7 N. Sa Slike 17 se može vidjeti da za istu primijenjenu silu treći FSR, koji ima najveću površinu aktivne oblasti, ima najmanju otpornost od 8,81 Ω, dok četvrti FSR sa najmanjom povšinom aktivne oblasti ima otpornost od 24,81 Ω.
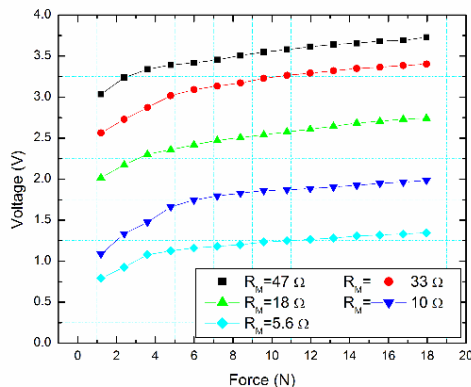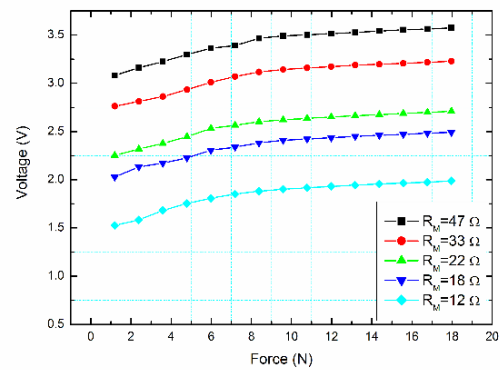

Slika 18 - Zavisnost napona od sile za 1. FSR.   *Slika 19 - Zavisnost napona od sile za 2. FSR.*
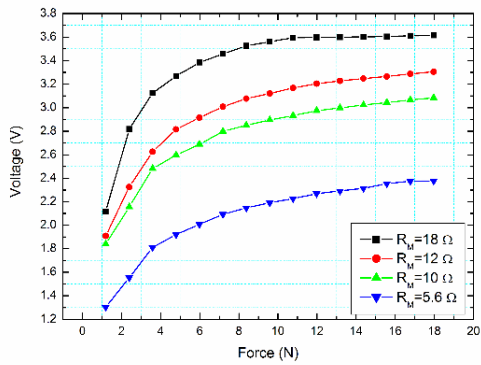
Slika 20 - Zavisnost napona od sile za 3. FSR.   *Slika 21 - Zavisnost napona od sile za 4. FSR.*

Slike 18-21 prikazuju promjene napona pri promjeni sile za nekoliko vrijednosti otpornika R_M. Različite otpornosti otpornika R_M su korišćene da bi se vidjela promjena napona FSR na cijelom mjernom opsegu. Sa povećanjem primijenjene sile raste i napon, što je moguće potvrditi i korišćenjem formule za naponski razdjelnik:

$$V_{out} = \frac{V_+}{\left(1 + \frac{R_{FSR}}{R_M}\right)} \qquad (1)$$

gdje je V_{out} izlazni napon, V_+ napon napajanja, R_{FSR} otpornost senzora, a R_M mjerni otpornik. Iz formule (1) se vidi da V_{out} raste sa smanjenjem R_{FSR} što se vidi i na Slici 18. Ova zavisnost je ista za sva 4 FSR-a.

R_{FSR} se može izračunati iz:

$$R_{FSR} = R_M \left(\frac{V_+}{V_{out}}\right) - R_M \qquad (2)$$

gde je V_+=5 V.

Korišćenjem formule (2) moguće je provjeriti vjerodostojnost dobijenih otpornosti prikazanih u Tabeli 1 i to zamjenom poznatih vrijednosti napona V_{out}, Slike 18-21, i vrijednosti R_M.

Na Slikama 18-21 se može vidjeti da je primijenjena sila u opsegu 1,19 - 17,96 N jer bi pri većim promjenama dolazilo do manjih promjena napona kao posledica manje promjene otpornosti R_{FSR}.
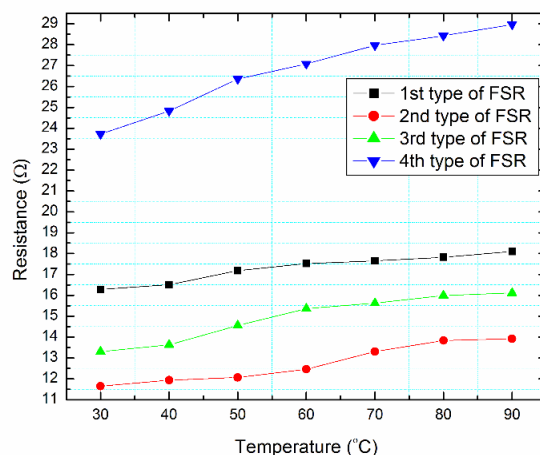
Slika 22 - Zavisnost otpornosti od temperature za sva 4 FSR-a.

Pri mjerenju temperaturne zavisnosti korišćen je isti opseg promjene temperature, za sva 4 senzora, 30-90 ˚C. Na Slici 22 se može vidjeti da pri povećanju temperature dolazi i do povećanja otpornosti, što se dodatno može se objasniti korišćenjem izraza za otpornost R_T na stvarnoj temperaturi T :

$$R(T) = R(T_0)(1 + \alpha_0 \Delta T) \tag{3}$$

gdje je α_0 temperaturni koeficijent, R_{T0} otpornost pri referentnoj temperaturi, $\Delta T = T - T_0$ razlika stvarne i referentne temperature. S obziom na to da je α_0 za srebro 0,0061 ˚C^{-1}, a za ugljenik -0,0005 ˚C^{-1}, iz izraza 3 se može vidjeti da pri povećanju temperature T, dolazi i do povećanja R_T. Ista zavisnost otpornosti od temperature važi i kod ostala 3 FSR-a. Dodatno su proračunati α_0 koeficijenti za sva četiri FSRa i prikazani su u Tabeli 2.

Tabela 2 - Temperaturni koeficijenti za fabrikovane senzore sile

	$\alpha_0(C^{-1})$
1. FSR	0.0019
2. FSR	0.0032
3. FSR	0.0035
4. FSR	0.0037

Pored električne karakterizacije fabrikovanih senzora, urađena je i strukturna i mehanička karakterizacija materijala od kojih su senzori napravljeni. Na Slici 23 prikazana su mjerenja skenirajućim elektronskim mikroskopom (*Engl. Scanning Electron Microscope - SEM*) za mjerenje debljine štampanih elektroda od srebra i ugljeničnog mastila, kao i mjerenja

mikroskopom atomskih sila (*Engl. Atomic Force Microscope - AFM*) koji nam je služio da bismo izmjerili debljinu sloja grafen oksida.


(a)

(b)

(c)

(d)

(e)
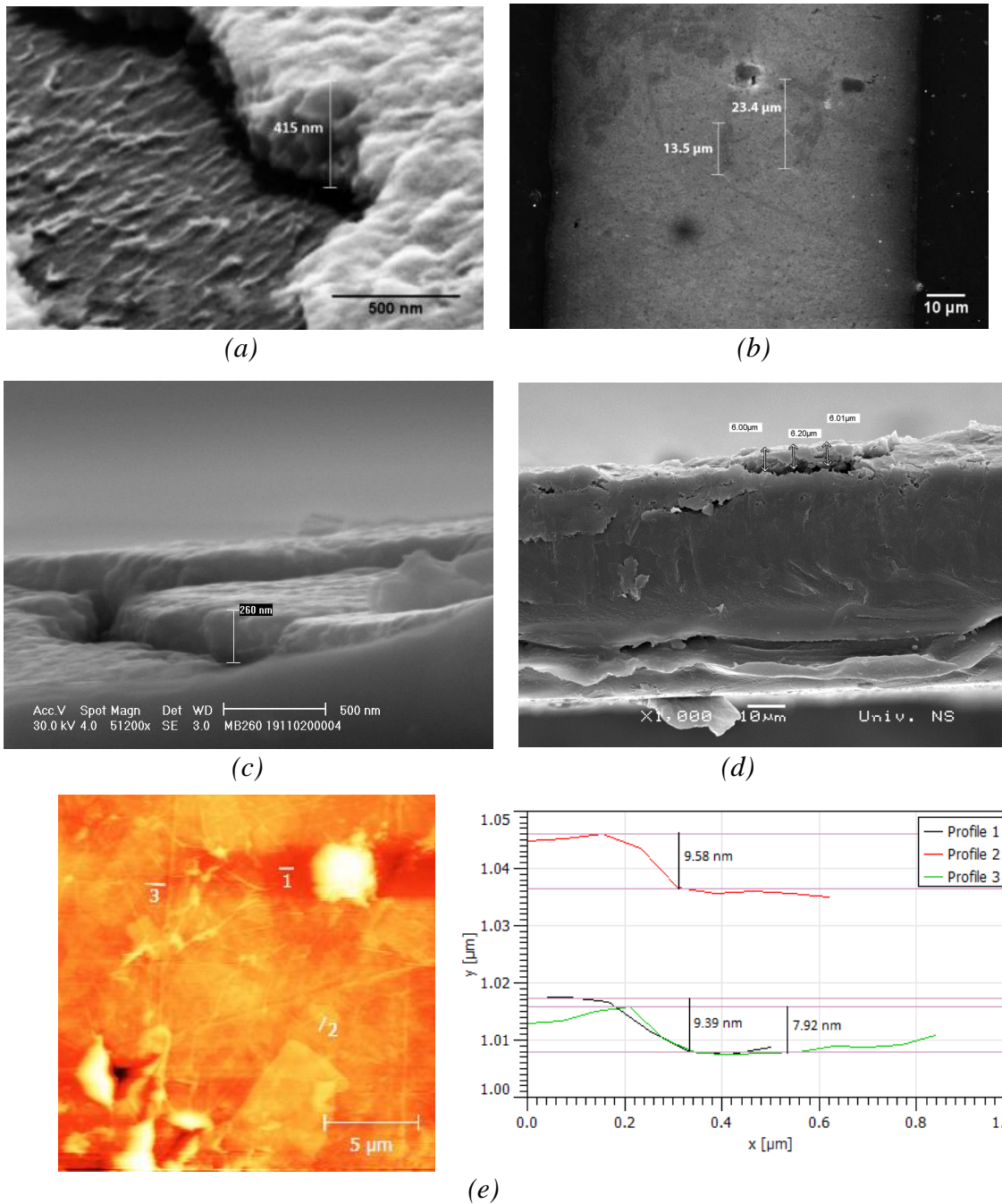
Slika 23 - (a) SEM prikaz štampanih srebrnih elektroda senzora vlage, (b) SEM prikaz elektroda srebra na kojima su vidljivi listići grafen oksida,(c) SEM prikaz štampanih srebrnih elektroda FSRa, (d) SEM prikaz poprečnog presjeka štampanog ugljeničnog mastila i (e) AFM mjerenja debljine sloja grafen oksida.

Sa Slike 23(a) se može vidjeti da je debljina sloja srebra u slučaju senzora vlage na bazi grafen oksida ~ 400 nm, kao i da su lateralne dimenzije listića grafen oksida reda desetak µm, dok je

njihova debljina ~ 9 nm, Slike 23(b) i 23(e) respektivno. Debljina sloja srebra za slučaj senzora sile je ~ 250 nm, dok je debljina ugljeničnog mastila ~6 µm.

S obzirom na to da se senzori često koriste u okruženju u kom se mogu oštetiti i da je njihova mehanička izdržljivost vrlo bitna, dodatno je urađena i mehanička karakterizacija slojeva srebra i ugljeničnog mastila. Karakterizacija je rađena nanoutiskivačem (*Engl. Nanoindenter*) G200. Zbog ograničenja u rezoluciji uređaja, nije bilo moguće uraditi mehaničku karakterizaciju sloja grafen oksida jer bi zbog njegove male debljine došlo do probijanja sloja GO. Rezultati mehaničke karakterizacije su prikazani na Slici 24.

(a)   (b)
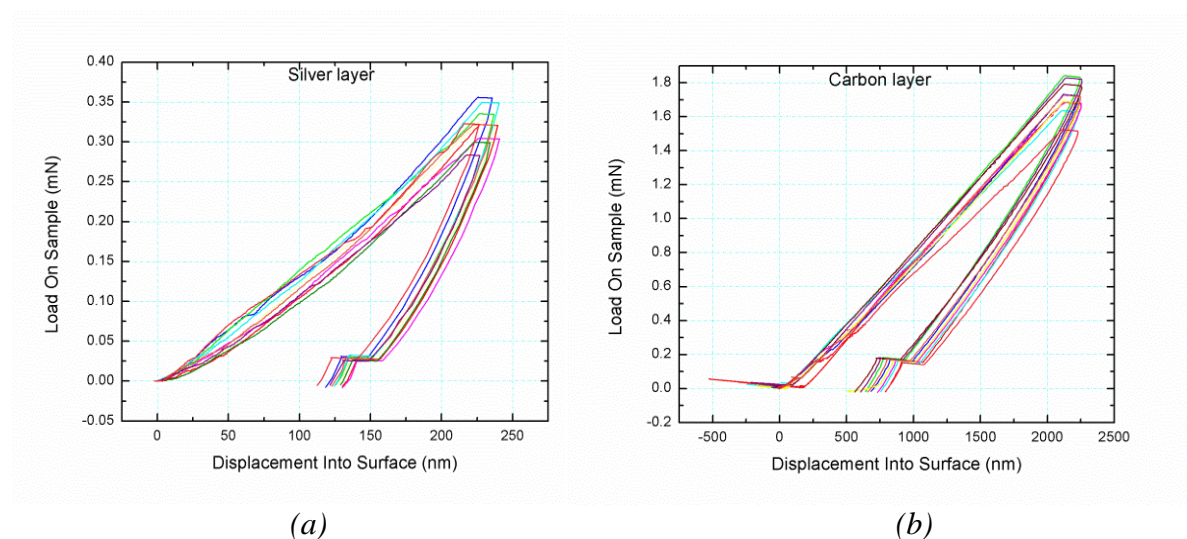
Slika 24 - Krive opterećenja na uzorak/prodiranje u uzorak za: (a) srebrno mastilo i (b) ugljenično mastilo.

Zaključak

U okviru ove doktorske disertacije opisan je značaj praćenja parametara životne sredine, kao i razvijanja senzora sile u svrhe robotskih aplikacija. Posebno je objašnjen proces izrade senzora u cilju minimizacije senzorskog elementa, a time i pojeftinjenja procesa izrade, i njihovog testiranja. Prikazani su do sada ostvareni rezultati gdje je pokazano da svi fabrikovani senzori reaguju na promjenu koncentracije vlage u komori za testiranje, kao i da otpornički senzori sile djeluju na promjenu primijenjene sile na uzorak. Dokazana je i ponovljivost procesa izrade senzora. Takođe je dokazana pretpostavka da sa povećanjem koncentracije vlage dolazi do povećanja provodnosti u slojevima grafen oksida, a samim tim i do povećanja kapacitivnosti senzora, odnosno do smanjenja njegove otpornosti. Takođe su proračunati osjetljivost senzora i vremena odziva i oporavka, kao vrlo bitne karakteristike svakog senzora vlage. Za slučaj

senzora sile dokazana je pretpostavka da će pri povećanju sile na senzor doći do smanjenja njegove otpornosti. Urađena su i mjerenja zavisnosti otpornosti pri promjeni temperature. Ispitan je i uticaj različitih geometrija elektroda senzora na odziv. Korišćenjem kvalitetnijeg i preciznijeg referentnog kompercijalnog senzora ostvarena je dobra kalibracija fabrikovanih senzora. Sve faze neophodne za realizaciju ove doktorske disertacije sprovedene su u Grupi za nanoelektronske uređaje u Komu, Italija i na Fakultetu tehničkih nauka u Novom Sadu, budući da ove dve institucije raspolažu svim neophodnim kapacitetima za realizaciju ove doktorske disertacije. Cilj ove doktorske disertacije je bila izrada kompletnog rešenja senzora za mjerenje vlažnosti u atmosferi, i njegova potencijalna primjena i za mjerenje gasova u životnoj sredini. Osim predloženih senzora na bazi grafen oksida fabrikovani su i testirani i senzori sile na bazi ugljeničnog mastila koji mogu naći svoju primjenu u mnogim oblastima poput robotike, medicine, protetske medicine, itd. Razvoj prototipa predstavljenih senzora bi bio polazna tačka za njihovu masovniju proizvodnju.

List of content

List of figures

List of tables

Abbreviations

AFM - *Atomic Force Microscope*

CAB - *Cellulose Acetate Butyrate*

CAGR - *Compound Annual Growth Rates*

CMOS - *Complementary-metal-oxide-semiconductor*

CNTs - *Carbon nanotubes*

d.c. - *direct current*

DMP - *Deposition Material Printer*

DOD - *Drop-On-Demand*

EDS - *Energy-Dispersive X-ray Spectroscopy*

F - *Force*

FET - *Field Effect Transistor*

FPCs - *Flexible Printed Circuits*

FSR - *Force Sensing Resistor*

GO - *Graphene Oxide*

IR- *Infrared*

LbL - *Layer-by-Layer*

MCLs - *Microcantilevers*

NAPSS - *Nanocomposites of Sodium Polystyrenesulfonate*

PANI - *Polyaniline*

PEDOT:PSS - *Poly (3,4-ethylenedioxythiophene) polystyrene sulfonate*

PES - *Polyethersulfone*

PETT - *Polyethylene terephthalate*

PEVCD - *Plasma-enhanced Chemical Vapour Deposition*

PMMA - *Polymethyl Methacrylate*

PPy - *Polypyrrole*

R – *Resistance*

R2R - *Roll-to-Roll*

RFID - *Radio Frequency Identification*

RH - *Relative Humidity*

SEM - *Scanning Electron Microscope*

T - *Temperature*

UV - *Ultra Violet*

V - *Voltage*

MEMS - *Micro-electro-mechanical-system*

1. Introduction

It is expected that global sensor market reach $241 billion by 2022, with an annual growth rates (CAGR) of 11.3 % in a period from 2016 to 2022.

During 2015, worldwide market of sensors valued more than $100 billion. It is predicted that in the next five years, the sensor market will reach more than $190 billion until 2021. The average rate of grow in the market of the sensors, for the period from 2016 to 2020, is expected to be around 11 % per year, Figure 1.1.

The market of sensors cannot be matched and it varies depending on the type of sensor, for that reason is very hard to accurately predict the growth on the global basis.

Several industries are making a profit from the sensor market growth, mainly the industry for environmental, automotive, and wearable sectors. These industries are expected to have markets of 35.2, 20.5 and 14.75 billion of USD by 2020, respectively [1].
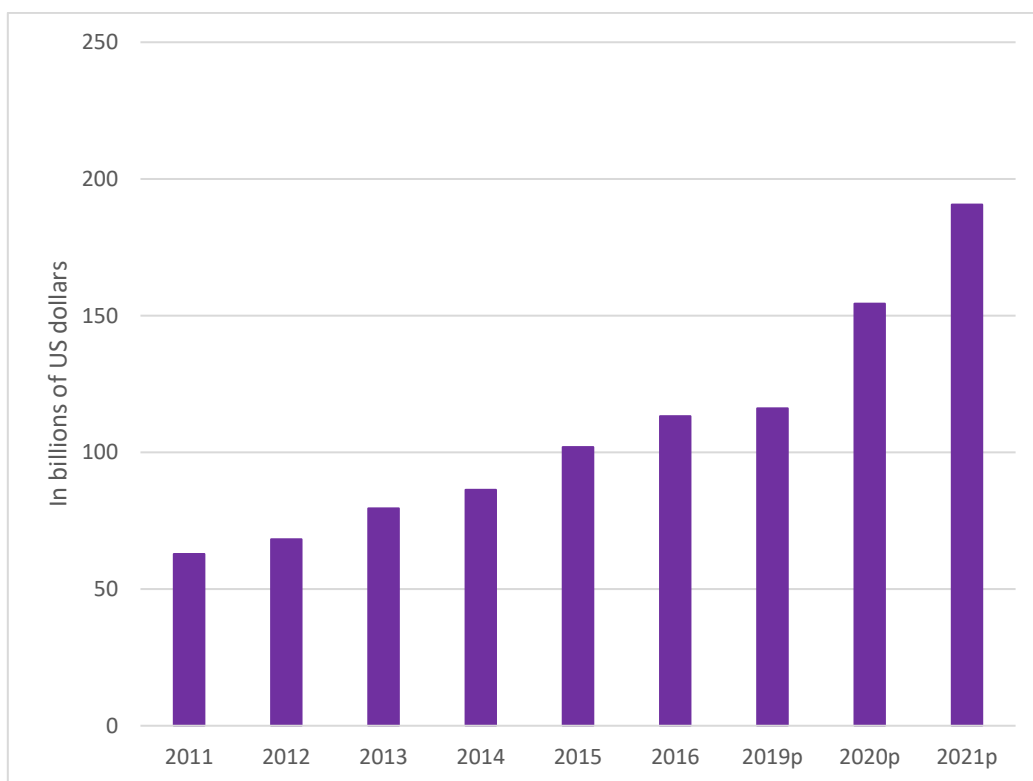
Figure 1.1 - Global market of sensors for a period from 2010 to 2020 [1].

Due to their high sensitivity, low power consumption, and low manufacturing costs, humidity sensors have a significant role in a wide range of applications, such as meteorology, agriculture, industrial control, and medical instrumentation [2]–[5]. In the previous period, many researchers have invested a lot of efforts to develop high performance humidity sensors which have properties of large sensitivity, fast response and recovery, and small hysteresis. Many principles, such as capacitive, resistive, acoustic, optical and mechanical, can be used for the design of humidity sensors [6]–[9]. New promising materials, such as graphene oxide (GO), have recently been introduced in humidity sensors [6], [10], [19], [20], [11]–[18].

The sensitivity of CMOS interdigital capacitive humidity sensors can be improved by means of GO as a sensing material [21]. Some of the GO based sensors have been manufactured by complex and expensive technological processes, such as etching [17] or layer-by-layer deposition (LbL) [15]. The humidity sensors based on gold nanoparticles and GO have been manufactured using self-assembly and the sol–gel techniques [22]. Spin coating chemically derived GO on a quartz crystal microbalance have been used for manufacturing humidity sensors with the frequency response dependant on the relative humidity (RH) [23]. A dip-coating technique have been applied to create uniform GO films for optical humidity sensing [11].

Together with humidity sensors, an important part of sensors industry belongs to force sensors. Measuring of force is an integral part of numerous applications. Force sensing resistor (FSR) have been used in a number of force sensing applications in many fields, such as medicine, rehabilitation, robotics, dentistry, etc. [24]–[26]. FSR is the device used to measure static and dynamic force which is applied to its sensing surface. The response range of FSRs is dependent on the change of its electric resistance. The FSR is usually a flexible device that shows the decrease of its electrical resistance with increase of the force which is used perpendicularly to its surface. Some of the most popular commercial types of FSRs are: FSR *Interlink Electronics* [27] and *FlexiForce-Tekscan* [28] sensors. A commercial FSR encompasses of two layers, a sensitive layer and electrodes. These two layers are facing each other allowing a contact between itself. This gives an opportunity of short circuiting of sensitive layer (conductive layer) and electrodes in order to reduce the resistance between them while force or pressure are applied. FSRs can be found in a few shapes such as round, square and strip and their small thickness and mechanical flexibility allow them extensive applicability. FSRs are usually used in the robotic fields, particularly for control application of robot interactions [29].

1.1. Subject and goal of the research

The subject of this PhD dissertation is capacitive humidity sensors and force sensing resistors based on carbon nanomaterials. Humidity and force sensing studies have made a big progress and humidity and force sensors have been extensively implemented in industrial and household applications. The technology used for the fabrication of proposed sensors was ink-jet printing technology, but because of the limitation of materials used for the fabrication of active layers this technology was combined with spin coating technology (for humidity sensors) and flexography printing technology (for FSRs). Ink-jet printing technology was used to fabricate the electrodes of both types of sensors, humidity and force. The electrodes of all were printed on polyimide flexible foil using commercially available silver nanoparticle ink. Different geometries of electrodes were presented for both types of sensors. For the fabrication of humidity sensors on top of ink-jet printed electrodes commercially available graphene oxide ink was spin coated, while for the fabrication of FSR a graphite ink was flexography (flexo) printed. Both types of sensors, humidity and force sensors, can be applied in many fields, such as environmental protection, food packaging, meteorology, health, medicine, robotics, rehabilitation, etc.

The increasing development of science and technology, have stricter requirements that the sensors must fulfil. Due to the diversity, strengths and shortcomings of various technologies and materials, the development of hybrid types of sensors is a real challenge and need.

The goal of this dissertation is to investigate the use of combination of various fabrication technologies, materials and their good electrical and mechanical properties for the fabrication of sensors, followed by manufacturing of sensor prototypes (humidity and force sensor), improvement and optimization of their performances. The main characteristics of the sensor are a simple design, low cost production and no need for power supply. The fabrication technologies investigated in this thesis are ink-jet printing, spin coating and flexo printing. All sensors were manufactured on flexible polyimide foil allowing in that way placement of the sensor and measurement of humidity and force in rough and inaccessible places.

The research on the capacitive and resistive sensors represent a new direction of research which has been enabled by the procurement of equipment for the production of the flexible electronic circuits, primarily thinking on *Dimatix* deposition material printer (*DMP 3000*). In addition to all already known good properties of capacitive and resistive sensors, low cost production and simple structures make them very suitable for use in systems where humidity and force have to be measured.

The goal of this study was to develop a simple sensor, with optimal geometric parameters suitable for humidity and force measurements in many fields, such as environmental protection, food packaging, meteorology, health, medicine, robotics, rehabilitation, etc.

1.2. The hypothesis and methodology of the research

Capacitive and resistive sensors are used in a large number of measurements where the specific environmental parameters, such as humidity and concentration of some gases, as well as clinical merits needed in experimental clinical studies on the biomechanics of prosthetic applications can be calculated from changes of capacitance and resistance.

The advantages of the described sensors are that they are completely manufactured on a flexible substrates, unlike sensors which can be found in the literature, allowing their application in very inaccessible places and their fabrication in low cost technologies.

The first part of the research included the analysis of the technical literature and scientific journals that deal with this topic.

The second part of the research is dedicated to the design of new sensors for humidity and force measurements.

The next step was the prototype fabrication of humidity and force sensors based on carbon nanomaterials.

After that, an experimental method which involved measuring the humidity and force in laboratory conditions was presented.

At the end the following processing of the obtained results and their publishing was done.

1.3. Organisation of PhD thesis

The thesis consists of six chapters including the introduction and the concluding chapter.

In the first chapter, after the introduction, a subject, problem and goal for research in the field of humidity and force sensors based on carbon nanomaterials, as well as framework phases of the research are presented.

The second chapter gives an overview of the proposed state-of-the-art of numerous types of sensors and their characteristics. Special focus is given on humidity and force sensors and their major performances, such as hysteresis, response and recovery time, sensors size, etc. Fabrication technologies, substrates and materials for sensor fabrication, as well as their applications, are presented as well.

The third chapter describes a design and fabrication of proposed sensors. Design of structures, and fabrication procedure are described in details. In this chapter the overall look of fabricated sensors is also given.

The fourth chapter describes in-house developed setup for electrical testing and characterization of sensors, structural characterization (Scanning Electron Microscopy-SEM and Atomic Force Microscopy - AFM), as well as mechanical characterization of fabricated structures.

Chapter five is dedicated to obtained results and their discussion.

The six chapter gives a general conclusion of the thesis.

The concluding section offers an overview of the literature referenced in this dissertation.

2. State of the art

There are numerous definitions of sensor, one of them describes it as a device which gives a measurable output with respect to a specific input, which is usually a physical quantity called the measurand [30].

Defining sensors as an "input device" means that the sensor is a part of a bigger system which provides an input to the main control systems, such as processors or microcontrollers. Another unique definition describes it as a device that transfer signals from one energy domain to electrical domain. In other words sensor is a device that transfer a physical input (temperature, humidity, force, etc.) to a proportional output signal (electrical, mechanical, magnetic, etc.) [31].

Many of the fundamental sensing mechanisms for physical and chemical sensors have been used for decades. However the improvement and development these sensors has made a huge progress in the last 20 years. The definition of a sensor also varies based on the type of sensor, i.e. its final application [32].

Many classifications of sensors are made by different authors and experts. The first classification of the sensors divides them in to active and passive. Active sensors are those which require an external excitation or a power signal in order to generate an output. Passive sensors, on the other hand, directly generate output response without the need for an external power signal.

The other type of classification is based on the type of the detection used in the sensor: electric, biological, radioactive, chemical, etc.

The next classification is based on the type of conversion phenomenon: photoelectric, thermoelectric, electrochemical, electromagnetic, etc.

The final classification of the sensors divides them to analog and digital sensors. Analog sensors produce an analog output which is a continuous output signal as a function of the quantity being measured. Digital sensors work with discrete or digital data.

There are many types of sensors that are typically used in various applications: humidity, force/pressure, temperature, proximity, light, touch, etc. sensors. All these sensors can be used for measuring of physical parameters such as temperature, resistance, capacitance, conduction, etc.

In a selection of a suitable sensor for measuring of desired physical quantity a certain static and dynamic parameters have to be taken into account. Static characteristics can be determinated after stabilizing of all transient effect to their steady state. These characteristics are related to issues such as: change of an output as a function of an input, selectivity of the sensor, stability of operation of sensing system, influence of internal and external factors to sensor's response, etc.

Some of the characteristics, which are very important for an optimal operation of each sensor are: precision, accuracy, repeatability, reproducibility, resolution, stability, sensitivity, hysteresis , response and recovery time [33]. Some are defined in detail as follows:

- Precision represents an ability of a sensing element/system to have the same response after measuring of the same physical quantity in the same measuring conditions for endless number of trials.

- Repeatability is sensing element/system capability to produce the same response for consecutive measurements. It is closely related to precision.

- Reproducibility of sensing element/system is its ability to give the same response after altering of measurement condition. For example, if measurements obtained by a sensing system in different laboratories are similar it can be said that the system is reproducible.

- Resolution is described as the smallest detectable change of the input which can lead to a measureable change of the output.

- Stability represents an ability of sensing element/system to produce the same output after measuring of the same input for a certain period of time. Sensitivity represents the ratio of the gradual change in the output of the sensor (Δy) to the gradual change of the physical parameter measured at the sensor's input (Δx). Figure 2.1 represents a usual curve for the calibration of sensors and sensitivity can be measured from its slope ($y = f(x)$). As it is visible in Figure 2.1 the sensitivity for low values of measured input ($\Delta y_1/\Delta x_1$) is larger than of the other section of curve where this change becomes slowly constant ($\Delta y_2/\Delta x_2$). In an ideal case sensor will reach saturation at certain point and will no longer respond to the changes of the input signal.
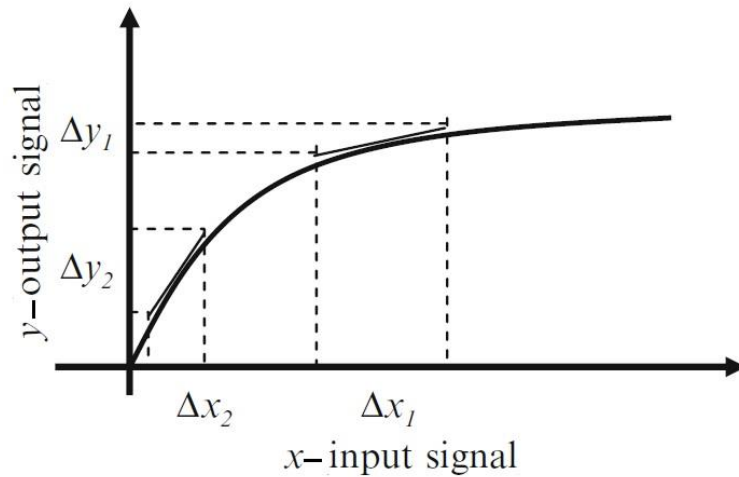
Figure 2.1 - Calibration curve: it can be used for the calculation of sensitivity [33].

➢ Hysteresis is the dependence of sensor response on its previous inputs. The sensor has a different response when increasing the input then when decreasing the input. Figure 2.2 shows the input-output response of a system which has hysteresis.
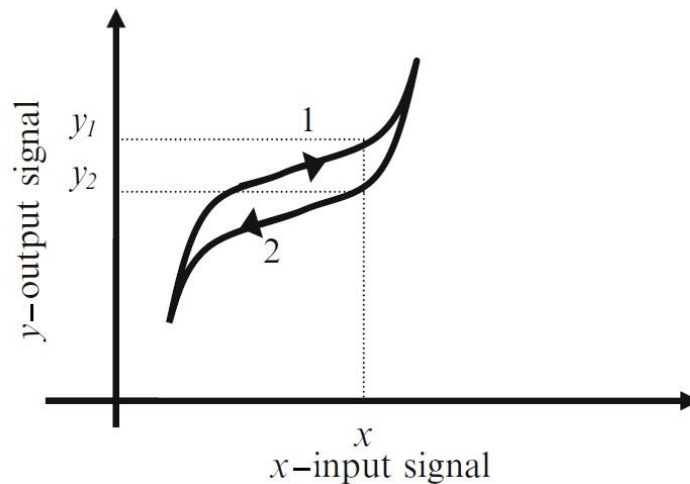
Figure 2.2 - Hysteresis curve of a sensor [33].

➢ Response and recovery time. Response time represents the time required to reach a stable value, certain percentage of its total change (usually 95 %), after exposing to measuring physical parameter. Recovery time is the time needed for a sensor to come back from 95 % to its initial value after removal of measured physical quantity.

Because of its high sensitivity, low consumption of power, and low production price, humidity and force sensors are very important in various applications, such as meteorology, agriculture, medical instrumentation, medicine, rehabilitation, etc. In the last decades, a lot of progress has been made in the development of humidity and force sensors with high performance, i.e. large sensitivity, quick response and recovery, and small hysteresis. Numerous transduction techniques, ranging from capacitive, resistive, acoustic to optical and mechanical, have been approved for the development of sensors used for the detection of humidity and force.

2.1. Humidity sensors

The climate system of the Earth is constantly changing across all space and time scales. Since the 18th late Century, measurements by thermometers and other surface instruments on land have been available. Most of our modern measurement systems have been used primarily for weather forecasting purposes [34].

As it is well known that measurement of humidity is very important for whole Earth's ecosystem and is of great importance of commercial and industrial applications, including those related to building ventilation control, clean rooms, environmental chambers for different types of testing, electronics, food control, biomedical analysis industries, and many others [35]. In order to have a wanted environment, it is necessary to constantly monitor the ambient humidity in different conditions while temperature is changing or it is combined with other gases. Humidity is affecting many substances and it is experienced on a daily basis that is why the interest about humidity is more and more focused on the products compatibility with relative humidity. During the production of any goods it is necessary to have an adequate level of relative humidity otherwise they properties will be lost. For example, if paper is printed at a wrong level of humidity it will lose its properties because of its hygroscopic ability, fruits and vegetables will dry or ripen too fast if they are kept under wrong humidity conditions, etc.

In atmosphere air is composed of following elements by volume: 78.1% N, 20.93% O, 0.93% Ar, 0.03% CO_2, 0.01% H, He, Ne, Kr, and Xe in smaller amounts. This structure of air is named „dry air" and happens very rarely in nature. „Moist air" comprises greater or a lesser extent of water content [36].

Moisture technically refers to the water content (mechanically mixed rather than chemically combined) of any solid, liquid, or gas, whereas humidity specifically means the water vapour content of a gas. Atmospheric humidity ranges from nearly 0 to more than 4% of the mass of air and averages about 3% making it the third most common atmospheric constituent. It comes

from evaporation from open water surfaces (oceans, lakes, rivers), evaporation from wet exposed content solid surfaces (soil, animals, plants, ice) or by formation during chemical reactions (i.e., burning or other oxidation of organic substances). Humidity is lost from air by condensation into suspended water droplets or ice crystals in the atmosphere (clouds or fog) or onto solid surfaces, Figure 2.3. Humidity also decreases through chemical reaction with atmospheric or terrestrial constituents [37].
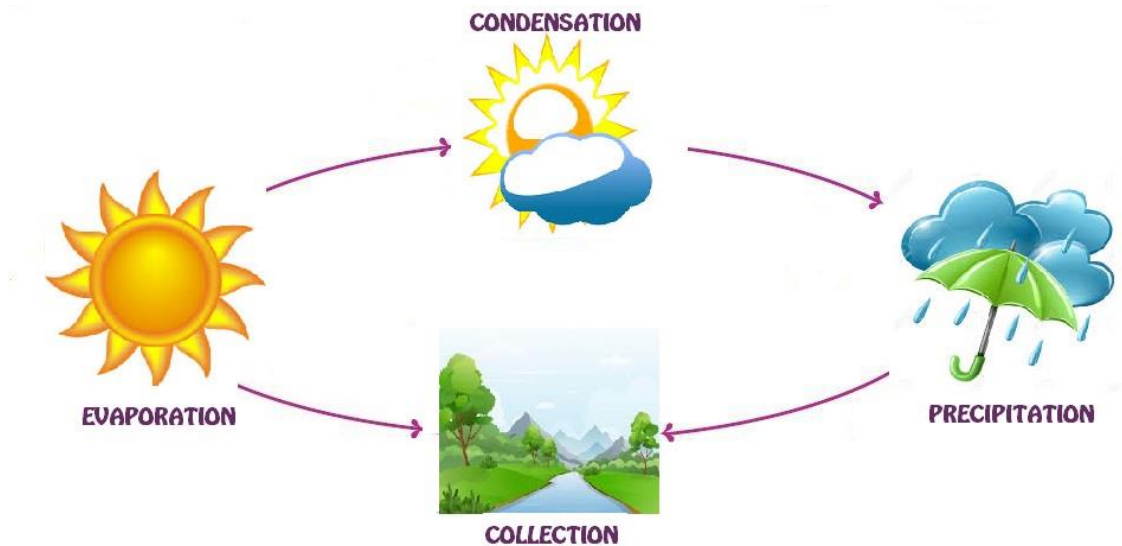
Figure 2.3 - The water cycle in nature

The most frequently used term related to humidity is relative humidity and it can be described as ratio of the maximum amount of moisture content in air that can be hold in the air at constant temperature and pressure of the gas. Relative humidity depends on a temperature and therefore it is a relative value which can be expressed by following equation, in %:

$$RH = \frac{P_v}{P_s} \times 100 \qquad (1)$$

where P_v is the actual partial pressure and P_s is the saturated pressure of moisture content in air at constant temperature.

Relative humidity changes with temperature, even if water vapour density does not. As air temperature increases, its water vapour capacity increases and relative humidity decreases, even though no actual change in water content or vapour density (evaporation potential) occurs. An understanding of relative humidity, however, is still important because it is easily the most commonly used term and will likely continue to be widely used.

Humidity is perhaps the most difficult environmental factor to monitor. Although accurate and relatively simple instantaneous measurement is feasible, no practical, reliable, continuous humidity measurement is available. Humidity measuring equipment is usually calibrated only

in terms of relative humidity. There are many methods for measuring humidity. Humidity measurement techniques include gravimetric, elongation, volumetric, psychrometric, hygroscopic, electrolyte resistance, electrolytic, radiation refraction, piezoelectric, electrical capacitance, thermal, etc. Direct measurements of humidity require isolation of the gas and a means of measuring the water content (chemical absorption, condensation, gravimetric) and are therefore impractical as a routine technique for monitoring humidity. Such measurements are usually employed during calibration. Almost regardless of the technique used, most sensors are not accurate throughout the entire humidity span. Capacitance hygrometers, which are used for measuring of the change in capacitance of a solid state or polymer absorptive element, seem to be the most reliable technique for routine humidity control and monitoring. Humidity is inferred from measurements of the capacitance of the oxide layer [37].

A humidity sensor based on lithium chloride was developed in 1937 [38], and has become the first and only humidity sensor available for many years after its development. Since then, humidity sensors have been expansively studied for many applications in industries, environmental monitoring human activities, agricultures, etc. [38], [39]. Different transduction mechanisms have been researched for the detection of humidity in the environment, including capacitance [6], [7], [40], resistance [8], [9], [41], field-effect transistor [8], microbalance [42], [43] and photonic crystal [44], [45], etc. Many effort has been given to an improvement of the performances of humidity sensors, where main focus was on the development of novel sensing materials, such as carbon based materials [46], [47], electrospun fibers [45], metal oxide nanowires [48]–[50], semiconductor particles [51], and composite nanofilms [52], [53]. The capacitive humidity sensors are the most frequently used sensors for the detection of the humidity in commercial field, because of their high sensitivity, low power consumption and low production prices [35], [54].

Based on the units which are measured, humidity sensors can be classified on relative and absolute humidity sensors. Relative humidity sensors, which are mostly used, can be divided on ceramic, organic polymer-based, and hybrid sensors (polymer/ceramic) [39]. All of the mentioned classes are changing properties of their sensitive elements (physical and electrical) when exposed under different conditions of atmospheric humidity, and supply a measure of the humidity related to adsorption and desorption of water vapour molecules [55].

2.1.1. Ceramic (semiconductor) relative humidity sensors

Ceramic type humidity sensors acquired special significance among other types of humidity sensors mainly due to properties of its sensing element, i.e. its mechanical strength, thermal, capability, resistance to the attack of different chemicals, etc. These properties are making ceramic as a promising material used for the development of humidity sensors for electrochemical applications. The exceptional structure of ceramic materials composed of grains, surface areas, grain boundaries, and controlled porous microstructures, makes them appropriate material for electrochemical sensors [56], [57].

Some of the capacitive humidity sensors have been fabricated using Al_2O_3, $MnWO_4$, boron phosphate, etc.

For many years, Al_2O_3, has been used as the dielectric layer in manufacturing of sensors for humidity measurements. A porous structure of Al_2O_3 makes it the most relevant material for humidity sensors due to the tunnelling mechanism effect of electrons inside of layer of water condensed inside of Al_2O_3, allowing it a detection of a very low levels of humidity.

One type of Al_2O_3 based humidity sensor was developed by anodization of an Al film, previously deposited by direct current (d.c.) sputtering, in sulphuric acid [54]. A layer of silicon dioxide was deposited by plasma-enhanced chemical vapour deposition (PEVCD) technique on silicon wafer. A double capacitor configuration was obtained by depositing of two titanium electrodes onto the p-type oxidized silicon wafer followed by deposition of thin film of aluminium. Both films were deposited using d.c. magnetron sputtering. Order to achieve oxidation of aluminium film electrochemical anodization was used. In order to obtain a porous structure of sample it has been dipped in acid solution (H_2SO_4). This was the most critical step in the fabrication of the sensor. Gold film electrodes were thermally evaporated on Al_2O_3 film. The complete structure of the sensor is shown in Figure 2.4.
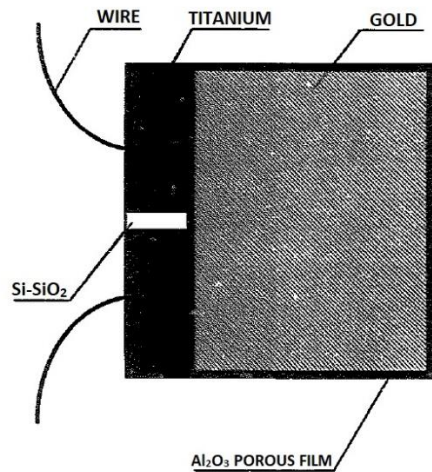
Figure 2.4 - Top view of fabricated Al$_2$O$_3$ sensor [54].

The measurements of the absolute value of sensor's impedance Z were done at three different humidity concentrations, 20 ppmv, 100 ppmv and 200 ppmv and at different temperatures. For the concentrations of 100 ppmv and 200 ppmv impedance remained constant as a function of temperature but have increased by ½ order of magnitude with humidity change. In the case when the humidity concentration is 20 ppmv sensors showed also a temperature sensitivity.

Another type of Al$_2$O$_3$ based humidity sensors used Al$_2$O$_3$ modified microcantilevers (MCLs) for the detection of small amounts of humidity [58]. Onto a commercially available silicon a thin film of Cr followed by Ag, were deposited using e-beam evaporation. Other side of microcantilever was covered with a thin film of aluminium. The aluminium was exposed to oxygen to form a layer of alumina. The bending of MCL was detected by constant checking of the position of a laser beam which was reflected from the side of the MCL coated with gold on a photodiode of AFM. The measurements were done at four different humidity concentrations, 10 ppm, 30 ppm, 100 ppm and 200 ppm. Figure 2.5 shows deflection of Al$_2$O$_3$ modified MCLs vs. time for different level of humidity.
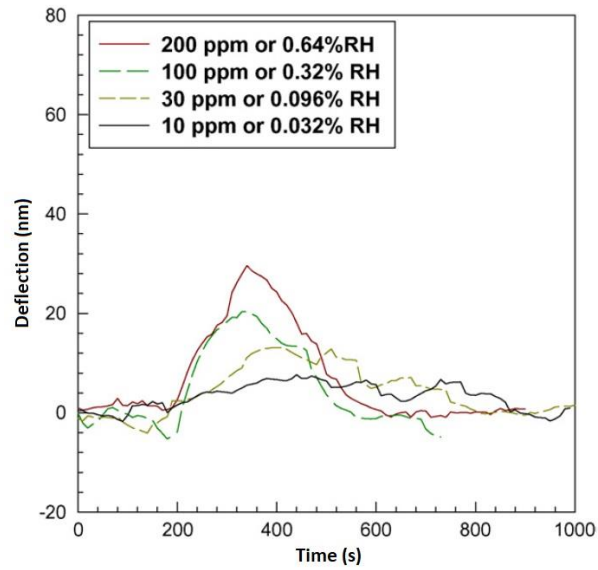
Figure 2.5 - Deflection of Al$_2$O$_3$-modified MCLs vs. time at four different humidity levels [58].

Measurement showed an increase of the MCL deflection with an increase of humidity which makes MCLs coated with Al$_2$O$_3$ as excellent sensors for the detection of low level of humidity in the environment.

Humidity sensors which use reactively evaporated A$_2$O$_3$ films as sensitive dielectric for humidity measurements have been reported [59]. The sensor, shown in Figure 2.6, was fabricated on Pyrex glass substrates by depositing of nickel electrodes using conventional vacuum evaporation from a tungsten heater, next step was deposition of oxidized aluminium particles previously obtained by oxidation from pure aluminium. In the last step thin films of moisture adsorptive gold were deposited by conventional vacuum evaporation on top of porous Al$_2$O$_3$ films.
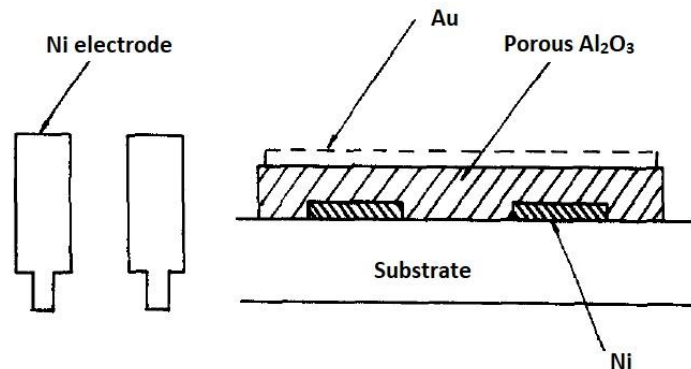
Figure 2.6 - Structure of the Al$_2$O$_3$ humidity sensor [59].

Dependence of sensor's capacitance and resistance on humidity was measured at 100 Hz. The measurements showed that for high level of humidity, the change of capacitance and resistance is large. For the low levels of the humidity, less than 100 ppmv, the change of both measurands is small, but still enough sensitive to detect extremely low humidity. Measured capacitance and resistance for different ranges of humidity are shown in Table 2.1. The drop of capacitance sensitivity can be noticed if the humidity decreases, whereas the change of the resistance sensitivity is not significant [59].

Table 2.1 - Capacitance and resistance sensitivity of Al_2O_3 sensors in various humidity rages at 100 Hz [59].

Humidity range (dew point in ˚C)	+20 ÷ –10	–10 ÷ –30	–30 ÷ –50	–50 ÷ –76
Capacitance sensitivity (pf/˚C)	700	90	30	8
Resistance sensitivity (kΩ/˚C)	11	21	14	11

A low melting temperature and adequate bulk conductivity are making $MnWO_4$ as an adequate material for the manufacturing of humidity sensors [60]. The sensor's electrode was fabricated on double sided sapphire substrates using lift-off procedure. After that a layer of titanium and a layer of platinum were thermally evaporated. The sensing films, used to obtain $MnWO_4$, were spin coated using sol–gel technique.

Two types of sensors, thick and thin film, were fabricated with the same geometric sensing area, as shown in Figure 2.7.
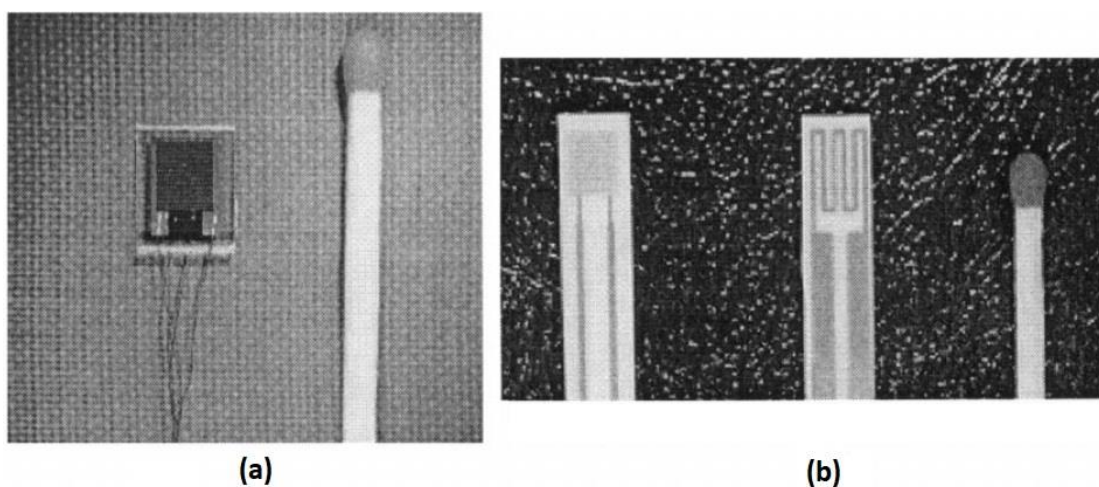
Figure 2.7 - The thin-film (a) and thick-film (b) MnWO₄ humidity sensors [60].

Humidity sensors fabricated by thick- and thin-film technology exhibited a significant differences in their characteristics when exposed to different concentrations of humidity, 30, 50, 70, and 90 %RH, shown in Figure 2.8.
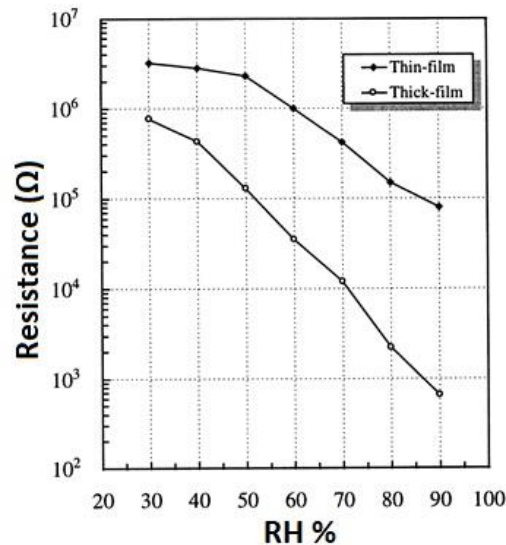
Figure 2.8 - Resistance as a function of humidity of the thin and thick film MnWO₄ humidity sensors [60].

Both sensors showed great sensitivity to humidity by decreasing their resistance when humidity increases. With increasing of humidity, layers of water molecules were physisorbed on MnWO$_4$ layer leading to an increase in protonic conductivity. This can be the result of the difference in structures of the thick and thin films of MnWO$_4$ sensing layers.

2.1.2. Organic polymer based relative humidity sensors

Due to the changes of electrical conductance when they are exposed to humidity, polymeric based materials are increasingly being used for the fabrication of humidity sensors. They can be used for resistive and capacitive humidity sensors. Advantages polymeric materials are simple fabrication process, low cost production, decent sensitivity, but they cannot stay long under water and in harsh environments, have slow response time, etc. Because of that, in past years organic/inorganic compounds are gaining a lot of interest as a promising sensing materials. Capacitive type sensors for measurement of relative humidity based on polymer materials are showing some advantages compared to resistive type [61]. One of the advantages is their fast response, linearity and small hysteresis [62]. For the fabrication of humidity sensors

most frequently used polyimides [63] and esters are: cellulose acetate butyrate (CAB) [64], polyethylene terephthalate (PETT) [65], and polymethyl methacrylate (PMMA).

Thirteen different commercial polyimide film were used for fabrication of capacitive RH sensor [63]. The performances of fabricated sensors were characterized before and after 28 days. The series capacitance and resistance Kapton® HN polyimide based sensor were measured as a function of relative humidity at 10 kHz immediately after fabrication, and after 1, 14, 21 and 28 days of aging. In Figure 2.9, hysteresis of Kapton® HN sensor is presented. The highest value of capacitance for this sensor, after its fabrication, was about 63 pF. The sensitivity of presented sensors was calculated to be about 23% at 100 %RH [63].
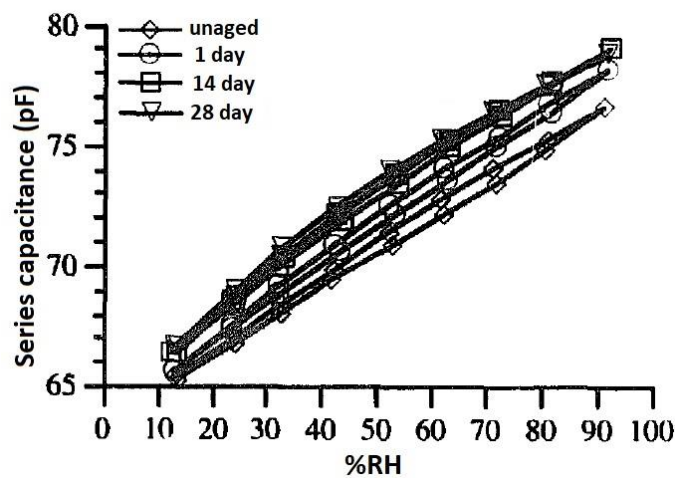
Figure 2.9 - Capacitance as a function of relative humidity of Kapton ® HN sensor in the unaged state, and after aging for 1, 14 and 28 days [63].

Another type of sensor was fabricated on 25 mm polyethersulfone (PES), and three different thicknesses: 7.6 mm, 12.5 mm and 25 mm, respectively. The capacitance of all sensors was measured from 10 %RH to 90 %RH, and results are presented in Figure 2.10.
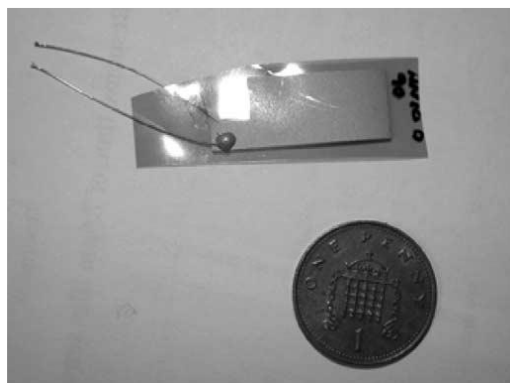
Figure 2.10 - Printed sensor structure on polyimide film [61].

The same range of humidity was used for testing the PES sensor too, and obtained result are presented in Figure 2.11. Both PES and polyimide sensors showed linear behaviour for the changes of humidity.
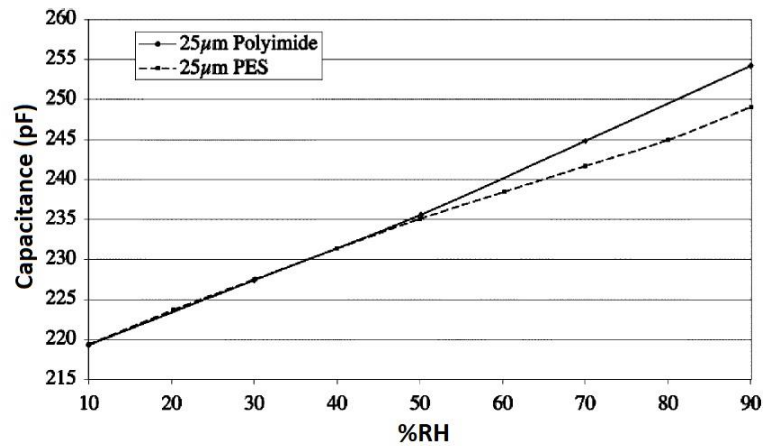
Figure 2.11 - Capacitance as a function of humidity of 25 mm film polyimide and PES sensors [61].

Nominal values of capacitance for both types of sensors was almost the same, while polyimide sensor had bigger change of capacitance when exposed to humidity, than PES sensor.

The development of capacitive sensors based on PETT was published [66] and structure of sensor is shown in Figure 2.12. The sensing mechanism, stability and linearity of sensor were investigated. These sensors showed the changes of their dielectric constant when exposed to humidity, which comes as the result of water sorption inside of sensing material.
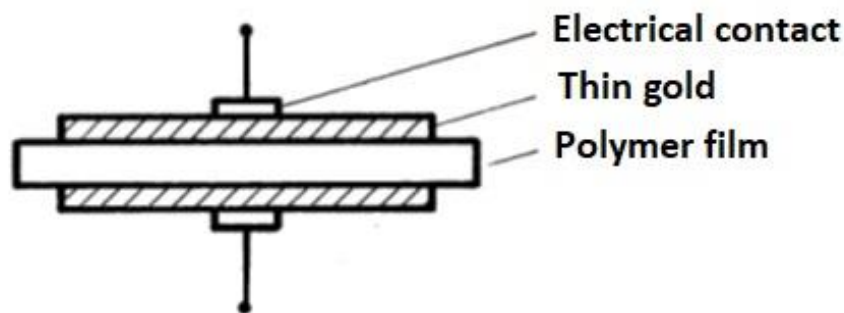
Figure 2.12 - The capacitive structure of PETT sensor [66].

The capacitance changes observed for humidity change from 12 %RH to 97 %RH, were linear, as it is presented in Figure 2.13.
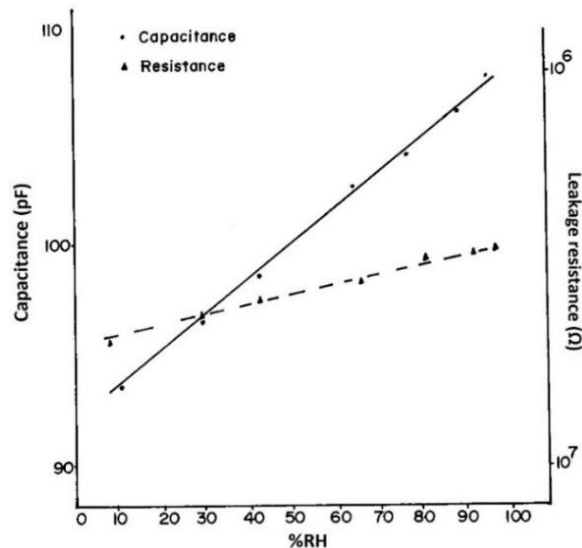
Figure 2.13 - Representative capacitance and leakage resistance characteristics of PETT sensor [66].

2.1.3. Hybrid composites humidity sensors

In recent years, there is an increase in usage of composites developed by combining organic and inorganic substances for fabrication of humidity sensors. Nanoparticles are taking place in humidity sensing applications because of their excellent chemical, physical, magnetic, electronic and mechanical properties Organic/inorganic compounds have the best characteristics of both groups.

Sodium polystyrenesulfonate (NaPSS) and ZnO were combined by in situ synthesis and then used for the fabrication of humidity sensors, Figure 2.14 [67].
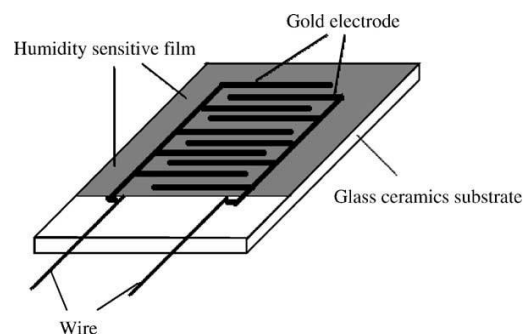
Figure 2.14 - Structure of sodium NaPSS and ZnO based humidity sensor [67].

In order to investigate their properties and sensing mechanism complex impedance was measured as a function of humidity. Logarithmic change of impedance was about 4 orders of magnitudes when humidity was changed from 11 %RH to 97 %RH, Figure 2.15.
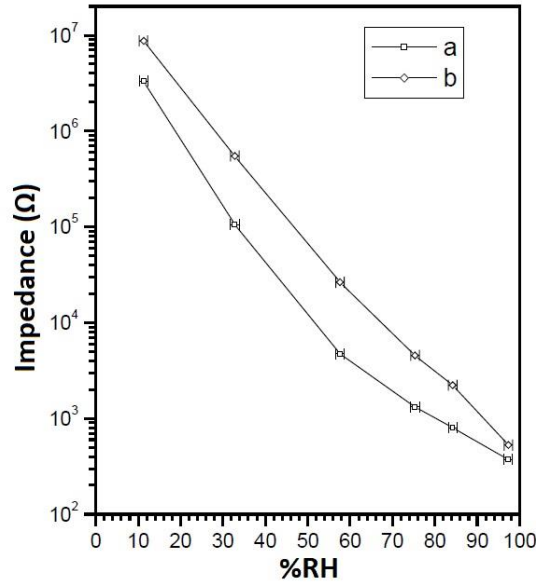
Figure 2.15 - Impedance of NaPSS and NaPSS/ZnO as a function of humidity [68].

Sensor has also exhibited a quick response and small hysteresis. It was showed that composite film have better sensitivity than NaPSS film, as well as improved linearity and faster response. Another type of organic/inorganic based humidity sensor was fabricated using pure polypyrrole (PPy) combined with TiO_2 nanoparticles/polypyrrole (TiO_2 NPs/PPy) thin film compound on top of Al_2O_3 substrate [68]. Using a ultra-violet (UV) light polymerization method an Al_2O_3 substrate with Ag interdigitated electrodes was coated with prepared compound, as shown in Figure 2.16. Four sensors with different amount of TiO_2 inside composite solution as shown in Table 2.2.
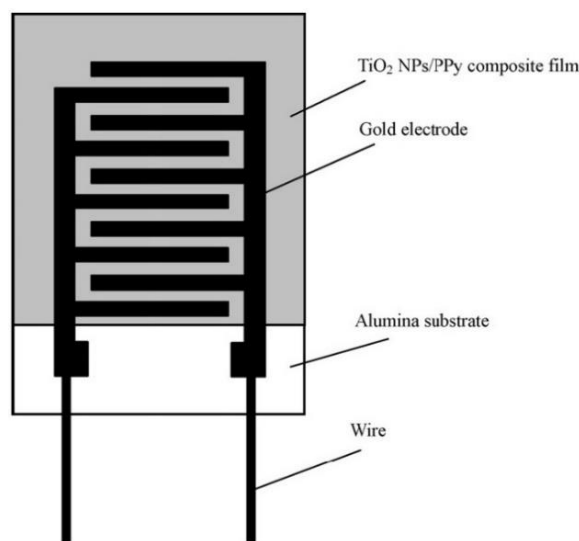
Figure 2.16 - Structure of TiO₂ NPs/PPy based humidity sensor [68].

Table 2.2. Composition of films used for fabrication of the sensors

Sample number	Pyrrole (g)	AgNO$_3$ (g)	TiO$_2$ (g)
1	0.125	0.0314	0
2	0.125	0.0314	0.0012
3	0.125	0.0314	0.0118
4	0.125	0.0314	0.0480

The humidity sensing principle of TiO$_2$ NPs/PPy composite thin films was tested using the results of activation energy and impedance spectroscopy. It was found that sensor made of PPy and TiO$_2$ NPs (0.0012 g) thin films, had the highest sensitivity, the best linearity and smaller hysteresis [68].

2.2. Ink-jet printing as a technology for the fabrication of sensors

Solution-based techniques such as spin coating, ink-jet, screen and flexography printing have attracted much interest in the fabrication of sensors. Printing methods can be classified as contact and non-contact ones. There are numerous printing methods that can be categorized into contact printing and non-contact printing processes. If the substrate is directly in contact with the ink reservoir method is than called contact method. Contact method has some disadvantages such as risk of damaging or contamination of substrate, which is not the case of non-contact method [69]. In last years, ink-jet printing becomes a main process for the fabrication of different types of sensors on flexible substrate, which are very important for the future of printable electronics. One of non-contact printing technologies is ink-jet printing, an alternative to screen printing or flexography [70]–[72], and it is very simple, precise method, which does not require any additional steps in fabrication process, i.e. there is no need for masks or etching, need of high temperatures or vacuum [73], and the most important printing design can easily be changed without additional costs. It has been used in many applications, such as biology, space science [74], flexible displays [75], solar cells [76], [77], sensors and actuators [78], organic memories [79], RFID tags [80], etc. These are some of the examples that ink-jet printed devices are without competition compared to the traditional semiconductor processes in terms of integration, performances and cost [81]. Ink-jet printing enables fabrication of flexible electronic devices with performances equal to conventional methods and covers large areas applications [74], [82] which were not satisfied by a traditional rigid devices.

The market of ink-jet printed devices is still at its beginning, but it is already taking place to many traditional method for electronic devised fabrication.

One of the most important steps for the fabrication of flexible electronic devices is the choice of materials, both ink and substrate. Selection of materials have to be compatible with the used deposition method. Different parameters such as viscosity, surface tension, conductivity and compatibility to other materials need to be taken into account when selecting the printable material [83]. Also, the properties of a substrate material should be taken into consideration. Such characteristics include, for example, dimensional stability, thermal stability and solvent resistance [84]. Ink-jet allows fabrication of micron size patterns depositing a drops of ink and achieving the resolution of tens of microns with a very precise volume of ink that is ejected through nozzles [84]–[88]. The first ink-jet printer was invented in 1960s [89], and it has used a pressure applied to the ink stream and caused its breaking in drops of uniform size and distance. Later, massive development of ink-jet printers brought to the application of this method to computer printers. Two main modes of operation of ink-jet printers are continuous and drop-on-demand (DOD). In a continuous mode, the droplet is constant, and it is controlled by a high-pressure pump which produces a vibration of nozzles made of piezoelectric material. The other method, named the drop-on-demand, ejects the droplet only when it is needed. The drop-on-demand printers relies on a pulse of pressure which forms ink droplets and deposits them on a substrate through micron sized nozzle head. The DOD ejection principle can be piezoelectric, thermal, or electro hydrodynamic, as it is shown in Figure 2.17.
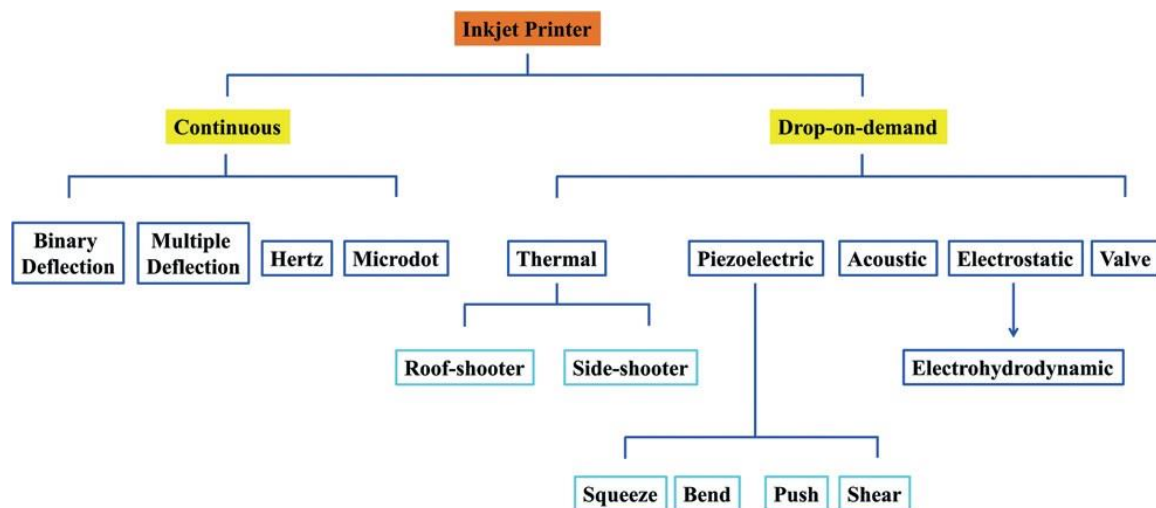
Figure 2.17 - Categories of ink-jet printers [90].

The two major factors that affect the drop formation when jetting are the ink properties and the waveform. Waveform controls applied voltage signal that triggers the drop ejection, and typical

basic waveform which is used as a starting point has four different segments. Each segment has three properties: duration, level and slew rate, shown in Figure 2.18.
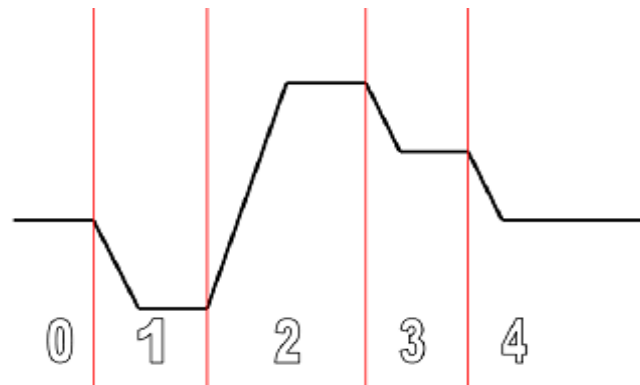
Figure 2.18- Basic waveform

The change of each of these properties effects on jetting process differently. The amplitude (voltage) of the first two segments has much influence. Especially changing duration in the first segment and the slew rate and/or the duration of the second segment effects drop formation very much. The applied voltage is related to how far the fluid chamber membrane is bending. The slew rate is how fast it bends and the duration is how long it stays in that position. Each fluid has its own optimal waveform so the user himself have to experimentally reach the best solution. Additionally by modifying waveform parameters, smaller or larger drop could be achieved. The exceptional chemistry of any ink is crucial to the ink-jet printing system. This is because the characteristics of ink are not only influencing the quality of printing but are also determining the drop ejection characteristics and the accuracy of the whole system.

The most frequently used conductive materials for the fabrication of ink-jet printed sensors are silver [91], gold [92], carbon nanomaterials [93], graphene [94], and conducting polymers [95]. Some of the dielectric materials are used to form a conductive tracks in order to create the active area of electrode. These materials are usually some polymers [96], or SU-8 [92] that is most often used as a photoresist in device fabrication.

2.3. Flexible substrates

Substrates used for flexible electronics are facing a different challenges compared to currently faced by rigid substrates. The most critical parameter for flexible devices is their flexibility, which at the same time is one of the most important differences that separates them from

traditional microelectronics. There are a number of characteristics that have to be fulfilled before some substrate is chosen for the fabrication of flexible devices, such as resistance to humidity and solvents, its thermal and mechanical stability, etc. Additionally, the smoothness, surface tension, transparency, price and commercial availability have to be taken into account. Since the quality of the material and its properties dictates the price of the material it is expectable that different quality materials will be used for different applications. For more challenging applications the substrate will most probably be a multi-layered structure [97]. Flexible substrates are mainly used for the fabrication of low cost, flexible, stretchable sensors that have a large area of production comparing to the silicon based technology [98]. Polymer based organic and inorganic materials are the two types of materials used in flexible electronics [99]. The most commonly used substrate in ink-jet printed flexible electronics is polyimide film. It provides important advantages for fabrication of the devices as well as for their functionality. Processing advantages are related to possibility of R2R fabrication, resistance to high temperature bonding stations and corrosive aqueous etchants, high mechanical strength. Thickness and flexibility of polyimide based flexible printed circuits (FPCs) allows them to be installed in small volumes and to be folded which leads them to various applications, such as mobile phones, digital and video cameras, flat displays, laptops, connections to printheads in printers, electronic packaging, and many others. Polyimide FPCs can also be used in membrane switches and single layer structures making an alternative for wire coupling [97].

2.4. Carbon nanomaterials

In the last 30 years, carbon nanomaterials have attracted substantial interest due to their exceptional electrical, optical, mechanical, chemical, and thermal characteristics. Carbon is already known as a material which forms different solid state allotropes with different structures such as fullerenes, carbon nanotubes (CNTs) and graphene. It can be found in mixed states where it forms the basic block of amorphous carbon, diamond-like carbon, and anocrystalline diamond. In contrast, graphite is the thermodynamically the most stable form of carbon and it is composed of two dimensional layered structure both layers have a hexagonal honeycomb structure of sp^2 bonded atoms of carbon. Weak bonding between the layers of graphite allows the exfoliation of a single layer of graphite using mechanical or chemical methods. That single layer of graphite is called graphene.

Very high delocalization of electronic structure of sp^2 bonding in carbon nanomaterials makes carbon nanomaterials as high mobility electronic materials. Because of this, carbon

nanomaterials tends to replace traditional semiconducting materials in the production of electronic and optoelectronic devices [100].

2.5. Graphene oxide as a material for the fabrication of sensors

Graphene is a free standing flat monolayer of carbon atoms tightly packed into honeycomb lattice with one atom thickness, and is basis for all graphitic materials. It is possible to wrap it up into 0D fullerenes, roll it into 1D nanotubes or stack it into 3D graphite, as it is presented in Figure 2.19. In last years, graphene has become one of the most important topics in many fields such as physics, chemistry, materials science, nanotechnology, etc. [101] because of its high mechanical strength, high elasticity and thermal conductivity, very high electron mobility at room temperature, tuneable band gap, etc.
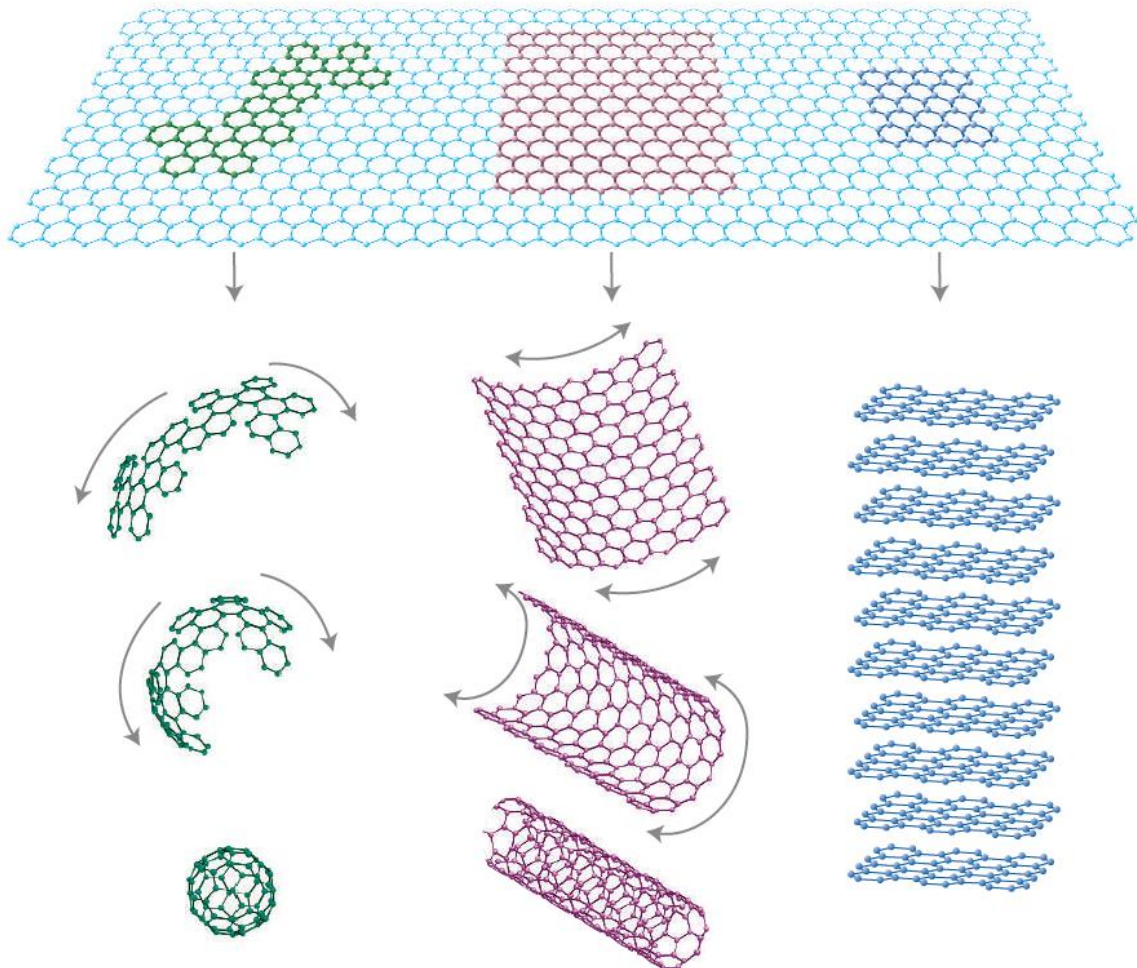
Figure 2.19 - Graphene as a base of all graphitic materials [101].

Due to its conductivity and transparency, its low cost, high surface area, high electron mobility graphene is an ideal material for the fabrication of batteries, super-capacitors, nanoelectronic and sensors [102]. On the other hand, for the fabrication of devices, where a dielectric material is needed graphene oxide (GO) have recently attract much interest as one of the stages in the production of graphene [103]. In GO the surface of carbon sheets is decorated with epoxy and hydroxyl groups while carboxyl groups are localized on its edges [102]. The presence of this O functional groups, shown in Figure 2.20, makes graphene oxide a hydrophilic and electrically insulating material, which can easily be dispersed in water, opposite than graphene which is hydrophobic.
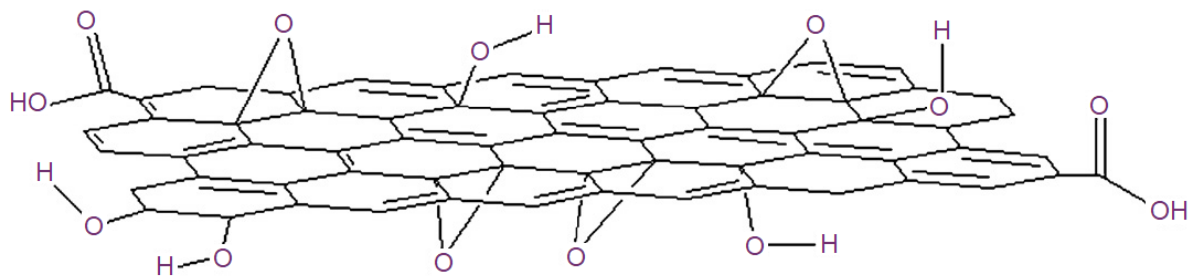
Figure 2.20 - Chemical structure of graphene-oxide [23]*.*

The conspicuous sp^3 fraction in GO is responsible of its insulating behaviour. By simple removal of oxygen from graphene oxide it can be turned to semiconductor and eventually to a graphene like semimetal [104]. The oxygen in graphene oxide makes higher interlayer distance, almost twice than interlayer distance in graphite. This is the consequence of insertion of water layer in between of graphene oxide layers. Beside water, other solvents can also be integrated in the layers of GO [105]. It is possible to tune the size of graphene oxide flakes too, and their size can vary from a few nm to mm. The ability of changing of GO chemical structure and flakes size makes it an attractive material in many applications, such as electronics, specially sensors, biology and medicine, etc. [104].

Sometimes, the fabrication of more complex devices by using only ink-jet printing seems to be complicated. For that reason combination of ink-jet printing with other techniques improve the fabrication of devices. Due to its simplicity screen printing [106], spin coating [107] and flexography printing [108] remain the major technologies used for the fabrication of planar electrodes. Some of the GO based sensors have been fabricated by complicated and expensive technological processes, such as etching [14] or LbL [15].

Humidity sensor based on reduced graphene oxide (rGO) was fabricated using LbL deposition. An interdigitated capacitor was fabricated on polyimide structure, as shown in Figure 2.21.
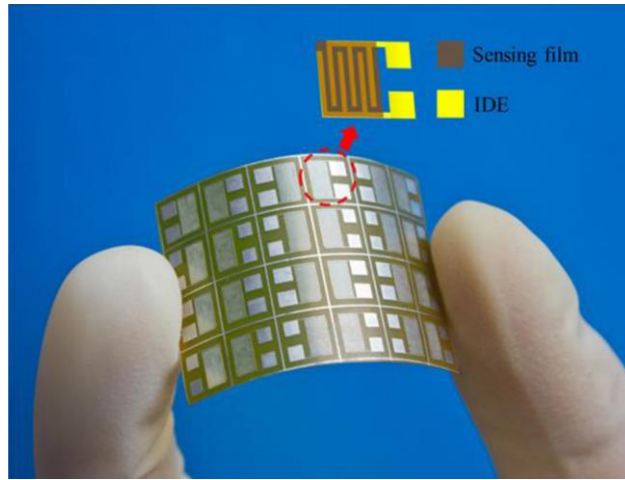
Figure 2.21 - Layer-by-layer deposited rGO humidity sensor [15]*.*

Humidity properties of the sensor were tested by exposing it to different humidity environments, changing the humidity from 11 %RH to 97 %RH and measuring its resistance as a function of time. Normalized response of sensor was from 8.69% to 37.41%, for used range of humidity, Figure 2.22.
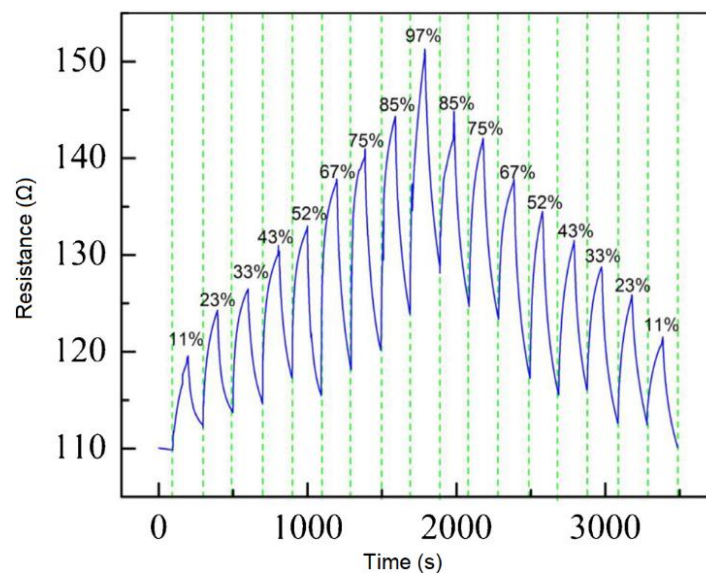
Figure 2.22 - Resistance as a function of time for the layer-by-layer fabricated GO sensor [15]*.*

Spin coating of chemically derived GO on a quartz crystal microbalance (QCM) have been used to manufacture humidity sensors with the frequency response of the microbalance dependant on the RH [23]. Three sensors with different number of spin coated GO layer were fabricated. Humidity response was tested from 6.7 %RH to 97.3 %RH, and it was observed that the sample with largest number of GO layers, i.e. sample number 3, has the highest sensitivity, as shown in Figure 2.23.
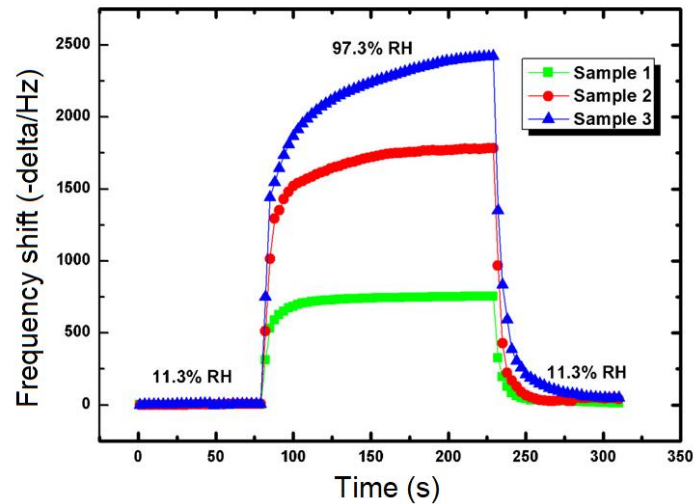
Figure 2.23 - Frequency response as a function of time for 3 fabricated QCM GO humidity sensors [23].

The humidity sensors based on Au nanoparticles and GO have been fabricated using self-assembly and the sol–gel techniques [22]. The optical humidity sensing was achieved by means of uniform GO films deposited by a dip-coating method [11]. Ink-jet printed GO has been applied in temperature-modulated resistive humidity sensors which employ CMOS MEMS micro-hotplate technology to monitor and control indoor air quality [109].

2.6. Spin coating and flexography printing techniques

Spin coating technique is frequently used for the fabrication of sensors. If applied on smooth and flat substrates, spin coating technique coats the substrate with a thin and reproducible layer of material, which can be used in a wide range of applications [110]. Presently, it is the leading technique for production of uniform thin films of photosensitive organic materials with thickness of few micrometres and nanometres. The first analysis about spin coating were done more than 50 years ago. Those analysis investigated the spreading of Newtonian fluid on a flat

substrate while the substrate was rotating with a constant speed [111]. Centrifugal force spreads the liquid radially from the centre of substrate to its edges. The surface tension of the substrate and viscose force of the liquid are causing a formation of thin film of liquid on top of the substrate. The formation of the film is predominantly influenced by two independent parameters, viscosity and spin speed. The thickness of the film that can be formed by spin coating goes from 1 µm to 200 µm [112].

Flexography, or flexo, is a direct printing, simple and cost-effective printing technique, which is used to print a wide range of materials such as plastic films, cardboard, cartons, rolling paper, cellophane, etc. Flexo print has a rapid development trend, both in terms of technology and in terms of printing materials on the market. Due to its characteristics of print on different surfaces flexo print is preferred in the field of printing on packaging materials. Flexography is one of the modern printing process which today covers about 40% of the commercial market printing in total printing production in the world, and around 55% of printing on packaging. Basic principle of how flexography is working is presented in Figure 2.24.
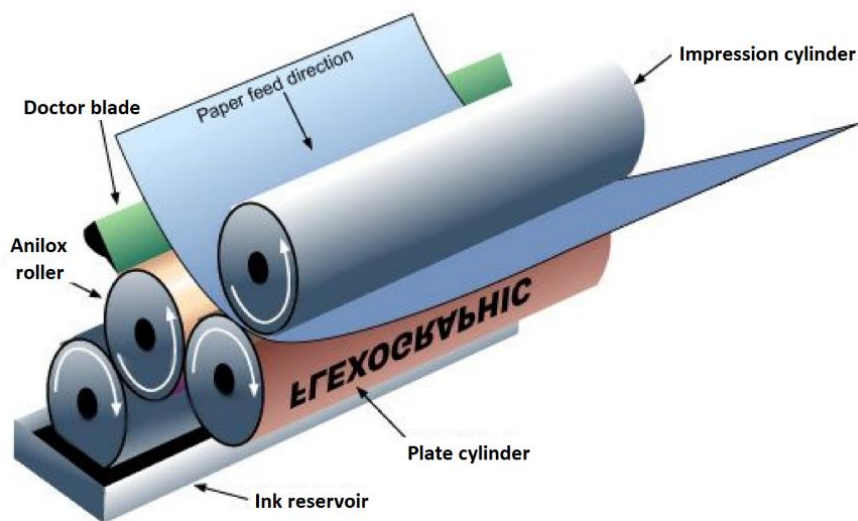
Figure 2.24 - Schematic view of flexography printing [108].

A roller covered with ink, also known as the "anilox roller", applies ink to the plate which has raised portions on its edge and ink is then transferred to the substrate. The roller is equipped with the cells that are carrying certain amount of ink to the plate. The number of cells varies according to the type of printing and the quality [108].

2.7. Force sensing resistors

Robotic devices are slowly entering into human lives, which has brought to an immense interest about robotic interaction and their ability to learn. This is very important for further development of robots in order to provide them to learn independently and to have a safe interaction with its surrounding. Along with its ability to learn and interact robots should not harm the surrounding and objects they are interacting with. Because of this it is extremely important to completely examine the paths and methods of robotic movement and its communication with the environment. Humans are communicating and exploring the environment using five senses: touch, vision, audition, smell and taste [113]. Human's dexterity is a spectacular skill, people are able to grasp different objects, to accomplish difficult tasks, and to easily switch their grasp from one task to another. This is the result partly because of physical construction of human's hand and partly of human's sophisticated control skills. This control ability is mainly focused on tactile and force sensing, particularly the ability to feel different conditions during the contact between fingers and object. In the last two decades a lot of scientific work has been implemented in creation of an artificial sense of touch which will equip robots with same manipulation abilities that people have. Even though vision has attracted the highest attention in robotic applications, touch is crucial for many tasks. Tactile sensing can deliver information about compliance, adhesion, and mass. Information about parameters is crucial if robots are constructed to handle unknown objects in unknown surrounding [113]. Tactile sensing found its application in consumer electronics, as well as robotics. For instance, it was planned to use robots as assistants to improve the care of sick and old people. In order to fabricate such a robot it is necessary to develop sensors which will completely imitate the human skin while grasping objects. While human hand is able to move different object without any effort (for example paper sheet and bottle of water) robotic hand requires an adequate sensor to enable the same level of functionality for different objects. Elastomeric based force sensing resistors can be used for this purposes because they are able to both sense and grasp objects [114]. Force and position sensing became an essential part of various dynamical measurements, and human sense of touch is one of those applications. Force sensor provides constant reading for constant force, independent of position where force is applied or how it is distributed on sensor's surface [115]. Resistive sensors are usually constructed from two conductive layers distanced by air, silicone glue, microspheres, etc. One of the sheet behaves as a voltage gradient by applying a reference voltage and ground on its ends, while second works like the slider in a linear potentiometer. A resistive type of touch

sensors are usually sensitive and low cost in a term of material needed for its fabrication, but, they are expensive in term of power consumption [113].

The oldest and most frequently type of pressure sensors are piezoresistive pressure sensors. The sensors consist of four resistors embedded in a Wheatstone bridge, used to precisely measure electrical resistance. Two resistors are placed in a way to sense the pressure in the direction of current, and two other perpendicularly to their current flow, Figure 2.25 [116].
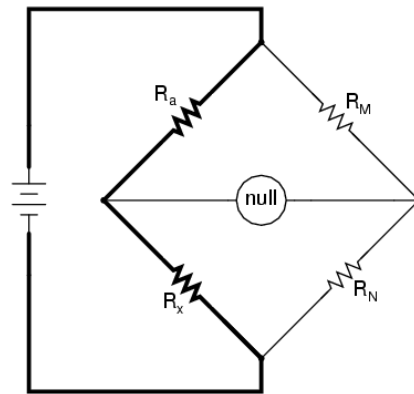
Figure 2.25 - Wheatstone bridge as a pressure sensor [116].

In this setup, the change of resistance of paired resistors is opposite compared to the other pair. The usage of mechanical pressure leads to the change of the resistance of crystalline silicone but will never break it [116].

The *SoftPot* sensor from *Spectra Symbol*, shown in Figure 2.26, is a strip potentiometer which resistance is changing related to the position of applied force to its surface. Thus it can be used to define precise position where the sensor is being pressed [116].
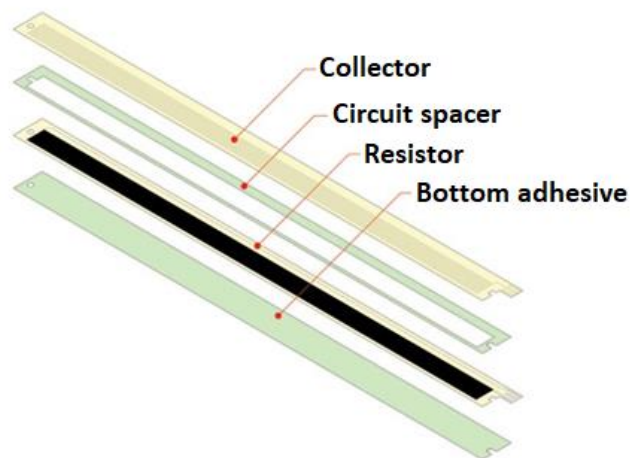
Figure 2.26 - Scheme of SoftPot pressure sensor [117].

The *Interlink* force sensing resistor consists of two polymer films. The first film is a conductive and it is facing the second film with interdigitated structure. A similar sensor is fabricated by *LuSense* in Luxembourg, and it comes in a few different shapes. The *FlexiForce* force sensor from *Tekscan* is made of two layers polyester/polyimide films, both with silver and conductive ink [118]. All three types of mentioned commercial sensors are shown in Figure 2.27.

Figure 2.27 - Force sensing resistors from Interlink, LuSense and Tekscan [118].

2.8. Scanning electron microscopy, atomic force microscopy and nanoindentation techniques

The SEM is one of the most useful techniques for the investigation of the microstructure morphology and chemical composition of material. The working principle of scanning microscopy is based on the interaction of an electron beam with a sample, i.e. with the atoms of the sampled sample, whereby a micrographic image is formed on the basis of the electron emission from the excited atoms of the sample. The SEM micrographs depend on the acquisition of signals produced from the electron beam and specimen interactions [108].

Atomic force microscopy offers a 3D profile of the surface on a nanoscale level, by calculating forces between a sharp probe and surface at very short distance. The probe is attached on a flexible cantilever and its tip is constantly tapping along the sample surface and records the small forces between the probe and the surface.

In the last decades, nanoindentation was used as a technique for verifying the modulus and hardness of materials by investigating nanomechanical response as a function of penetration

depth. Nanoscale characterization techniques are constantly challenged by the quick progress in nanostructures and functional materials requiring better resolutions and sophisticated measurement methods for mechanical, chemical, electrical, and thermal testing. Nanoindentation is usually used to examine the displacement of materials under specific applied loads to obtain load–displacement curves [119].

The *Berkovich* tip induces plasticity at very small forces which creates a meaningful measure of hardness, suitable for different types of measurements. The main principle of Nanoindenter G200 measurements is to employ a high-resolution actuator to force an indenter into a test surface and a high-resolution sensor to constantly measure penetration into sample. When the indenter is placed into the material, both elastic and plastic deformation is causing the formation of a hardness impression conforming to the shape of the indenter to some contact depth. After the indenter is withdrawn, only the elastic portion of the displacement is recovered, enabling the determination of the elastic properties of a material.

3. Design and fabrication of sensors

Fabrication of GO humidity sensors (presented in this dissertation) was done at University of Novi Sad, Serbia and Nanoscale device group, Politecnico di Milano, Italy, while FSRs were fabricated at the University of Novi Sad.

Both types of sensors, capacitive humidity and force sensing resistors, were fabricated in ink-jet technology, using *DMP 3000* [120] on *GTS* polyimide films [121], using commercial *SunChemical* [122] 20 %wt nanoparticle silver ink as electrode material. The *DMP 3000*, shown in Figure 3.1, is cartridge based piezo ink-jet printer which allows direct deposition of functional inks that offer simple, faster and cheaper product and material development for electronics, mechanics, optics, life science and medicine. It is mainly designed for laboratory purpose to allow researchers, scientists, and engineers to evaluate the use of ink-jetting technology for new manufacturing and analytical processes. A materials deposition printer is equipped with XYZ stage, ink-jet deposition system with thermally controlled and interchangeable printheads, thermally controlled platen, platen rotation, printhead rotation, 3 camera and lighting systems for examination of substrate and print, nozzle plate rotation calibration and drop watching system. Moreover, a full PC based user interface is provided allowing video capture of images, calibration of machine, drop-watching, and arbitrary waveform editing and pattern generation.

Figure 3.1 - Dimatix deposition material printer DMP 3000

Drop watcher camera system shown in Figure 3.2(a), allows direct view of the jetting nozzles, providing the real time monitoring of jetting of the ink.

(a)   (b)
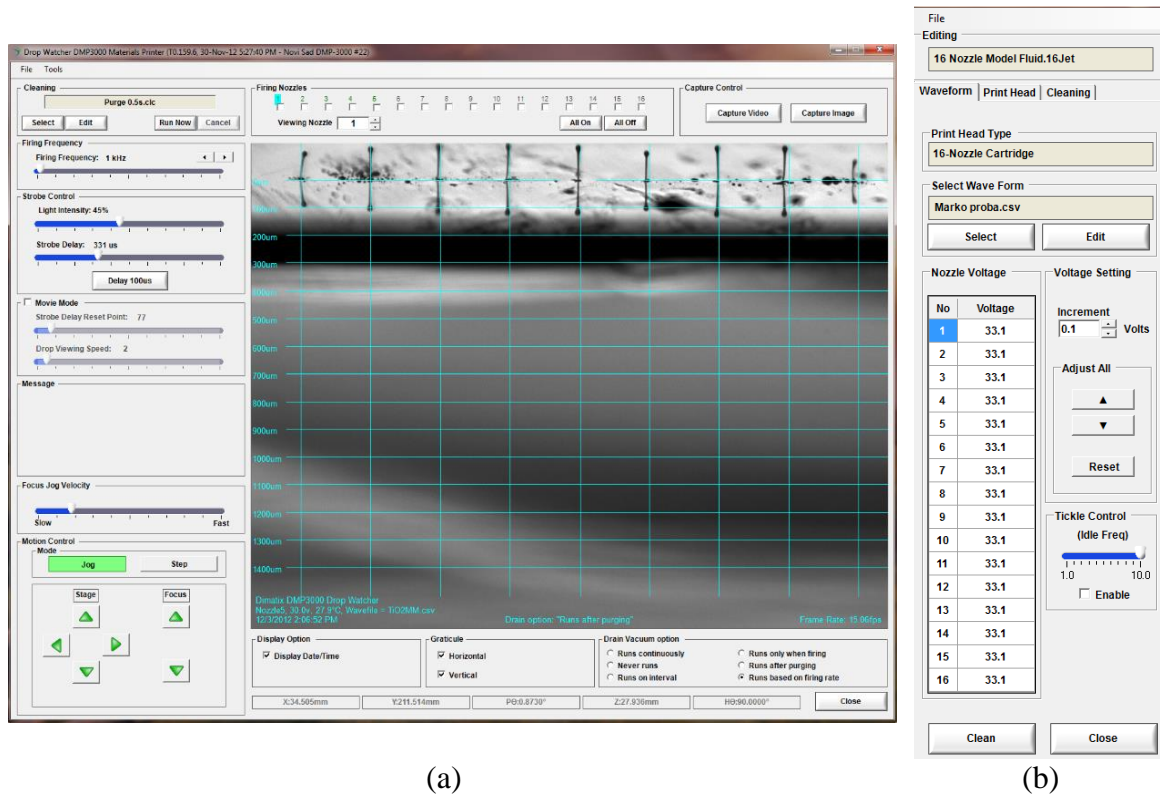
Figure 3.2 - DMP software (a) drop watcher screen and (b) voltage adjustment window

The *Dimatix* Drop manager software enables turning on or off any of nozzles or adjusting the voltage in the individual nozzle. The voltage change at the certain nozzle will actually change the velocity of the drop formed at that nozzle. Voltage adjustment window is shown in Figure 3.2(b).

The drop watcher system has two different viewing modes; one shows real time continuous jetting of the nozzles and the other for closer inspection and measurement where drops appear to be frozen in flight. By adjusting the strobe delay drops are frozen at different positions after they leave the nozzle, shown in Figure 3.2(a), where drops of silver nanoparticle ink used for fabrication of the sensors are shown.

The process of printing on DMP printer was optimized in order to achieve a stable stream of droplets from cartridge towards the surface, without the so-called "satellite" drops that are formed after basic drops and that cause shorting of printed electrodes and "tail" drops which usually leads to a "messy" and unsuccessful printing structure, Figure 3.3(a), and to obtain uniform drops the same speed without satellites and "tails", Figure 3.3(b).
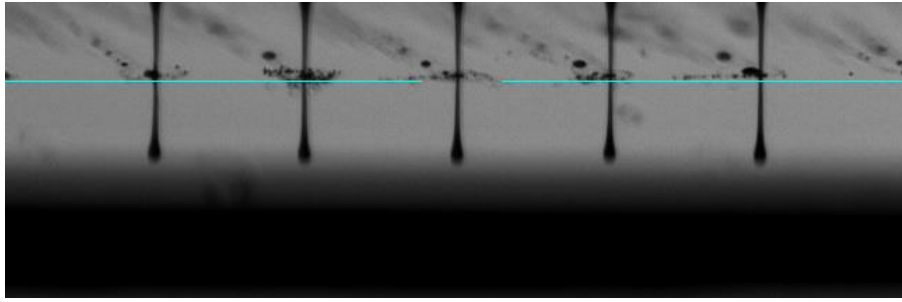
(a)
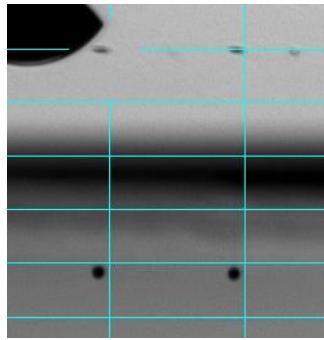
(b)

Figure 3.3 - Drops of silver nanoparticle ink after being fired from cartridge: (a) unadjusted drops with "tails" and b) appearance of droplets of ready for printing.

Using this application it is possible to observe how different voltage amplitude, firing frequency and waveforms affect printing and finding optimal parameters for best printing quality.

3.1. Design and fabrication of humidity sensors based on graphene oxide

Humidity sensors consist of a polyimide substrate, ink-jet printed Ag electrodes and sensing graphene oxide material and schematic view of the sensor is presented in Figure 3.4 [20].
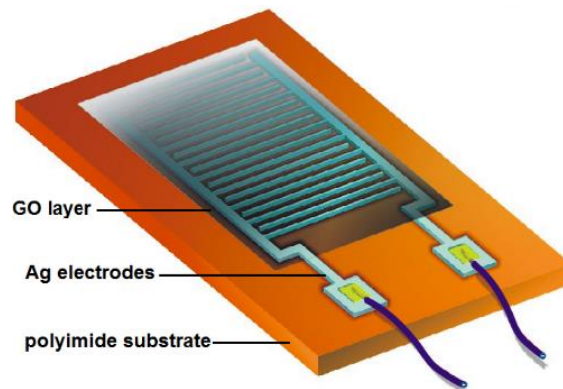
Figure 3.4 - Schematic of the GO sensor [20].

It is made of a polyimide substrate, ink-jet printed silver electrodes and sensing GO material. A capacitor with different patterns of interdigitated electrodes was designed, as shown in Figure 3.5.

<center>(a)   (b)   (c)</center>
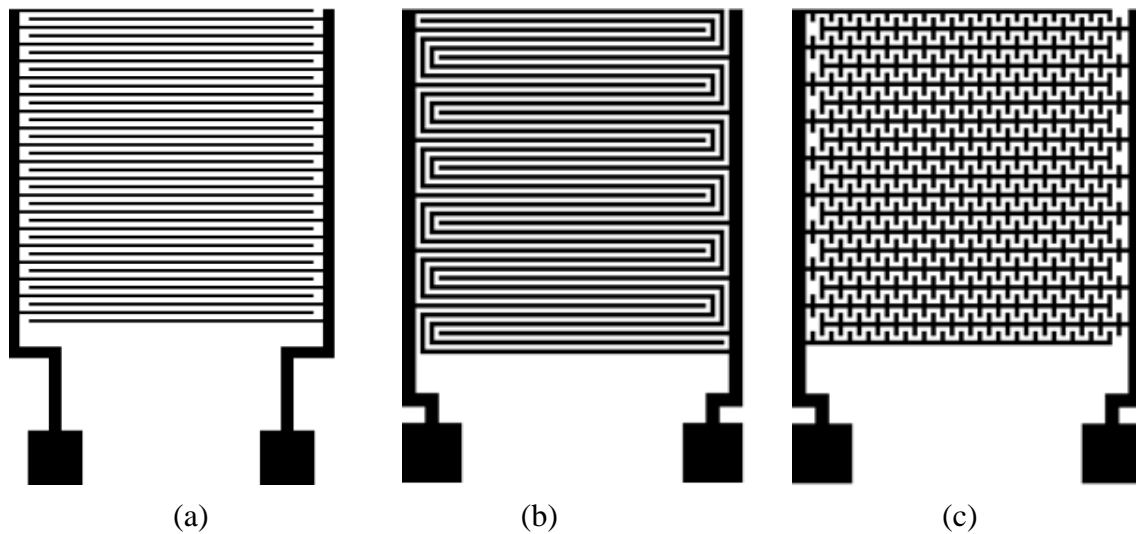
Figure 3.5 - Design of sensor's electrode. (a) interdigitated, (b) serpentine and (c) toothed design.

The length of each electrode was 7 mm, whereas the width of electrodes and spacing between them were 100 μm, which was within the resolution limit of the used ink-jet printer. Different designs were printed in order to increase active area of the sensor, without increasing its total dimensions. The total dimensions of all sensors was 8 mm × 9 mm. The first sensors' layer was fabricated by printing commercially available *SunChemical* Ag nanoparticle ink with 20 wt%. The *GTS* polyimide film had the thickness of 75 μm. The resolution of the ink-jet process using *DMP 3000* was limited by the nozzle diameter and the statistical variation of the droplet flight and spreading on the foil. In the case of printing with Ag nanoparticle ink, the minimum droplet diameter was ~ 36 μm, and center-to-center drop spacing was 18 μm. These were obtained by rotating the printhead. Three identical structures for all 3 designs were printed and then sintered at 240 ˚C for 30 min. The temperature of 240 ˚C was chosen as a tradeoff temperature between desired resistance of the structures and its mechanical flexibility [123]. Completed printed electrodes before and after sintering are presented in Figure 3.6.
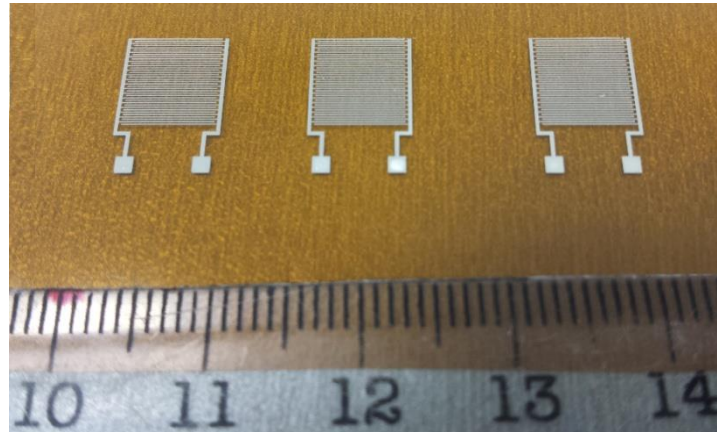
Figure 3.6 -Interdigitated sensor's electrodes before deposition of GO. The ruler is in cm [20].

Even though the projected width of the electrodes was 100 µm, due to the shrinking during sintering process, the printed conductive segments shrunk to 90 µm after printing and ~ 80 µm after sintering, Figure 3.7. This shrinking is the result of evaporation of organic solvent in which silver nanoparticles were dispersed.

(a)   (b)
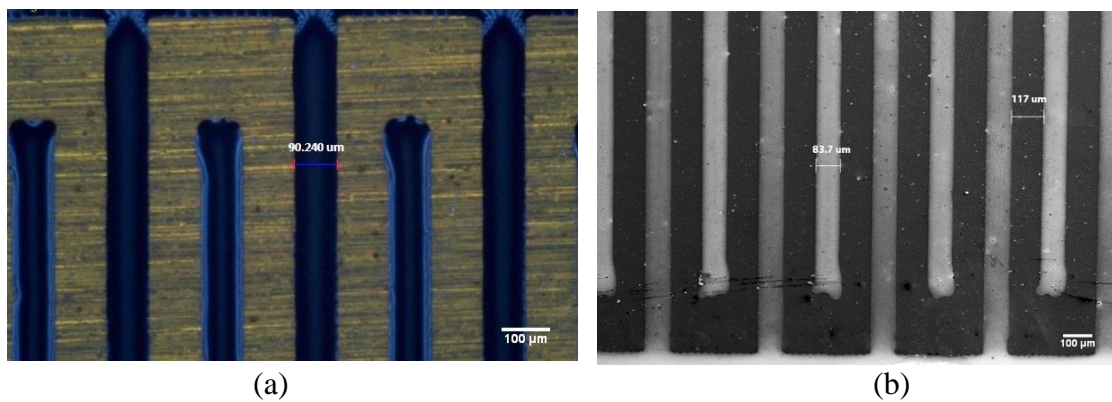
Figure 3.7 - Printed sensor's electrodes (a) before sintering and (b) after sintering [20].

After sintering of ink-jet printed silver electrodes second sensors' layer, graphene oxide, was spin coated on top of already sintered electrodes. Three layers of commercially available *Graphenea* GO ink, with a concentration of 0.4 wt%, were spin coated onto the electrodes at 750 rpm for 5 s and then at 1500 rpm for 40 s. Monolayer content in the ink was >95% at 0.05 wt% [20]. In this case spin coating was chosen because of the size of graphene oxide flakes inside of the solution. Graphene oxide dispersion was attempted, but the size of flakes caused clogging of cartridge nozzles. *Dimatix* cartridge nozzles are 25.4 µm in diameter and in order to be printable the size of nanoparticles in the ink has to be 100 times smaller than the nozzle

diameter, i.e. less than 200 nm in diameter. After spin coating of GO layer the samples were dried at 100 ˚C for 30 min and then cooled to room temperature.

Proper deposition of graphene oxide was firstly investigated by an optical microscope. Figure 3.8 presents optical microscope images of sensor's electrodes before and after spin coating of GO ink.

(a)   (b)
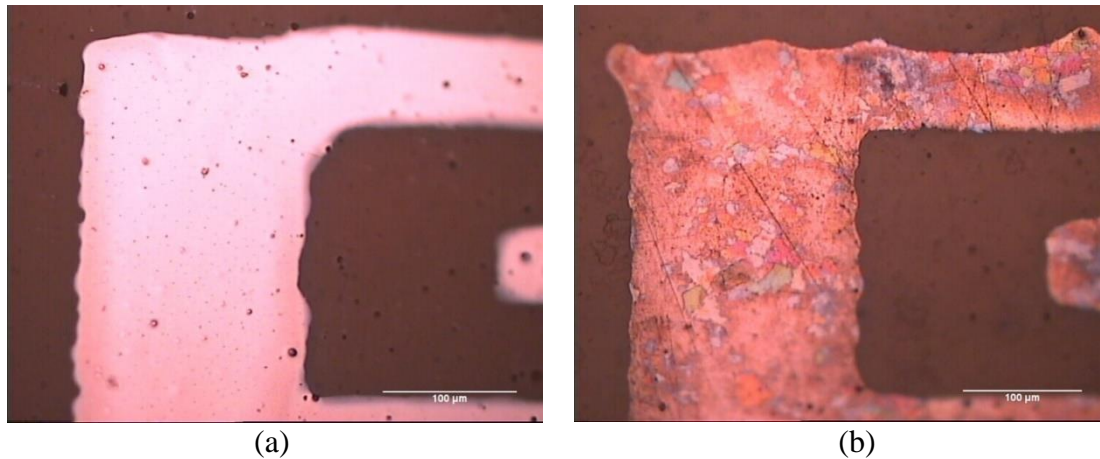
Figure 3.8 - Sensor Ag electrodes without and with the GO film. (a) An optical microscope image of bare sensor's electrodes and (b) An optical microscope image of sensor's electrodes after spin coating GO ink [20]*.*

The presence of the GO flakes on top of the Ag electrodes is clearly visible in the latter case. Wire contacts, necessary for measurements were glued using conductive silver paste, and complete sensor structure is shown in Figure 3.9.
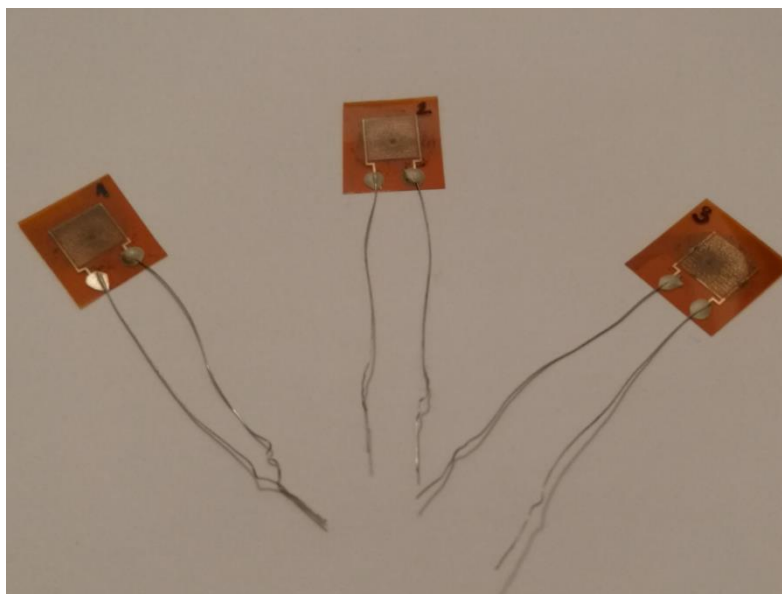
Figure 3.9 - GO humidity sensors after fabrication and placing contacts

3.2. Design and fabrication of force sensing resistors

Force sensing resistor consist of a polyimide substrate, interdigitated Ag electrodes and sensing carbon material and schematic view of sensor is presented in Figure 3.10.
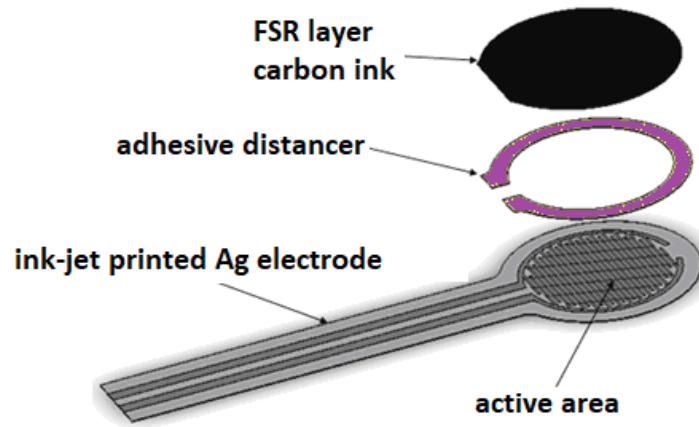

Figure 3.10 - Schematic of the force sensing resistor [27].

Four different designs of force sensing resistor were proposed, as can be seen in Figure 3.11.

(a)　　　　　(b)

(c)　　　　　(d)
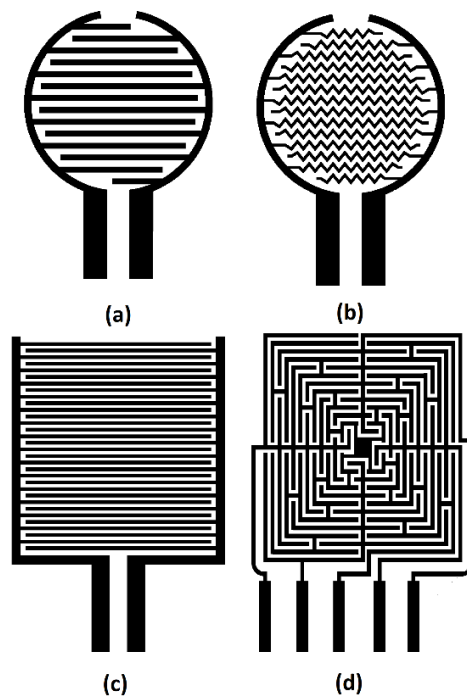
Figure 3.11 - Design of FSR electrode. (a) Round interdigitated, (b) Round wave interdigitated, (c) Square interdigitated and (d) 4 zones electrode.

First two structures are round and they have different shapes of interdigitated electrodes, while the third structure has square shape active area (Figure 3.12(c)). The fourth structure has 4-zones active area, and just first zone has been used for testing, due to identical geometry of other zones, shown in Figure 3.12(d). Presented structures were ink-jet printed using *DMP 3000* and then sintered at 240 ˚C for 30 min. Printed electrodes after sintering are shown in Figure 3.12 [115].
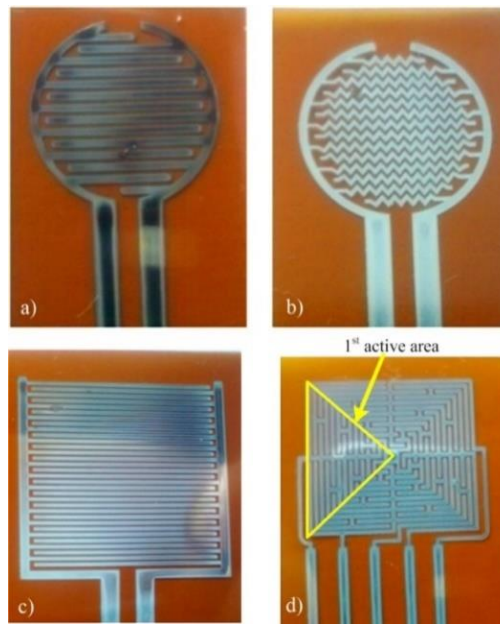
Figure 3.12 - Four different structures after sintering: (a) 1st type of FSR, (b) 2nd type of FSR, (c) 3rd type of FSR and (d) 4th type of FSR, respectively [115].

Dimensions of four types of fabricated sensors are shown in Table 3.1. All FSRs were manufactured by ink-jet printing made by printing of *SunChemical* silver nanoparticle ink with 20 wt%. The printer and the procedure were described above. Thickness of polyimide film was 75 μm.

Table 3.1 - Dimensions of 4 different types of FSRs

	1st type of FSR	2nd type of FSR	3rd type of FSR	4th type of FSR
Active area diameter/surface (mm)	12.7	12.7	24 x 24	18 x 18
Length of structure with terminals (mm)	51.4	51.4	63.4	38.83
Width of interdigitated electrodes (mm)	0.4	0.2	0.4	0.36
Distance between interdigitated electrodes (mm)	0.4	0.5	0.3	0.27

The second sensors' layer was made by printing of carbon ink using *RK* printing proofer, shown in Figure 3.13, on 50 μm *GTS* polyimide film.
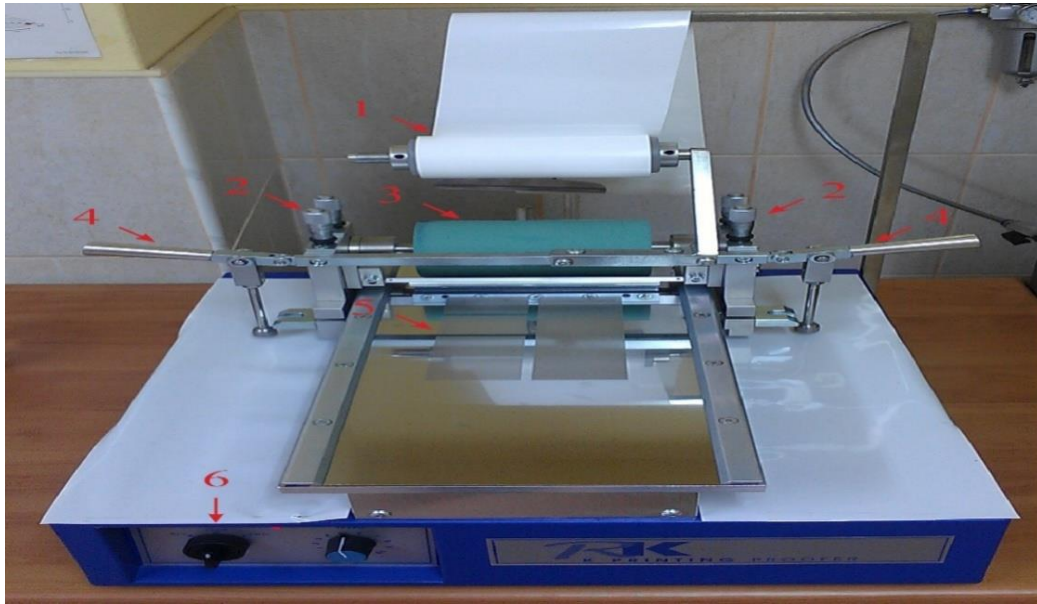
Figure 3.13 - RK printing proofer used

Carbon ink has been printed in several layers (three) on *GTS* film. After printing and cutting in the desired shape, depending on the required dimensions, a second layer of FSR looks like one of the circular form, shown in Figure 3.14.
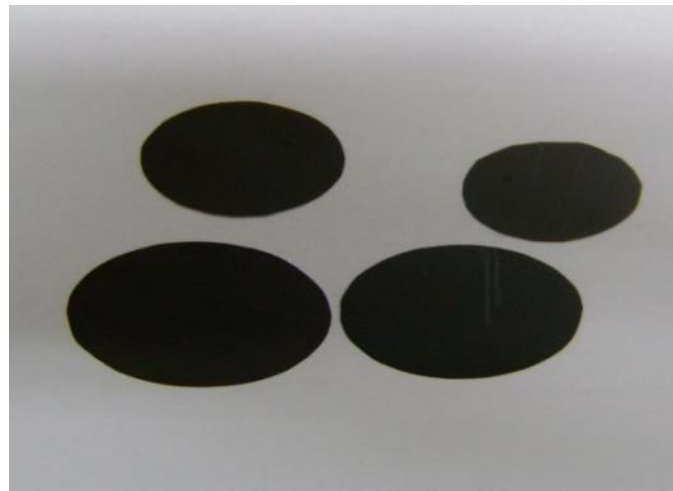
Figure 3.14 - Carbon layer of FSR after printing and cutting

After fabrication both layers have been attached using two component epoxy glue, which has been mounted around the edges of the active area. For the purposes of testing wire contacts were glued using silver paste, and complete FSRs are shown in Figure 3.15.
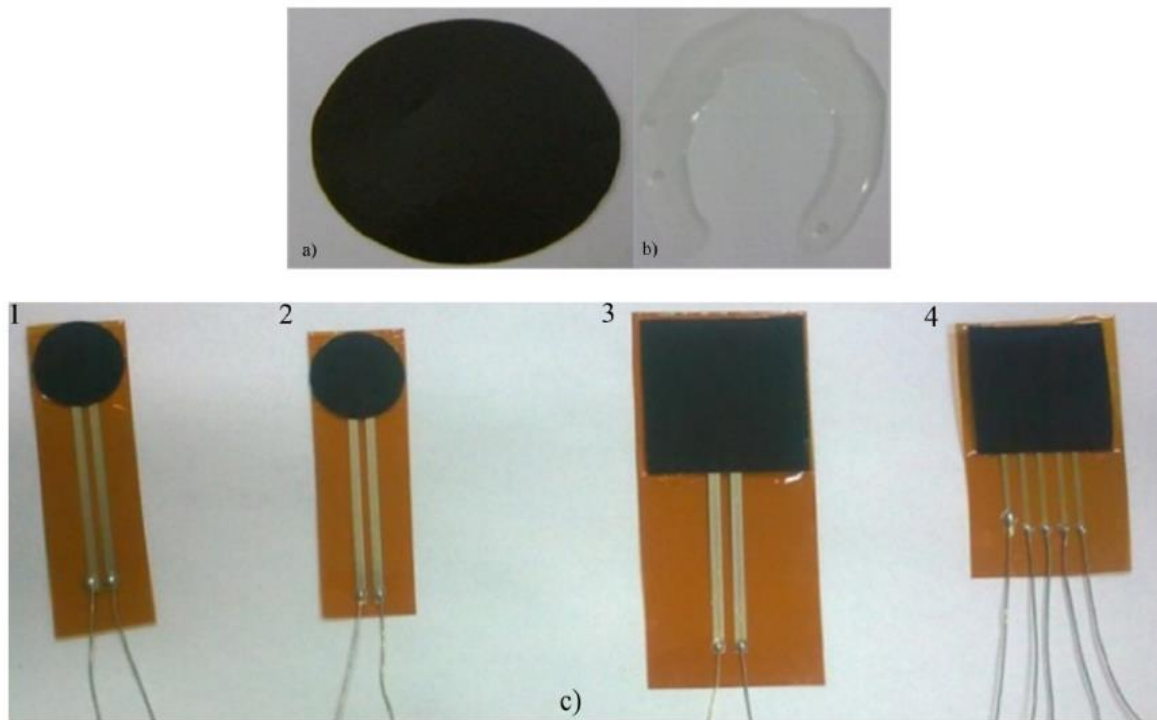
Figure 3.15 - (a) Printed carbon ink, (b) mounted two component epoxy glue and (c) four types of FSR sensors after manufacturing, respectively [115].

4. Testing and characterization of fabricated humidity sensors and force sensing resistors

For both, humidity sensors and force sensing resistors, in house developed measurement setups were used. An electrical, structural and mechanical characterization was done for all fabricated samples.

Structural and morphological characterization of fabricated structures was done by the SEM (Philips XL30 S-FEG and Hitachi TM3030 microscope) and the AFM (Veeco Innova).

4.1. Electrical characterisation of humidity sensors based on graphene oxide

Measurements were done using in-house developed measurement setup, shown in Figure 4.1. It involves a chamber (plastic box) and humidity source (aerosol). The Agilent LCR meter 4284A was used to measure capacitance and resistance at a frequency of 1 kHz.

Figure 4.1 - Schematic of a humidity sensing measurement setup [20].

Commercially available Omega RH USB probe with a temperature sensor was also inserted in the chamber and used as a referent sensor [124]. Sensors were placed inside of plastic box and at the same time connected to LCR meter, as it is shown in Figure 4.2.
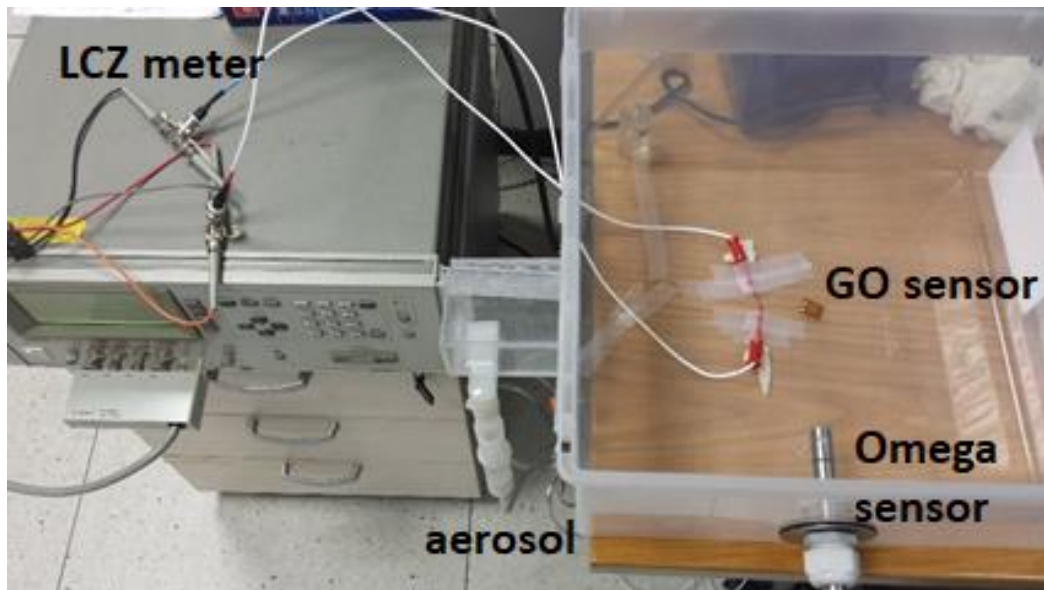
Figure 4.2 - Measurement setup used for the electrical characterisation of GO sensors.

Aerosol, as a humidity source, was also connected to the box and was turning on and off when needed.

The effect of flexibility on sensors' response was also verified. Sensors were bent around cylinder surface (pencil), as it is shown in Figure 4.3, with an angle of 120˚ and exposed under humidity conditions as without bending.

Figure 4.3 - Measurement setup used to test the flexibility influence on sensors' response.

4.2. Electrical characterisation of force sensing resistors

The testing of force sensing resistors was conducted using an in-house developed measurement setup shown in Figure 4.4.
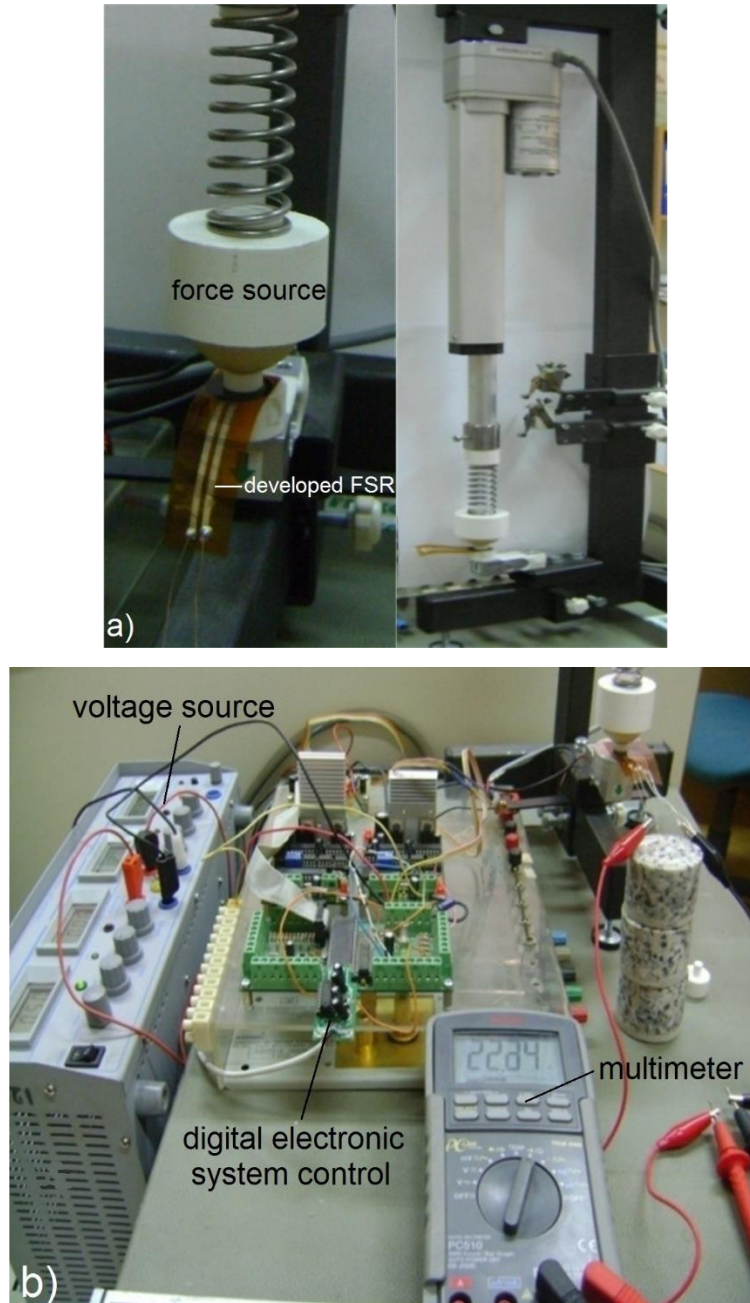
Figure 4.4 - (a) Positioning FSR and (b) complete measurement setup [115].

It involves a firm holder, linear actuators with position feedback, springs, and reference force sensor. At the top of the holder linear electric actuator is attached. At the bottom of linear actuator a rubber ball with 30 mm in diameter is attached. The rubber ball serves as an actuator sensor. On the lower part of the frame the reference force sensor is placed. In addition to these

mechatronic platform a digital electronic control systems together with software (user friendly in-house developed software tool, entitled Forcer), shown in Figure 4.5, is included.
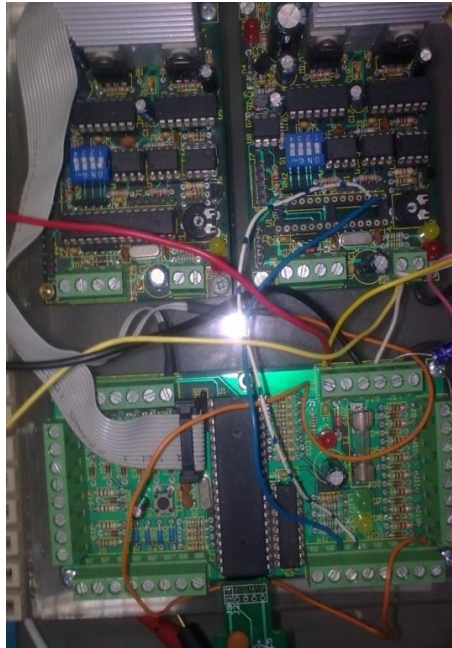
(a)

(b)

Figure 4.5 - (a) Digital electronic control and (b) software window [115].

Digital control system forms two independent closed control loops using position sensor and feedback sensor of the force. The first control loop controls the position, while the second and even more important, loop controls of the force. Force control loop enables to apply measured force and actual position, setting a new reference values for position and force and to set up a parameters of digital controllers embedded in the microcontroller. Resistance and voltage of fabricated sensors were measured using multimeter (shown in Figure 4.4(b)). For the purpose

of measurements a voltage source was used (Figure 4.4(b)). Force used for measurements was applied to the fixed part or all over the active part of sensor.

As addition to the setup, a voltage divider circuit which was connected to FSR, shown in Figure 4.6, was used. The measuring resistor, R_M, is selected to maximize the preferred force sensitivity range, to limit the current and to obtain the voltage on FSR in the range from 0 to 5 V. For resistance as a function of temperature heat source was used to reach the desired temperature and an infrared (IR) camera was used to monitor temperature variations.
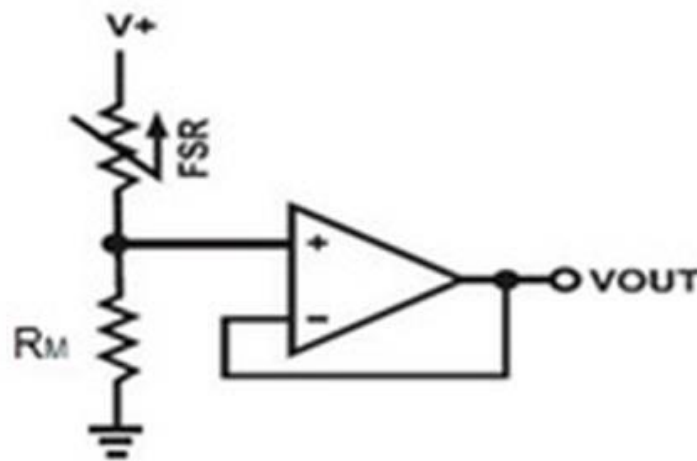
Figure 4.6 - FSR voltage divider circuit [115].

A simple conversion from force for voltage, was conducted by connecting the FSR to R_M in a voltage divider circuit. The output can be calculated from the following equation:

$$V_{out} = \frac{V_+}{\left(1+\frac{R_{FSR}}{R_M}\right)} \tag{4}$$

where V_{out} is output voltage, V_+ bias voltage, R_{FSR} resistance of FSR, and R_M measuring resistor. The current density through the force sensing resistor should not be more than 1 mA/cm^2 of applied force. A common way of using of FSR is to apply the force to the fixed part or the entire active area of the sensor. An elastomer is usually located between the force applied to the sensor and the sensor, in order to prevent the damage of the sensor and to distribute the force on the sensor evenly. The rubber ball elastomers is one of choice and in this setup the rubber ball is located in the described equipment, but beside the ball plastic discs, shown in

Figure 4.7, are used. These discs are used to provide uniform appling of the force on the active surface of the sensor.
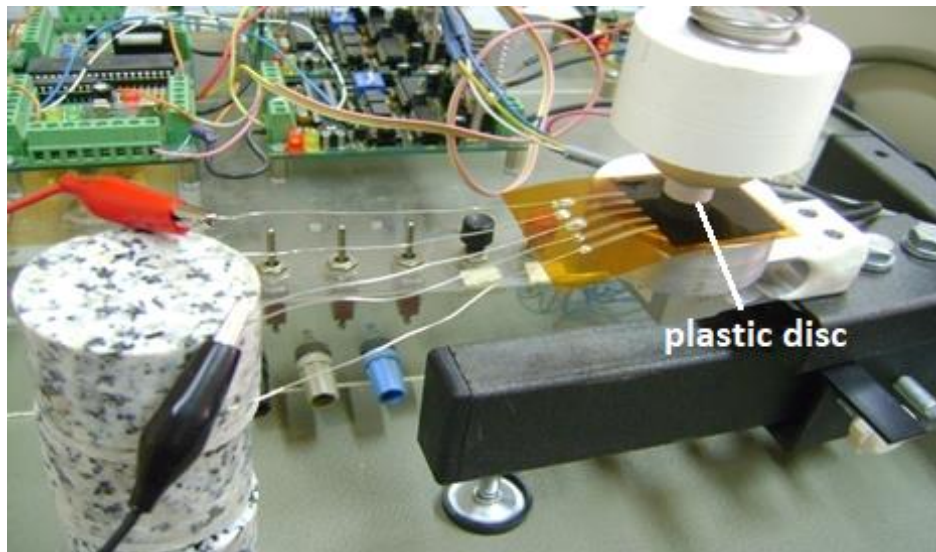
Figure 4.7 - FSR connected to the measurement setup together with plastic disk for even force distribution.

Force sensing resistors were also characterised to the temperature dependency, where a source of hot air with precise digital adjustment of the exact temperature and an IC camera to control the temperature, were used, as shown in Figure 4.8.

Figure 4.8 - Measurement setup for the measurement of sensor's resistance as a function of temperature

4.3. Structural and mechanical characterisation of fabricated sensors

With the aim to determine the exact thickness of silver conductive layer as well as graphene oxide and carbon layer, AFM and SEM were conducted.

The SEM micrographs are presented in Figure 4.9, and it is visible that thickness of FSR silver layer was around 260 nm, Figure 4.9(a), whereas the thickness of carbon layer was around 6 µm, Figure 4.9 (b).

(a)	(b)
(c)	(d)
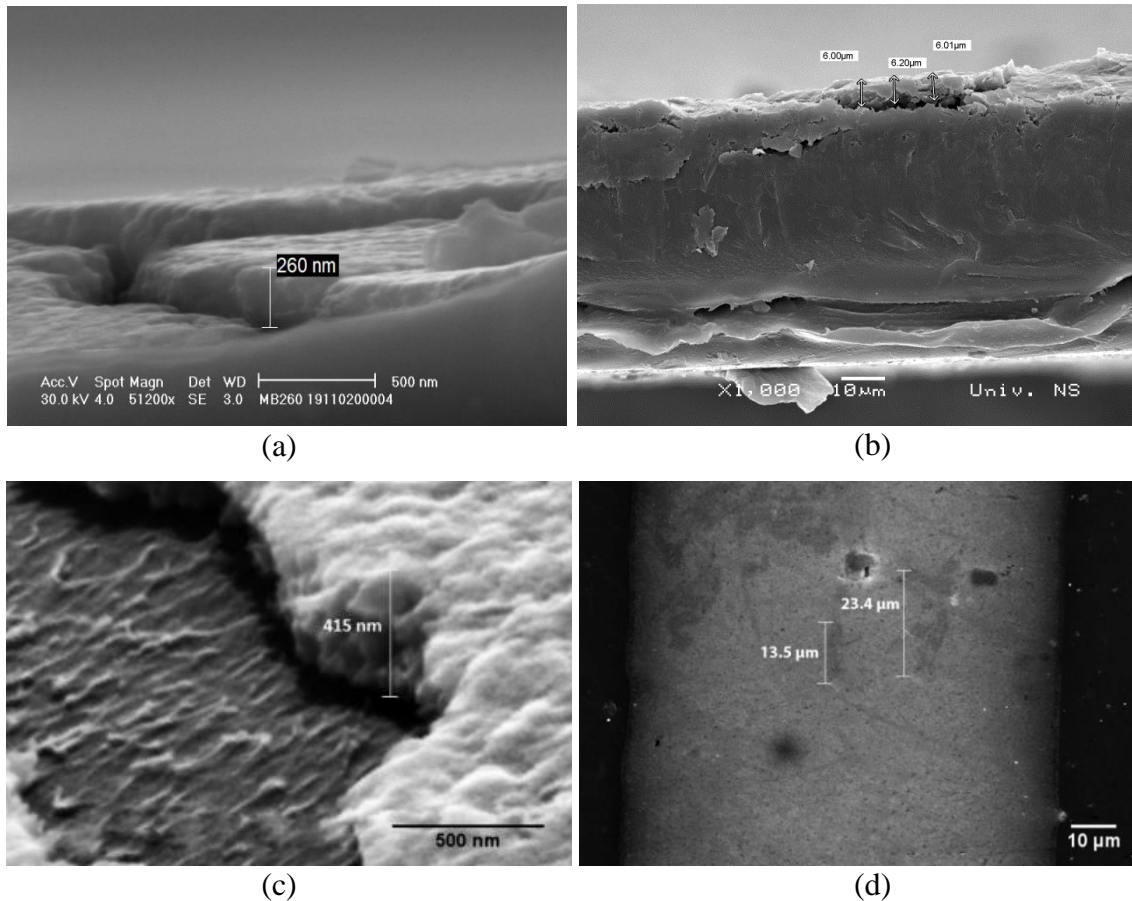
Figure 4.9 - SEM micrographs of (a) A tilted scanning electron microscope (SEM) image of a bare FSR electrode showing a typical thickness of ~ 250 nm of the printed Ag layer, (b) Cross section of carbon layer showing a typical thickness of ~ 6 µm, (c) A tilted SEM image of a bare GO sensor electrode showing a typical thickness of ~ 400 nm of the printed Ag layer, and (d) a top view SEM image of the sensor electrode showing a lateral dimension of deposited GO flakes [20], [115].

The thickness of the silver layer and the lateral dimensions of the flakes were ~ 400 nm and ~ 10 µm, respectively, as displayed in Figure 4.9(c) and Figure 4.9(d).

The presence and thickness of GO flakes were examined by AFM characterization, as it is presented in the same figure. The thickness of the GO flakes was ~ 9 nm which confirmed successful deposition, Figure 4.10(a).

(a)

(b)
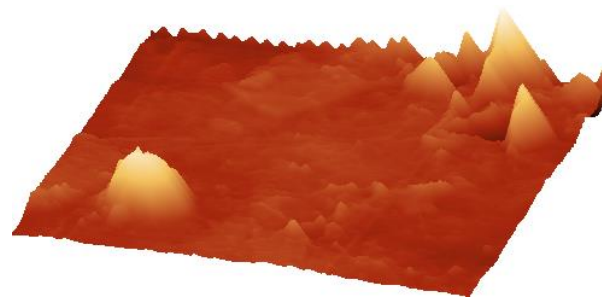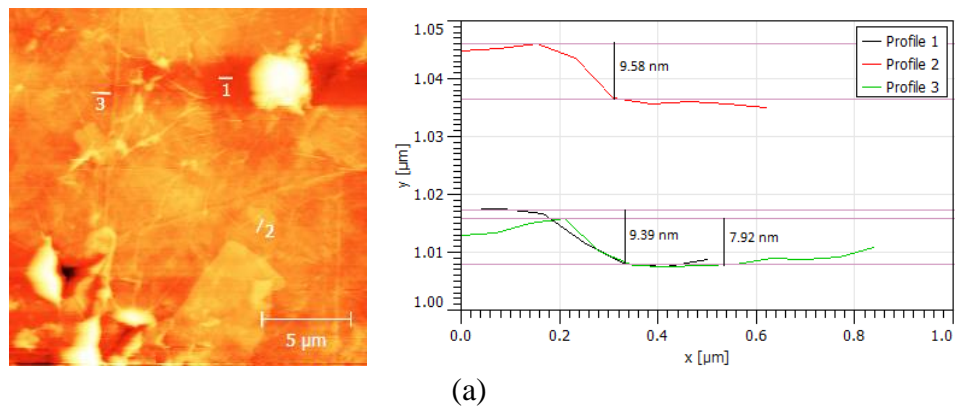
Figure 4.10 - An AFM image of the GO film deposited on the electrodes: (a) a topography analysis along the sections 1, 2 and 3 indicated in the image reveals typical thickness of the GO flakes of ~ 9 nm [20] and (b) 3D profile of graphene oxide layer.

The uniformity of GO layer was not achieved over the whole area due to limitations of spin coating process, which is visible in Figure 4.10(b). These agglomerated flakes were not homogeneously distributed over the sensor's structure, and they are also differences in their deposition in sensors' structures.

In order to investigate mechanical properties of sintered silver layers, as well as carbon layers, an *Agilent* nanoindenter G200 equipped with three sided pyramidal (*Berkovich*) diamond tip was used, shown in Figure 4.11. The reason why graphene oxide was not mechanically tested is the thickness of the GO layer, which is below the resolution of nanoindenter [119].
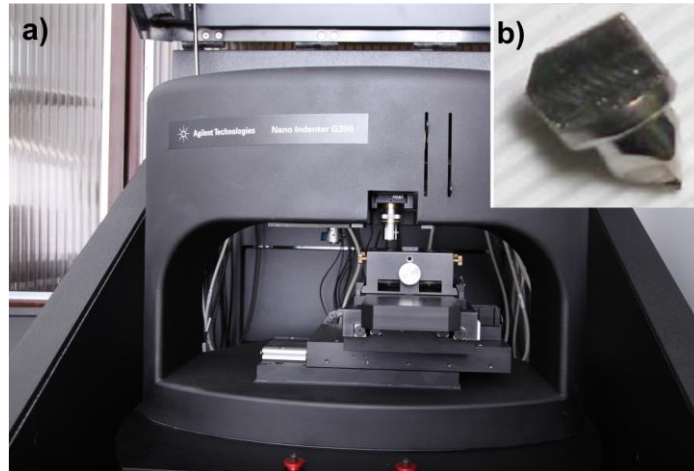
Figure 4.11 - (a) Measurement system - Agilent Nano Indenter G200; (b) Berkovich diamond tip [119].

Before measurements it is very important to prepare the samples by positioning them on a sample holder. For that purpose a double sided scotch tape was used. Prepared samples are presented in Figure 4.12.

Figure 4.12 - Samples mounted on holder and prepared for measurement [119].

Central position in sample holder is for reference material (*Corning 7980*, fused silica [125]). This material was used to indirectly check the instrument accuracy according to the standards. When the substrate with printed Ag layer was placed into the indenter, its height was adjusted to the height of the reference material. All measurements were performed at same depth of indentation, 200 nm to avoid possibility of perforation of printed layer. The Poisson's ratio for Ag was set as 0.37, while Poisson's ratio for carbon ink was set to 0.19. Ten indentations have been performed for each analysed specimen.

5. Results and discussion

In this chapter the main results about humidity sensors based on graphene oxide and force sensing resistors are presented and discussed. The chapter is divided in three sections. In the first section response of GO humidity sensor and an explanation is given, the second section gives the main results obtained by force sensing resistor, while the third section gives the result of mechanical characterisation of material used for the fabrication of all structures.

5.1. Humidity sensor based on graphene oxide

The obtained results can be explained by the equation for the capacitance of the sensing material [126].

$$C = \varepsilon^* C_0 = \left(\varepsilon_r - \frac{i\gamma}{\omega\varepsilon_0} \right) C_0 \tag{5}$$

where ε^* is the complex dielectric constant of the material, C_0 is the capacitance of the vacuum capacitor with the same dimensions as the sensing layer, ε_r is the relative dielectric constant of the material, ε_0 is the vacuum permittivity, γ is the leak conductance, and ω is the angular frequency. This illustrates that the capacitance of the sensing material is directly proportional to γ. With the increase of relative humidity, water molecules are physisorbed through single hydrogen bonding on the hydroxyl groups in GO [10]. When exposed to the external electric field, the water molecules undergo protonation (due to a transfer of oxygen from the large number of oxygen-containing groups in GO, e.g., epoxy groups) and produce a large number of hydronium ions (H_3O^+) which act as charge carriers [10]. As a result, the rise of RH increases γ which leads to an increase of the capacitance. An excellent sensitivity, noticed here at large RH, is due to the physisorbed water layers behaving as liquid which enables hydronium ions to freely move and contribute to the ionic conduction [10]. Large surface area of the GO flakes is also beneficial for increasing the sensitivity of the sensors, which ultimately depends on the film thickness and its uniformity. For instance, it was found that the uniformity of GO film was not achieved over the whole active area, Figure 4.10(c). Agglomerates of the GO flakes were present in many places lead to the better sensitivity. The different humidity response of different sensors can also be attributed to the nonuniformity of the GO film.

The change in resistance was influenced by the adsorption of water molecules on the surface of GO, as well as the absorption of water molecules into the GO thin film. The adsorption of

molecules on the surface leads to the change in resistance, i.e. the resistance decreases due to proton-exchange between graphene oxide and adsorbed water molecules. Absorption of water molecules in GO leads to the increase in resistance due to higher spacing between GO layers [127]. Absorbed water molecules at higher level of RH contribute to increasing ionic conductivity and cause a decrease of the sensor's resistance.

Frequency dependence measurements were performed at frequencies of 1, 10 and 100 kHz, for all three designs of sensors, and it was found that fabricated sensors have the highest sensitivity at 1 kHz, as shown in the Figure 5.1. For that reason all measurements were done at 1 kHz. Testing was also conducted at frequencies below 1 kHz, but resulted curves were not clear due to the presence of noise.
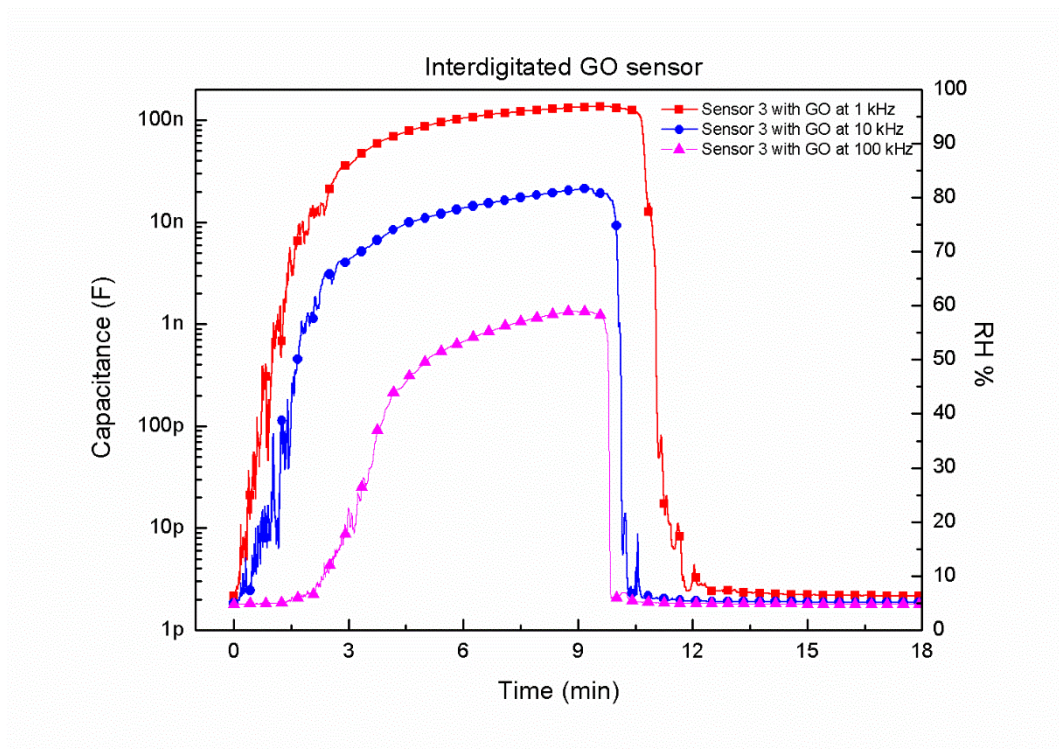
(a)
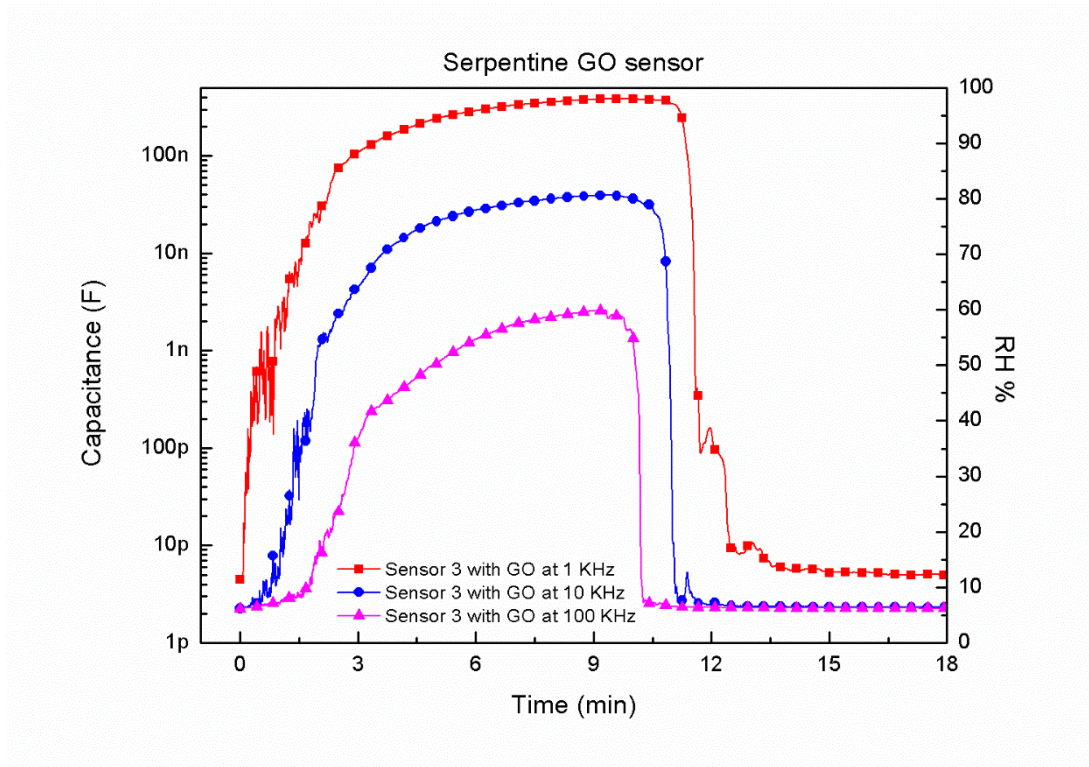
(b)
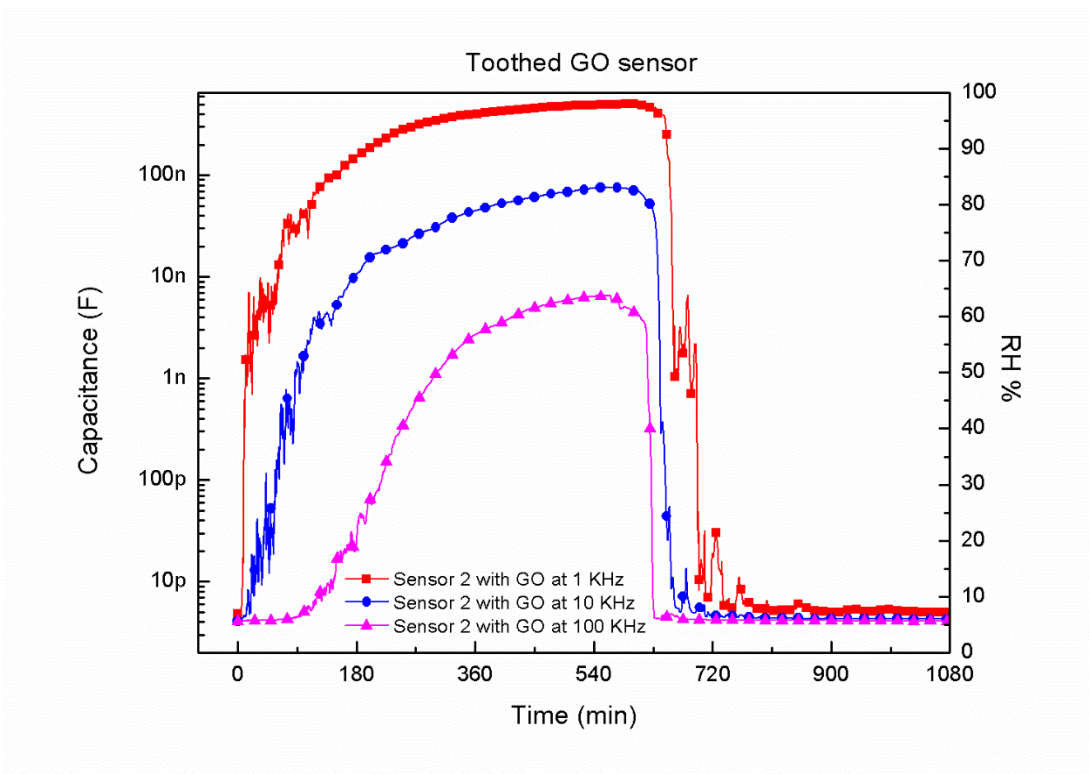
(c)

Figure 5.1 - Frequency dependence measurements for: (a) interdigitated, (b) serpentine and (c) toothed design of sensors. Capacitance as a function of time for different frequencies and humidity percentage is shown.

The C and R of all 3 sensor samples, for three designed patterns, were measured as a function of time while changing the RH as follows. The sensor was set in the chamber with laboratory atmosphere and its stable output was monitored. The humidity source was then turned on and it was kept running for 9 min after which the steady state with 95 %RH was achieved, as determined by the commercial sensor positioned in the same chamber. Finally, the humidity source was turned off and the sensor was exposed to laboratory atmosphere again. Figure 5.2 depicts the results obtained by measuring the capacitance of the sensors with the interdigitated, serpentine and toothed design, without (Figures 5.2(a) - 5.2(c)) and with the GO film (Figures 5.2(d) - 5.2(f)). In the interdigitated sensors without the GO film, the capacitance increased ~ 10 times in the humidity range from 55 %RH to 95 %RH, but it did not exceed 120 pF for interdigitated design. However, in the sensors with the GO film, Figure 5.2(d) - 5.2(f), the capacitance increased by almost 4 orders of magnitude, from 430 pF to 1.6 µF for interdigitated design, in the same humidity range. The other two designs followed the same behaviour.
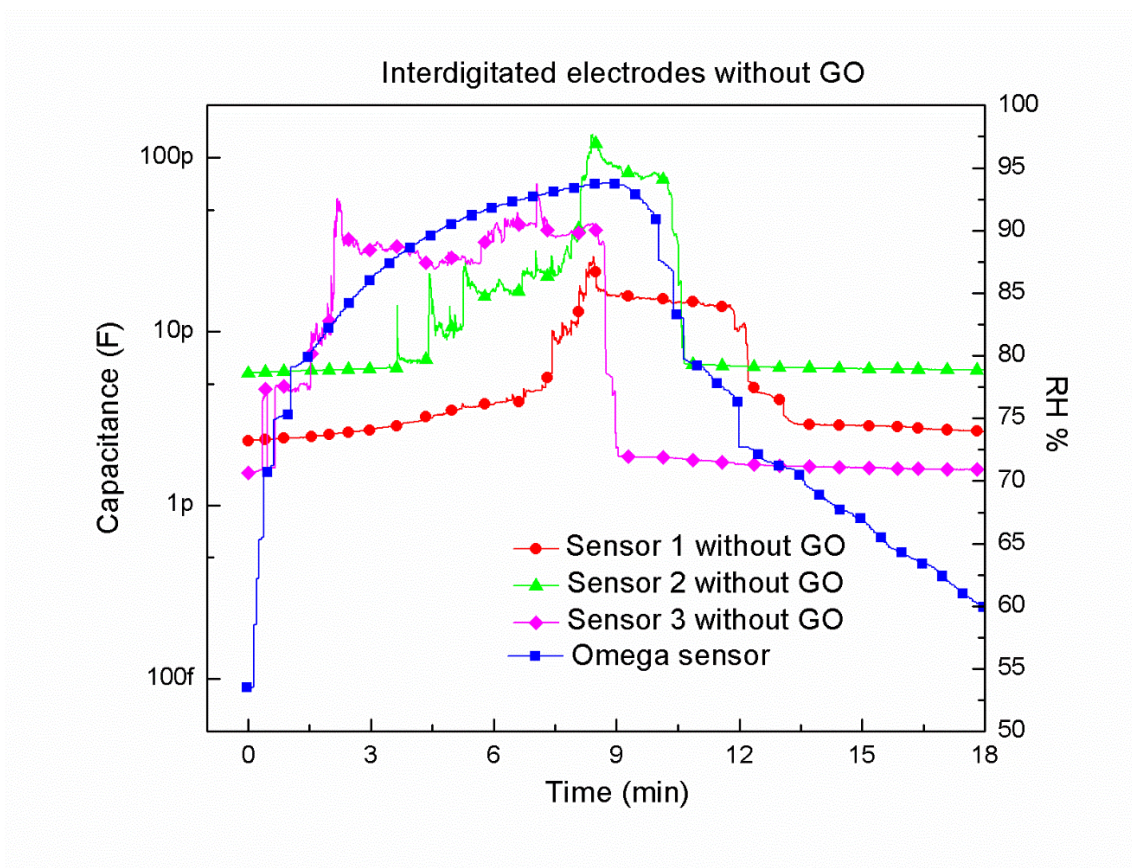
(a)
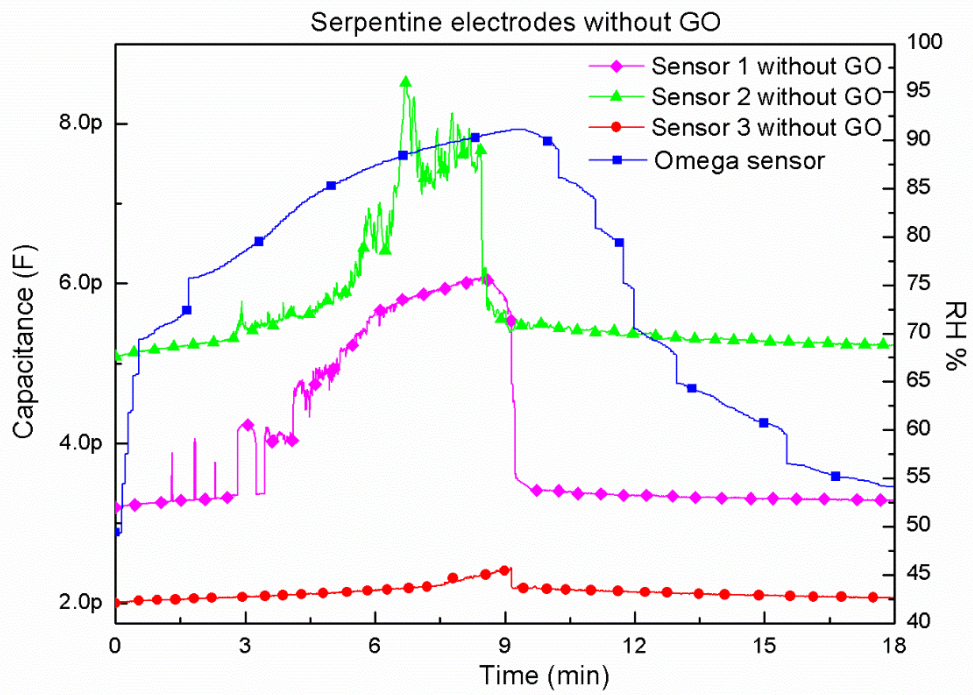
(b)
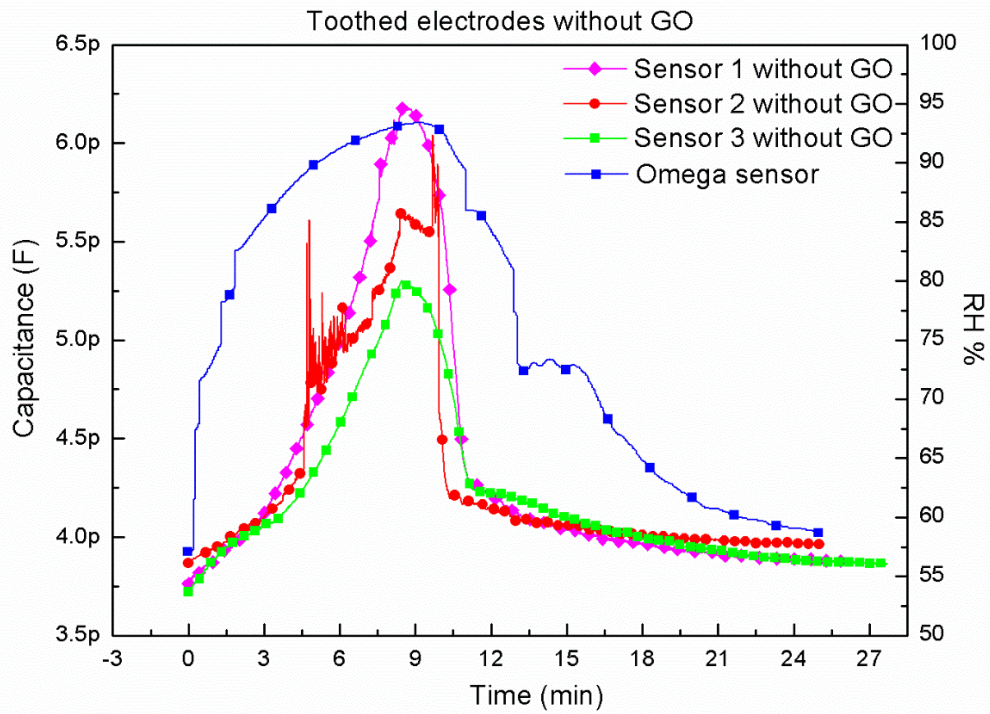
(c)
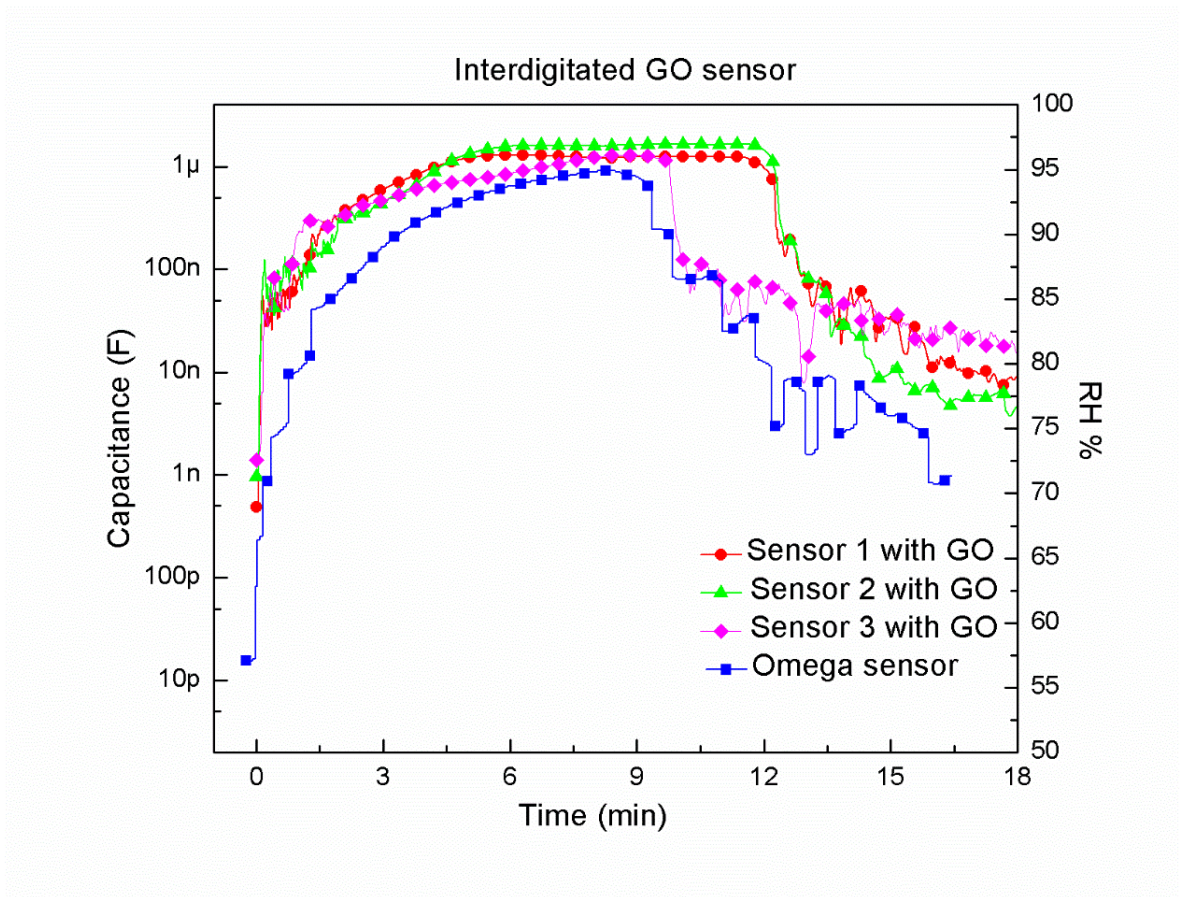
(d)
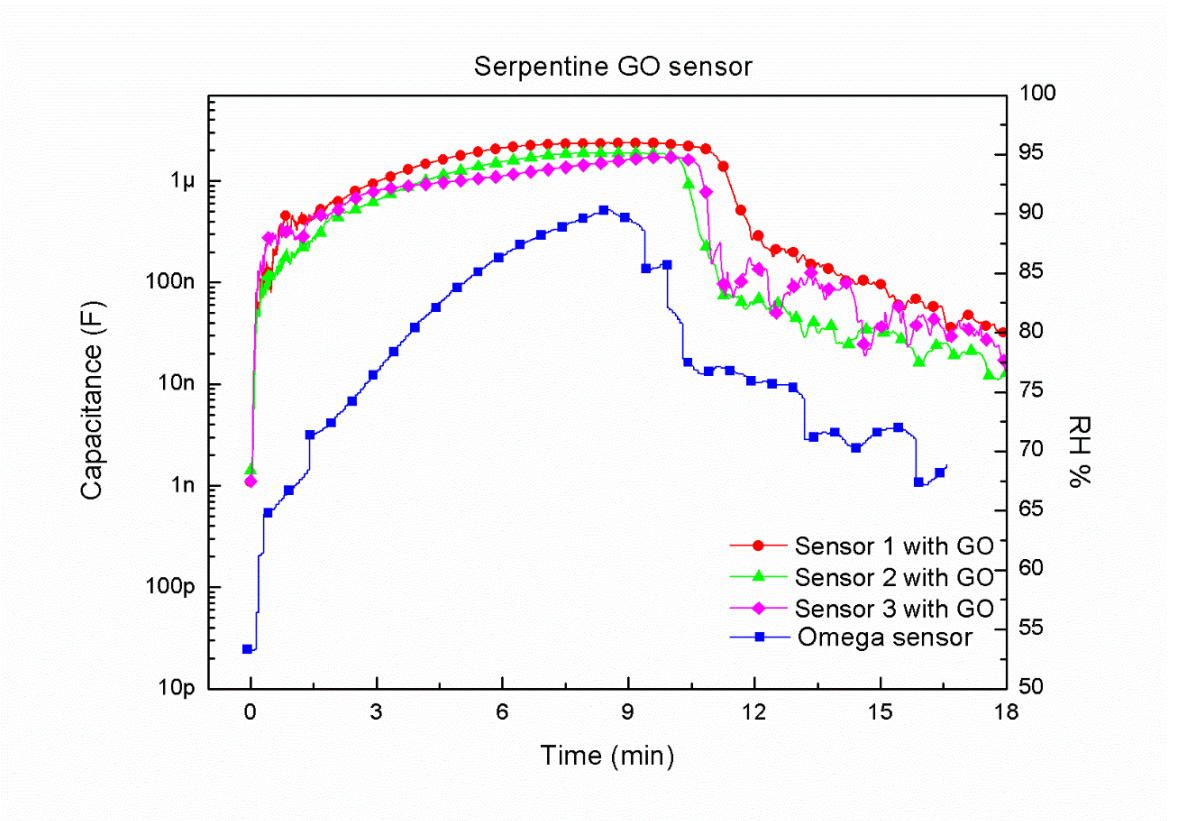
(e)
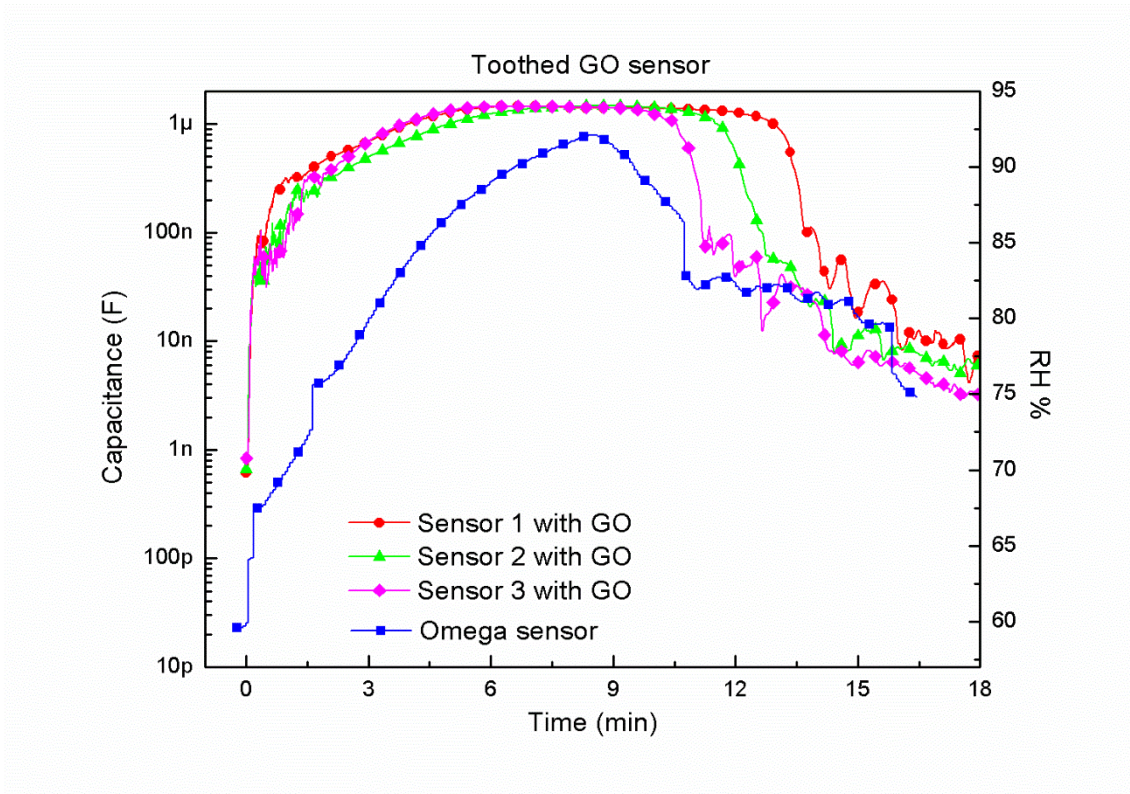
(f)

Figure 5.2 - Capacitance of 3 different geometries of sensors (encoded in different colours) as a function of time. Each geometry was fabricated in 3 samples. (a) interdigitated sensors without the GO film [20]*, (b) serpentine sensors without the GO film, (c) toothed sensors without the GO film, (d) interdigitated sensors with the GO film* [20]*, (e) serpentine sensors with the GO film, and (f) toothed sensors with the GO film. In all cases humidity was changed from 55 %RH to 95 %RH and then back to 55 %RH. The blue curves (with the scale on the right) show the RH measured by the commercial sensor at the same time.*

Figure 5.3 displays the time dependence of the resistance of the fabricated interdigitated GO sensors recorded at the same time as the capacitances, shown in Figure 5.2(d), 5.3(e) and 5.2(f).
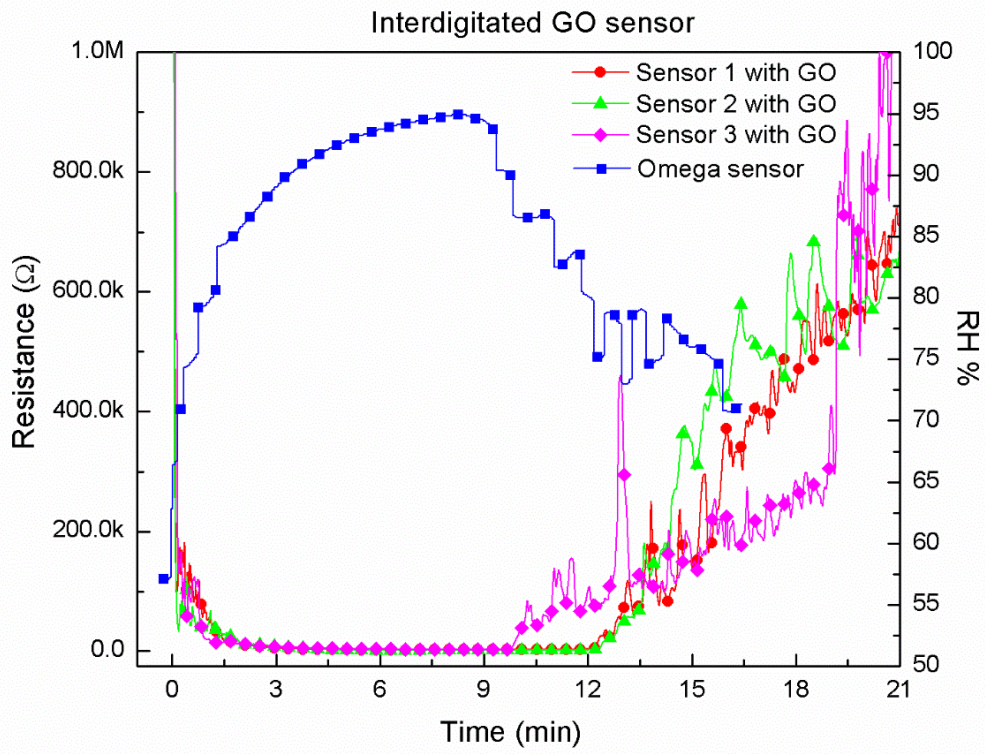
(a)
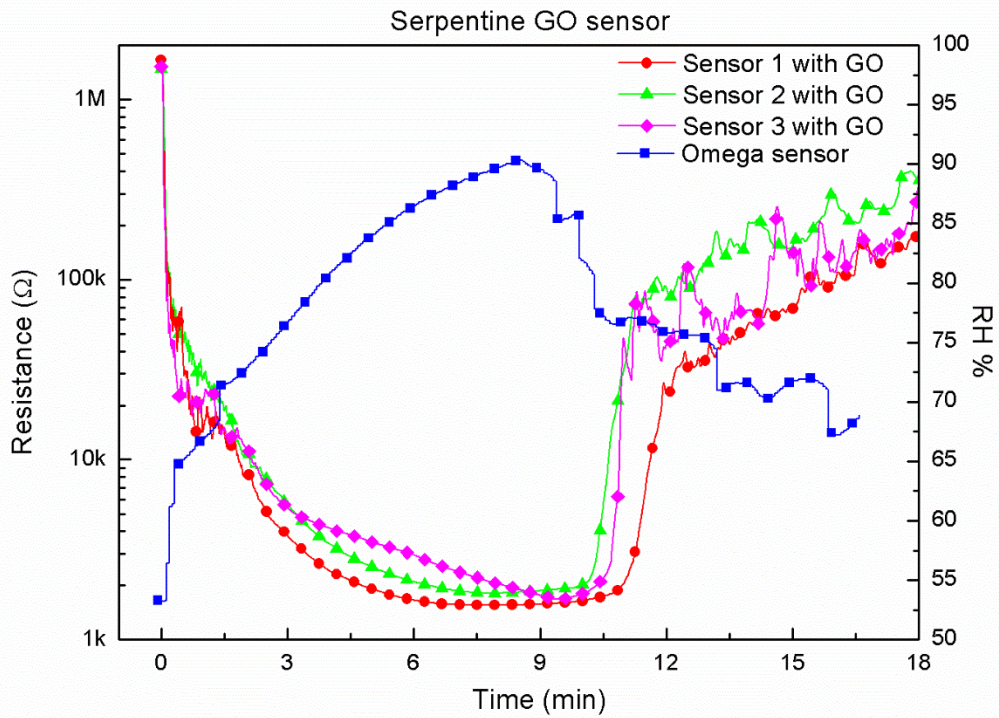
(b)
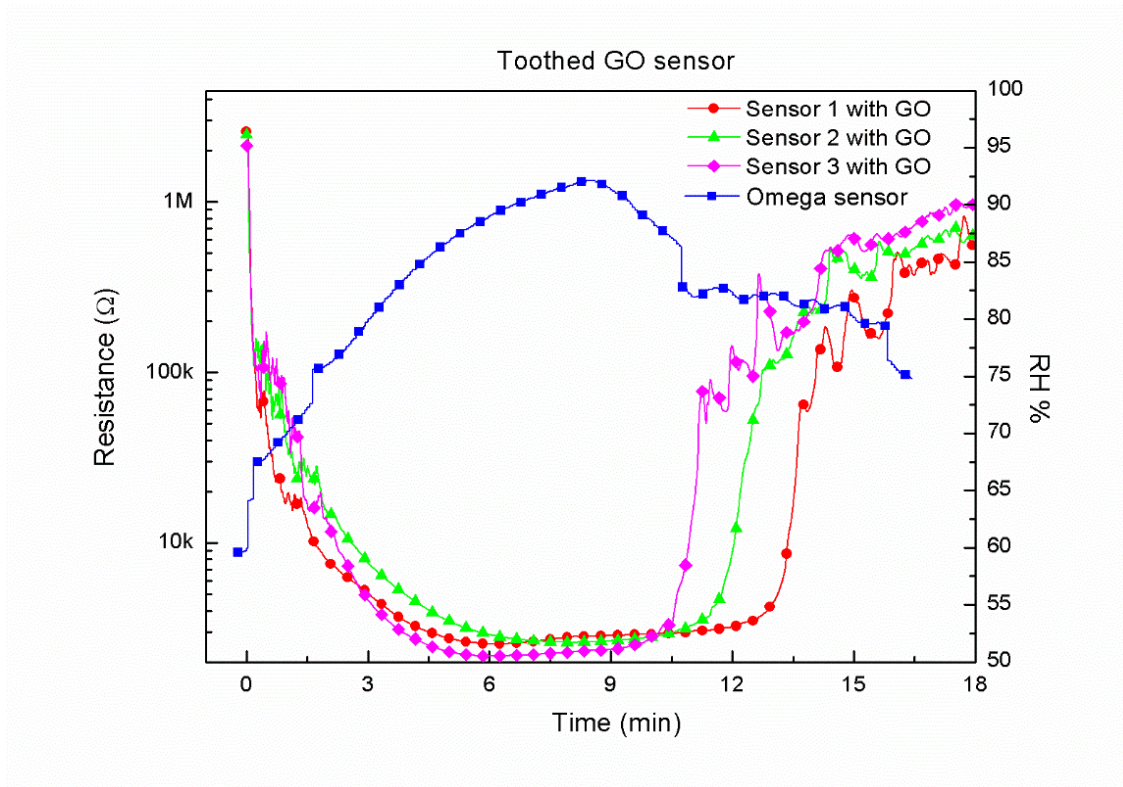
(c)

Figure 5.3 - Resistance of 3 different sensors (encoded in different colours) with GO as sensing material, for: (a) interdigitated [20], (b) serpentine and (c) toothed design of sensors. The resistances were measured at the same time as the capacitance of the sensors shown in Figure 5.2(d), Figure 5.2(e) and Figure 5.2(f), respectively. The blue curve (with the scale on the right) shows RH measured by the commercial sensor at the same time.

As it was previously reported, the change of resistance has been from 300 kΩ to 20 kΩ over the humidity range from 45% to 85% [127]. In this work, the obtained resistance change, for interdigitated design, was in the range from 2.5 MΩ to 5 kΩ under the similar environment. From Figures 5.2(d), 5.2(e) and 5.2(f) it can be noticed that with an increase of active area capacitance also increases, thus serpentine design has the maximum capacitance value of 2.4 µF. The comparison of capacitances for all three designs of GO sensors is shown in Figure 5.4.
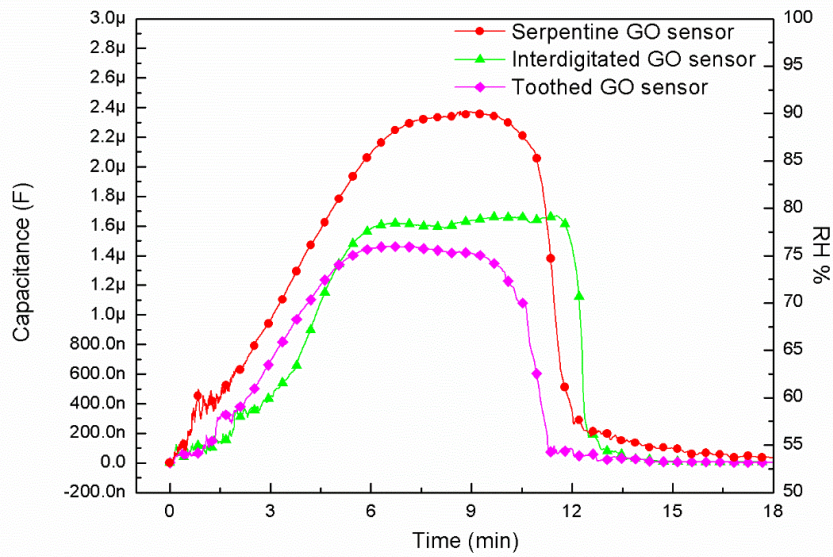
Figure 5.4 - The comparison of capacitances obtained for three different designs of GO sensor

Long term stability measurements were conducted for all 3 sensors, of each design, after 21 months from their manufacturing, Figure 5.5. The measurements demonstrated a decrease of capacitance response by an order of magnitude, for each design, which is not that substantial considering their total response.
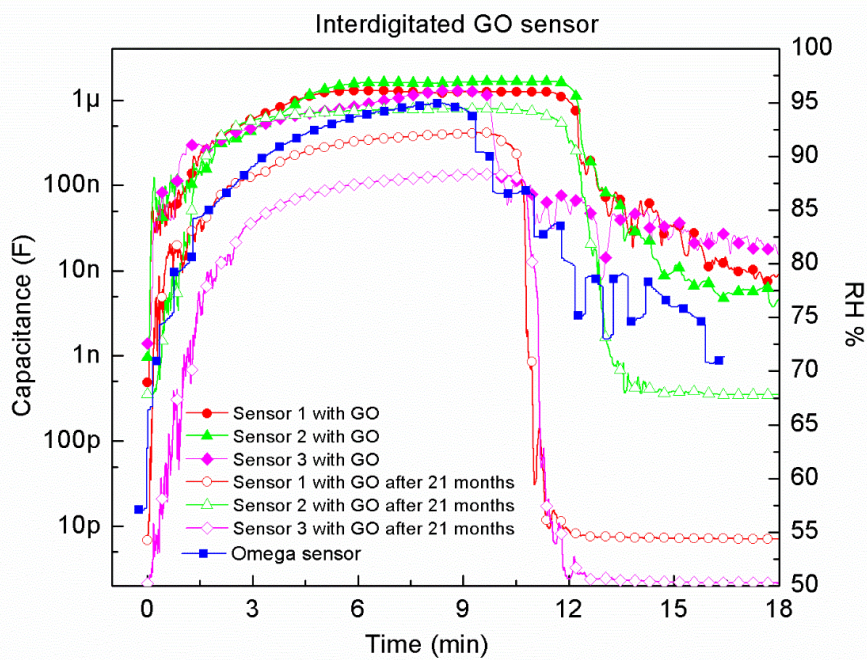
(a)
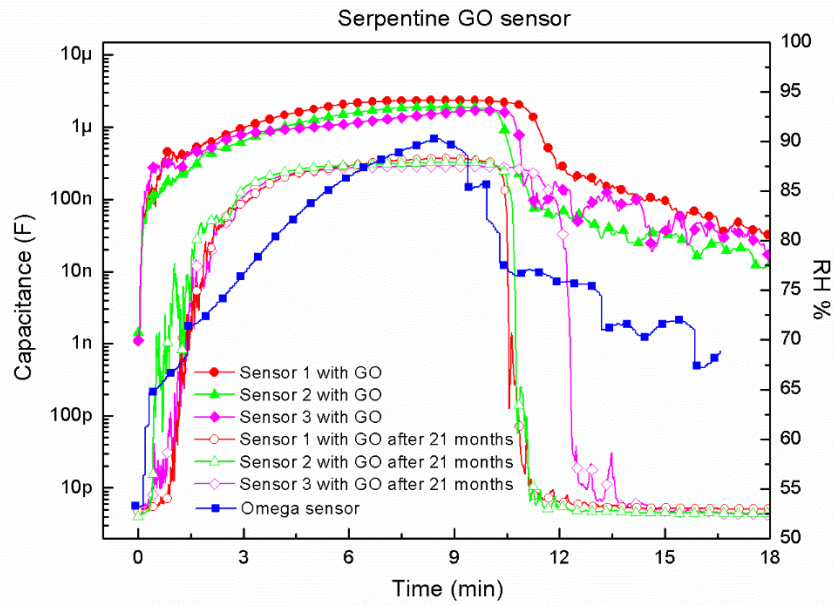
(b)
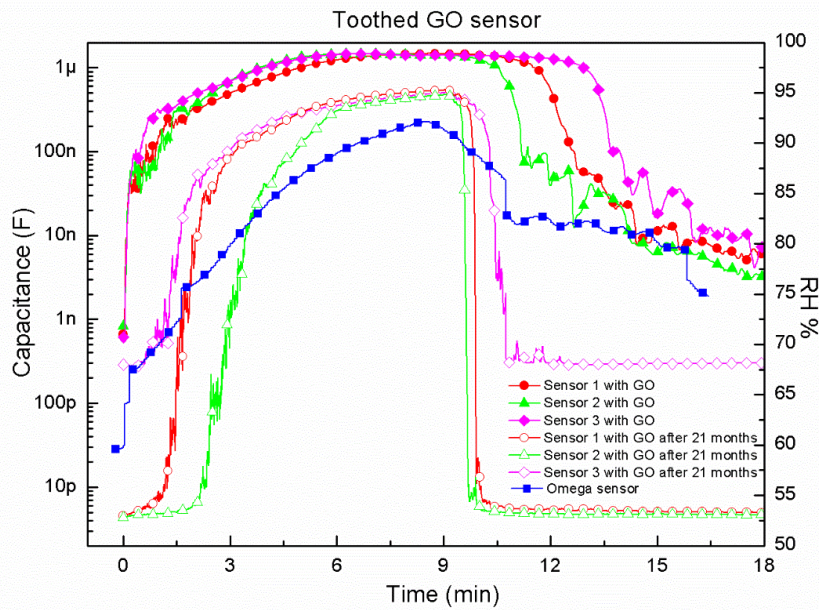
(c)

Figure 5.5 - Long term stability measurements of the sensors 21 months after its fabrication:
(a) interdigitated [20]*, (b) serpentine and (c) toothed design of sensors. Capacitance as a*
function of time is presented.

The difference in the Omega sensor's response, which can be noticed in Figures 5.2, 5.3 and
5.5 is a result of the drying process which was simply done by exposing the sensors to ambient
air. This probably left some residual humidity in the sensing area of the Omega referent sensor.

Response and recovery time were also calculated, from obtained curves, based on the time values at 10 % and at 90% of total change capacitance. Figure 5.2(d) and 5.3 also show the response and recovery characteristics of the GO based humidity sensors. The measured average response and recovery times, for interdigitated design, were 30 s and 150 s, respectively, for all fabricated sensors. This can be explained by different speeds at which the humidity was introduced and removed from the chamber (i.e., the plastic box depicted in Figure 4.1). The humidity was introduced into the chamber by an aerosol device, whereas the humidity exhaustion was performed by self-drying in laboratory atmosphere, similar to previous study [12]. However, the developed sensor had much higher sensitivity. The fast response–recovery behaviour benefited from the porous structure, hydrophilic functional groups, and large inter-layer space of the GO film.

Hysteresis is one of the most important characteristics of humidity sensors. Hysteresis leads to the measurement errors because different capacitances (i.e., RH readouts) could be obtained at the same RH depending on whether RH increases or decreases. Figure 5.6 presents the hysteresis curve in the adsorption and desorption phase for all 3 designs of the fabricated GO sensors. The humidity hysteresis curve of the sensors was measured by increasing the RH from 55% to 95% and then decreasing the RH back to 55 %. RH was measured by the commercial sensor which has a hysteresis width $\Delta RH \sim \pm 1$ %. The maximum hysteresis width of the fabricated sensors was $\Delta RH \sim 10$ % which can be noticed in Figure 5.6. This shows that further improvements would be needed if the high sensitivity of the proposed sensors in order to be used in commercial applications, which will be a part of the future research in this area.

(a)

(b)

(c)
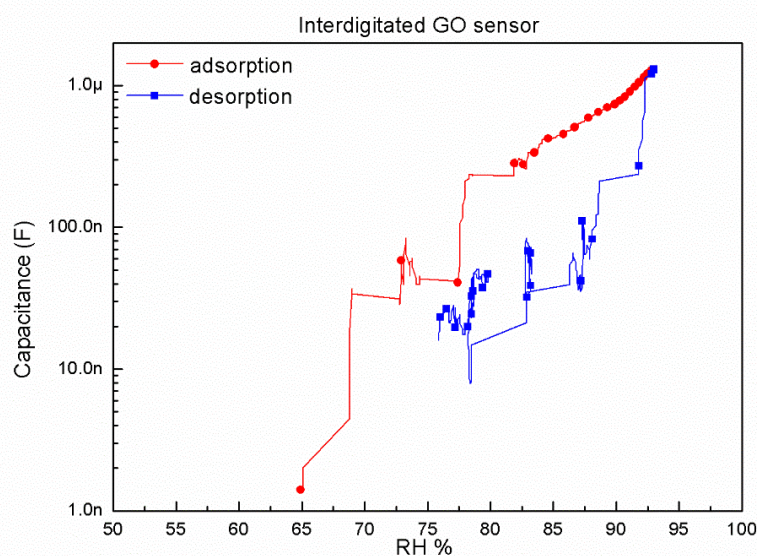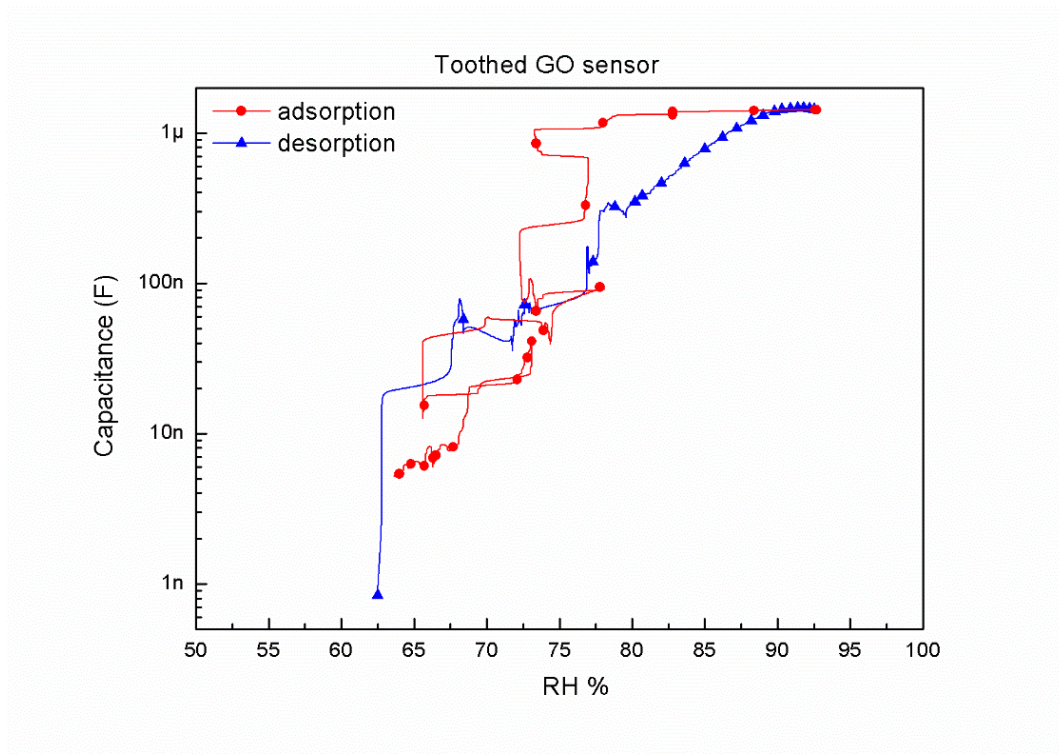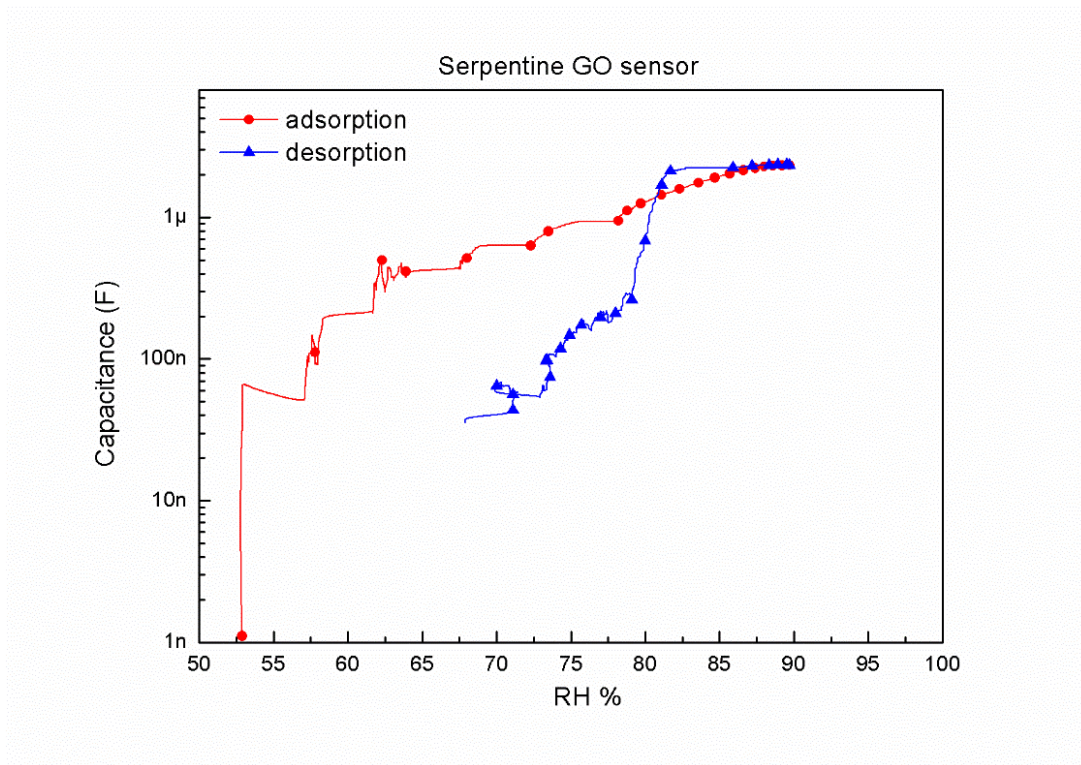
Figure 5.6 - Humidity hysteresis curves of the GO based sensor: (a) interdigitated [20]*, (b) serpentine, and (c) toothed design.*

Figure 5.7 shows the repeatability measurement of one from all three designs of fabricated GO sensors.
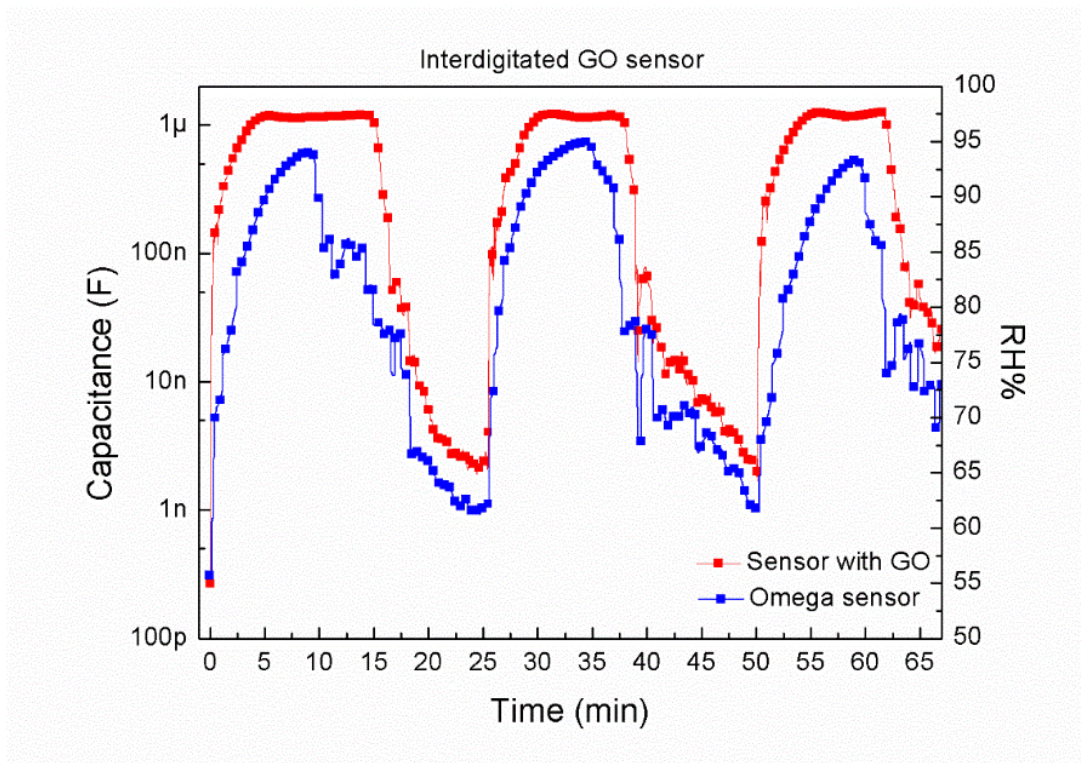
(a)
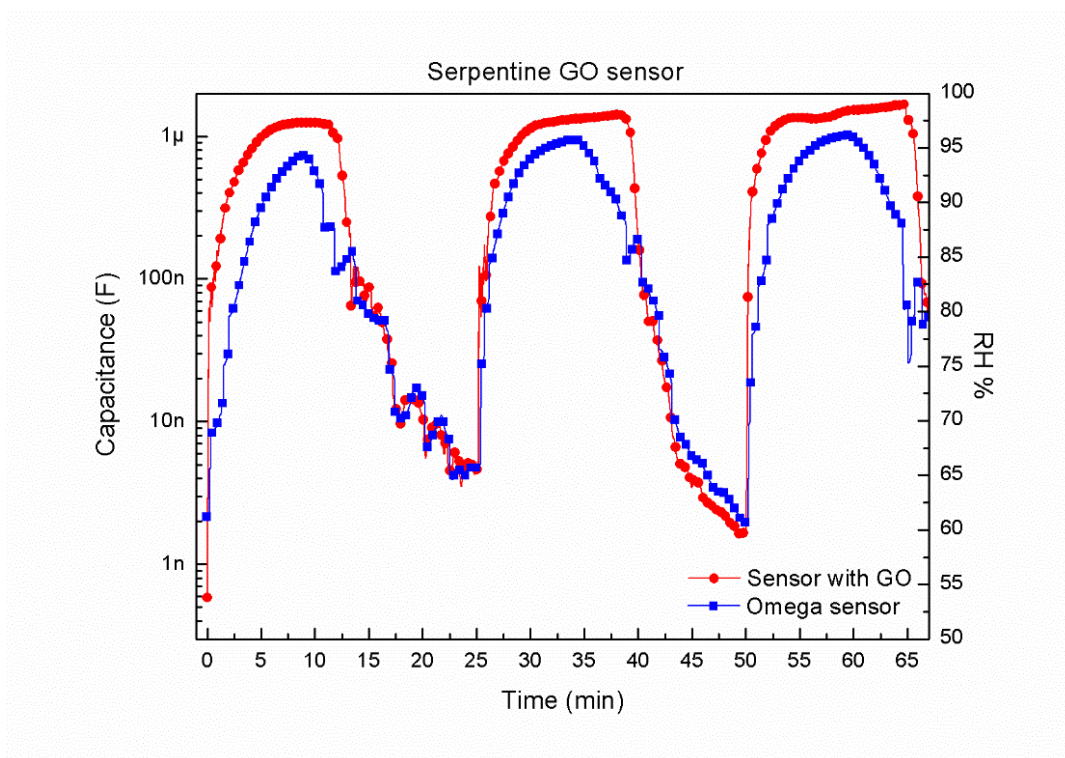
(b)
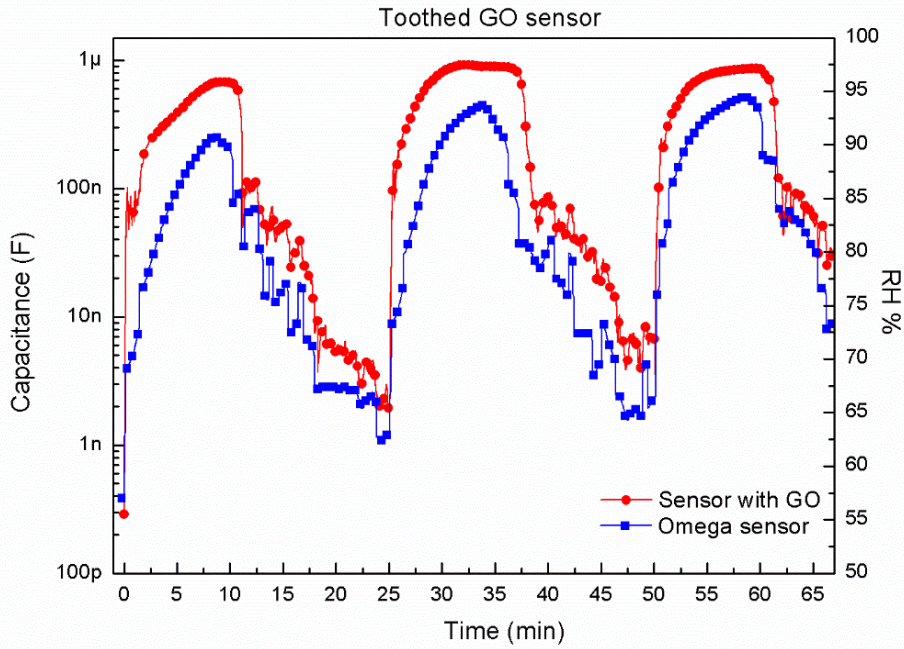
(c)

Figure 5.7 - Repeatability of the GO sensors compared to a commercial sensor (with scale on the right) over three response/recovery cycles: (a) interdigitated [20], (b) serpentine, and (c) toothed design.

The repeatability of the GO sensors was tested by exposing the sensors to 3 alternating RH cycles from 55 %RH to 95 %RH. During the response-recovery cycles, the capacitance response was highly repeatable demonstrating the advantage of the proposed sensors.

Sensitivity (*S*) used to characterize the sensor performance is defined as:

$$S = \frac{\Delta C}{\Delta RH} \tag{6}$$

where ΔC is the sensor's response change of capacitance and ΔRH is the RH change. In the present study, the sensitivity was ~35 nF/%RH, ~40 nF/%RH and ~60 nF/%RH, for toothed, interdigitated and serpentine design, respectively. The sensing characteristics of the presented sensor are comparable to previously demonstrated capacitive humidity GO sensors manufactured in different technologies [6], [10], [16]–[18], [22], [23] or with different sensing materials [5], [128]. The main advantage of the fabricated sensors are their very large change of capacitance with humidity, as presented in Table 5.1. The fabrication process was also found to provide a reproducible sensing which is of the utmost importance in the possible applications of the fabricated sensors.

Table 5.1 - Performance of the sensors presented in this work compared to the state-of-the-art sensors

Sensing material	Fabrication method	Measurement range (%RH)	Sensitivity(pF/%RH)		Reference
GO	Ink-jet printing	55-95	Toothed	~35000	this work
			Interdigitated	~40000	
			Serpentine	~60000	
ZnO	CMOS+ post process	40-90	3.18		[5]
GO	Drop casting	15-95	46.25		[10]
rGO/SnO2	Hydro thermal synthesis	11-97	1604.89		[17]
GO/MWCNT	magnetron sputtering+ drop casting	11-97	7980		[6]
GO/PDDA	LbL self-assembly	11–97	1552.3		[18]
GO	Simulation	0-100	7680		[19]

The influence of bending of sensor's response was also analysed. Fabricated sensors of all three designs were bent around a cylinder with a radius of 3.5 mm encompassing an angle of 120˚ and exposed to the same humidity tests. The obtained results were almost identical compared to that without bending, as shown in Figure 5.8 for interdigitated, serpentine and toothed design, respectively. This is an important advantage of the proposed sensors for simple monitoring of humidity because they can be placed on almost any surface without affecting their response.
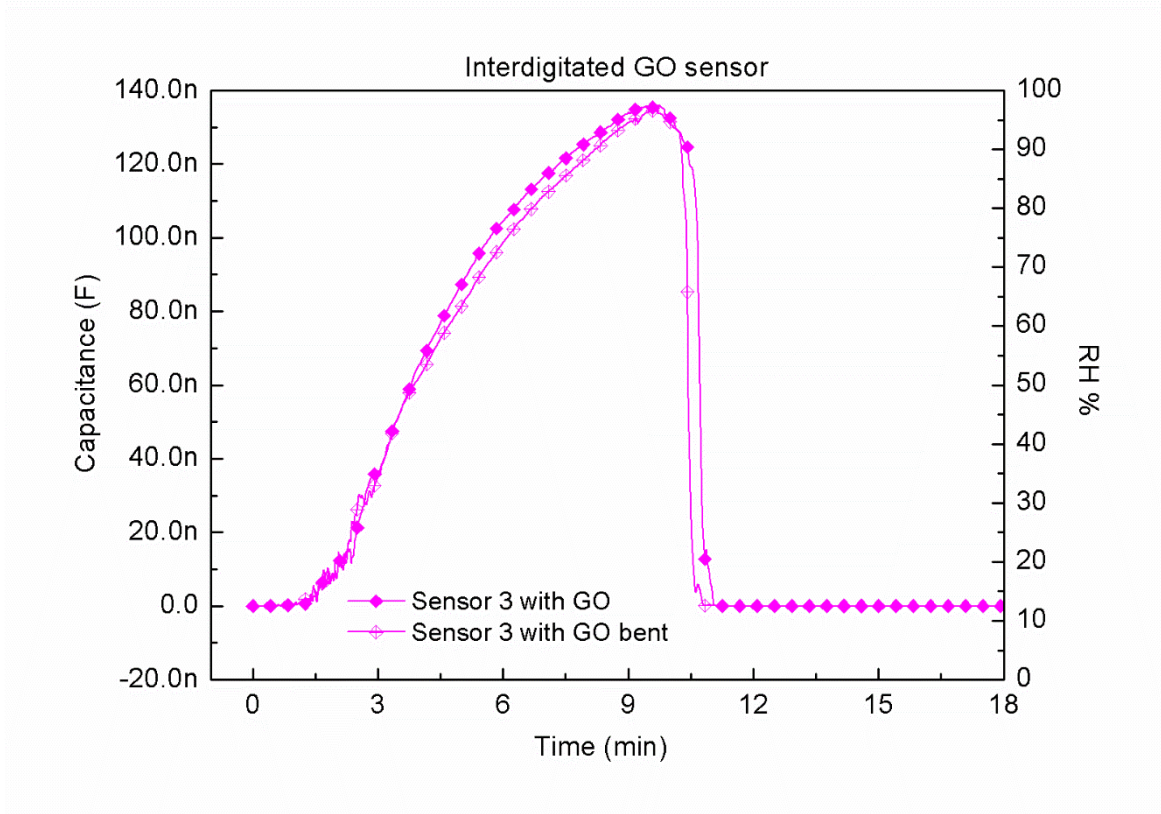
(a)
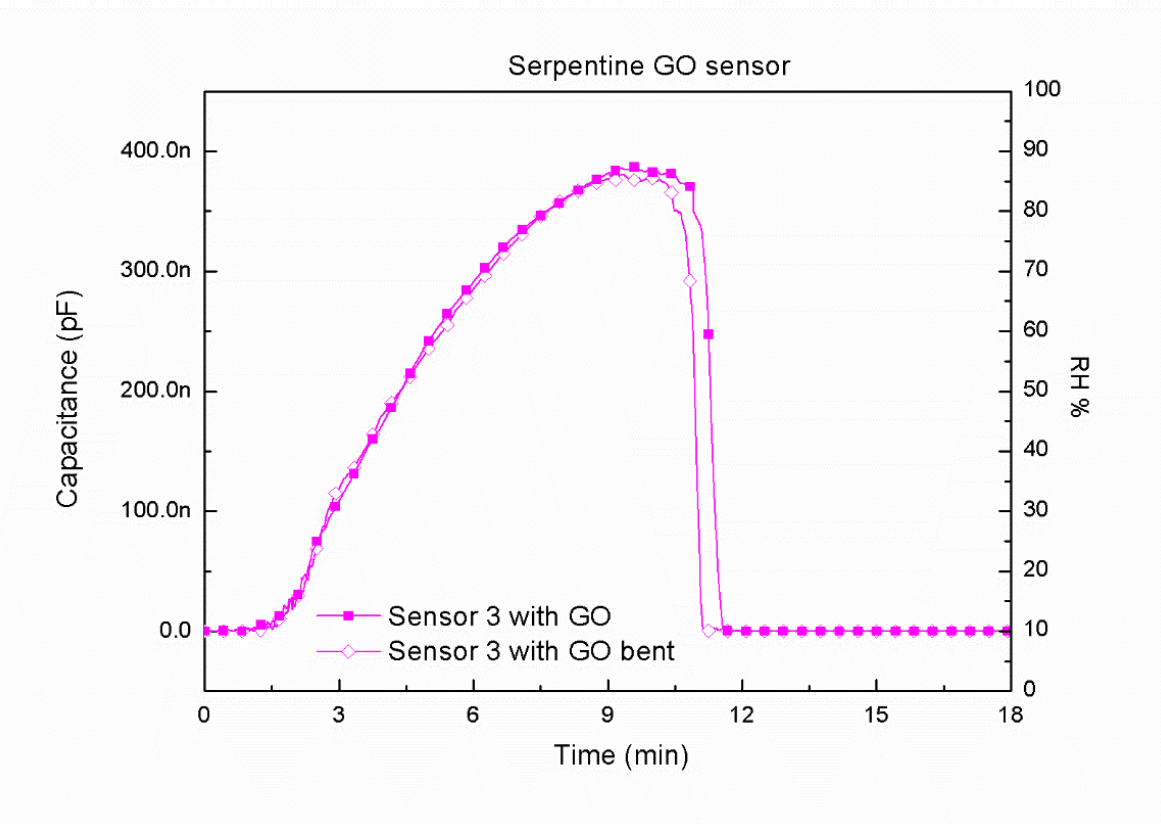
(b)
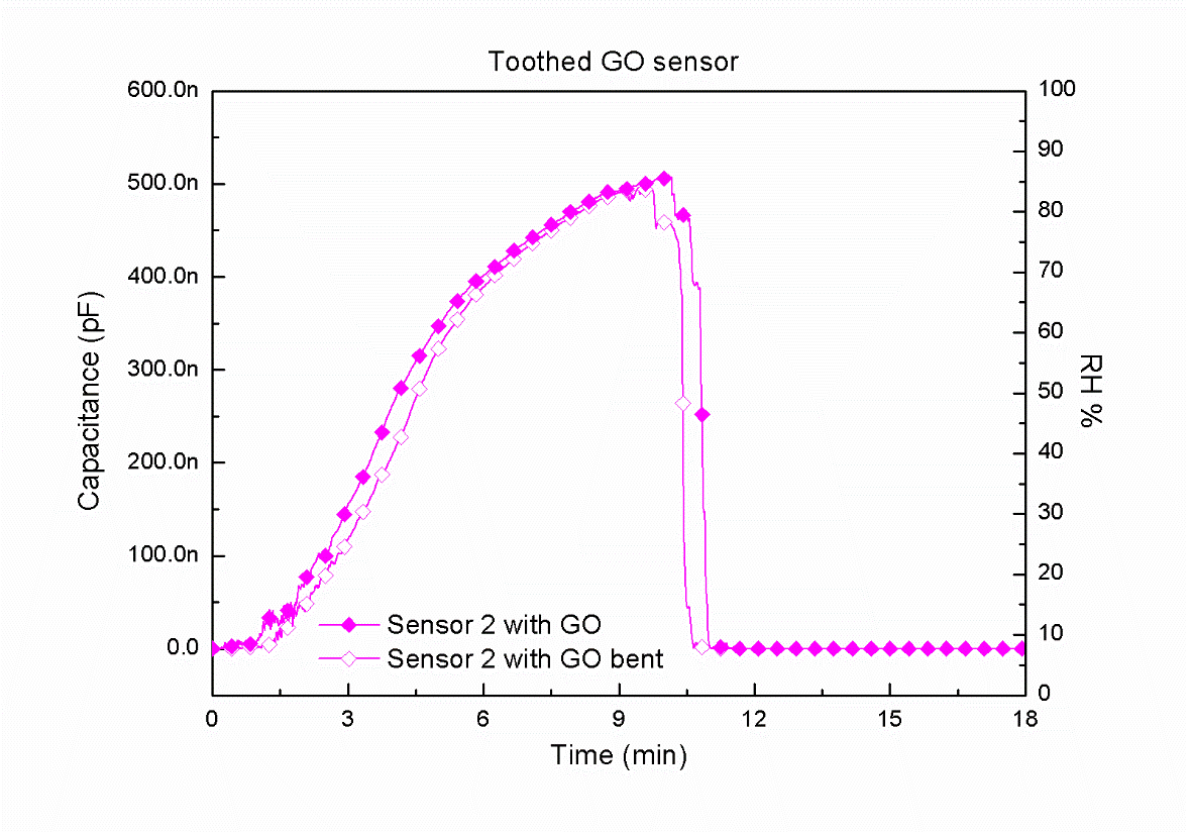
(c)

Figure 5.8 - The humidity measurements performed on one of the each design of sensors: (a) interdigitated [20]*, (b) serpentine and (c) toothed, without (solid symbols) and with bending (empty symbols).*

5.1. Force sensing resistors

The obtained results are directly connected with sensor's structure. When the force is applied to surface of sensor the FSR carbon ink acts as a short between the conductive traces from the contact area. This leads to a resistance that is dependent on the applied force. When the two layers are connected together, the microscopic protrusions on the FSR ink surface shorten across the interdigital fingers of the facing surface. At low forces, only the tallest protrusions make contact, while at higher forces, here are more and more contact points between the two substrates. As a consequence, the resistance between the electro conductive lines is inversely proportional to the applied force. A typical FSR's characteristic represents dependence of resistance vs. force, thus we analysed firstly this behaviour of the proposed sensors. The resistance as a function of force characteristic for four types of FSRs, at room temperature, is depicted in Figure 5.9.
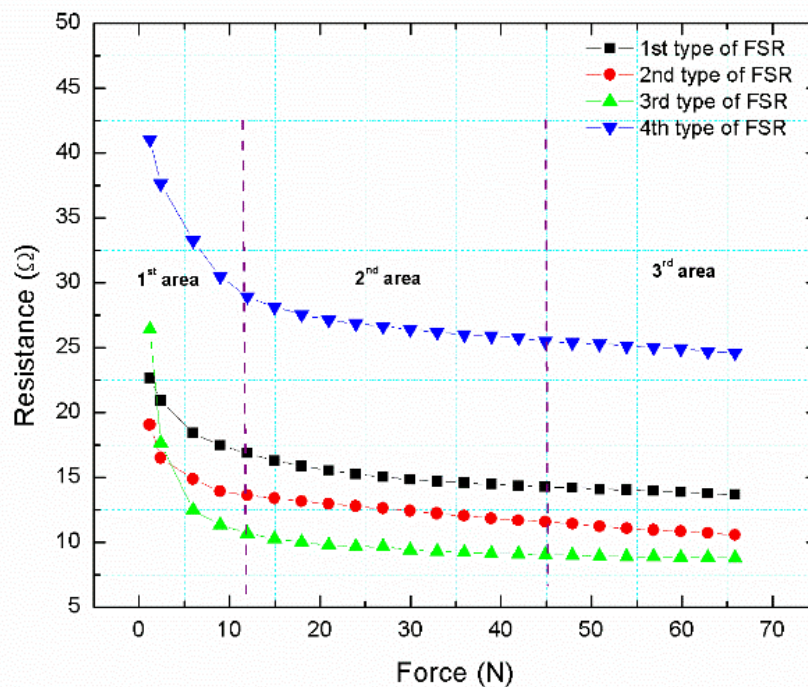
Figure 5.9 - Resistance as a function of force for four types of FSRs [115].

Three areas of different sensors' behaviour can be distinguished. The leftmost area is the area in which the resistance is high and the sensitivity is also very high [129]. This area has nonlinear characteristics at the beginning of the area characterized by a breaking force that introduces the

sensor in the high sensitivity area. The component abruptly switches into the second – the regular area, which is usually used for sensing. In this area the conductance fairly linearly depends on the applied force (force difference). Finally, when excessive force is applied, the component goes into saturation. The switch to the saturation is not abrupt, but rather gradual [130]. Figure 5.9 shows that resistance of sensor decreases with an increase in force, and it can be observed for all types of analysed FSRs.

The force range was from 1.19 N to 65.7 N and the same range was used for all four types of FSRs. This force was implemented on FSRs by means of in-house developed system, presented in Figure 4.4. In Figure 5.9 is visible that the third type of FSR, which has the largest active area, has lowest resistance, 8.81 Ω when applying maximal force, while the fourth type of FSR, with smallest analysed active area, has resistance of 24.81 Ω when applying the same force. For practical application point of view and connecting with electronic circuits, it is important to have voltage-force characteristics. FSRs are usually implemented into voltage divider circuits to achieve simple resistance-to-voltage conversion, as already shown in Figure 4.6. Voltage change due to change in force for several values of R_M resistor (depicted in Figure 4.6) is presented in Figure 5.10 and 5.11. Moreover, Figure 5.12 depicts voltage as a function of applied force for proposed types of FSRs, for constant values of R_M equal to 18 Ω. The linear regime of FSRs was present for the forces up to 18 N.
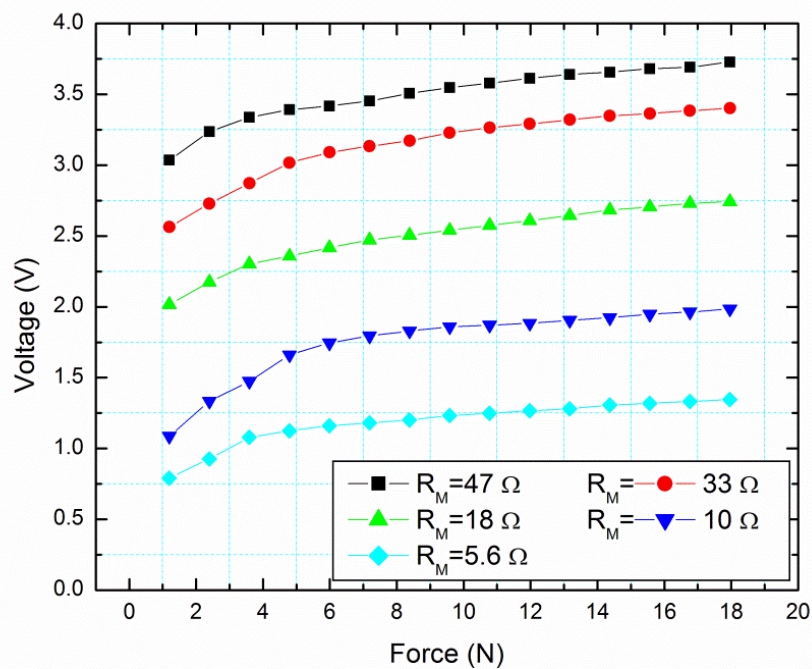
(a)
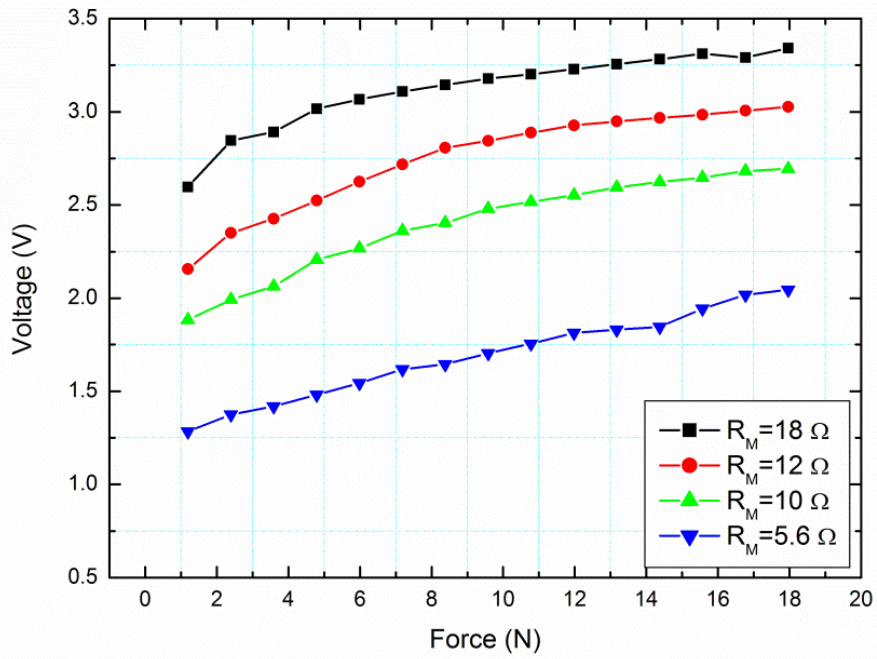
(b)

Figure 5.10 - Voltage as a function of force characteristics for: (a) 1st type of FSR, (b) 2nd type of FSR [115].
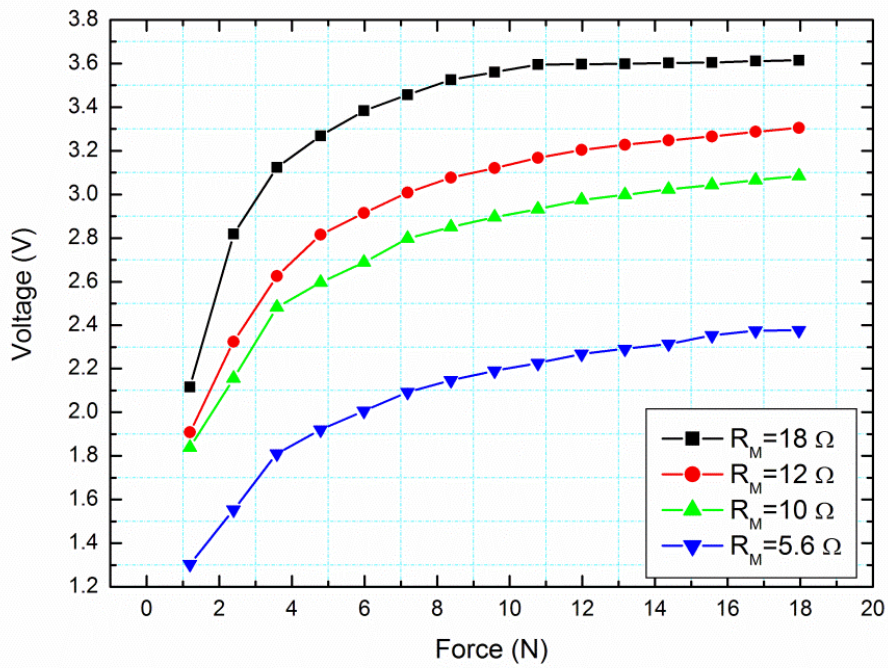
(a)
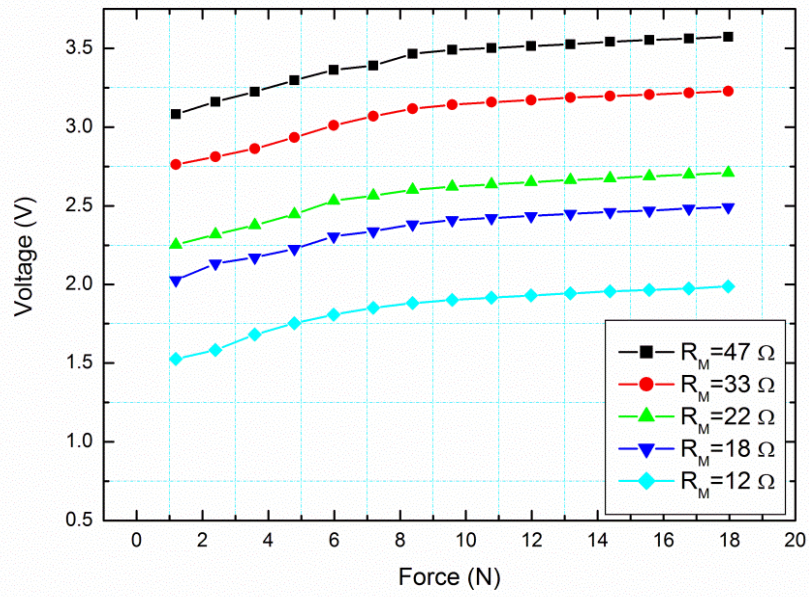
(b)

Figure 5.11 - Voltage as a function of force characteristics for: (a) 3rd type of FSR, (b) 4th type of FSR [115].
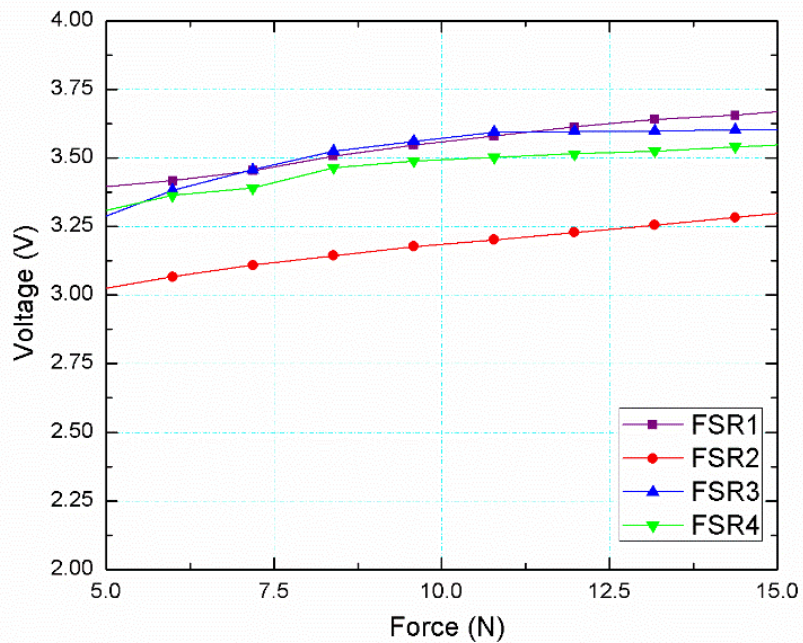
Figure 5.12- Voltage as a function of force for four types of FSRs and for R_M = 18 Ω in linear sensors' regime [115].

The resistance of FSR decreases with increasing force. Therefore, the voltage increases with the increase of applied force, which can be seen using voltage divider equation (4). Applying that in (4), V_{out} increases with R_{FSR} decrease, which can be seen in Figures 5.10 - 5.12. This is valid for all four types of the proposed sensors. From Figure 5.12, it can be seen that voltage range is from 2 V to 3.75 V, which is very appropriate range for further connection to read-out electronics or displays. Using (4) it can be also calculated which value of R_{FSR} will be obtained for already measured voltage shown in Figures 5.10 and 5.11. This will confirm validity of resistance values shown in Figure 5.9. R_{FSR} can be calculated from the following equation:

$$R_{FSR} = R_M \left(\frac{V_+}{V_{out}} \right) - R_M \tag{7}$$

where $V_+ = 5$ V.

In Figure 5.11 can be seen that applied force was from 1.19 N to 17.96 N, since at larger forces changes in voltage are negligible due to small change of R_{FSR}. Figure 5.11 shows that the output of the sensor was changing linearly with the force applied. The 2nd type of FSR demonstrated the best linearity, in a wide range of applied forces, due to effectively increased length of electrodes in interdigitated structure. This FSR has our novel design and cannot be found commercially.

FSRs may also find their application in systems with higher temperature than room temperature. Because of that, we analysed the behaviour of the proposed FSRs at elevated temperature. Figure 5.13 shows that resistance of FSRs increase with an increase in temperature. Temperature was changed in the range from 30 ˚C to 90 ˚C, while applied force was constant with value of around 12 N (which belongs to a linear range). This increase of resistance can be explained using following equation for $R(T)$ at room temperature [131]:

$$R(T) = R(T_0)(1 + \alpha_0 \Delta T) \tag{8}$$

where α_0 is temperature coefficient, $R(T_0)$ is resistance at room temperature, and $\Delta T = T - T_0$ is difference between actual and room temperature. As α_0 for silver is 0.0061 ˚C^{-1} and for carbon -0.0005 ˚C^{-1}, using (8) it can be seen that with an increase in temperature, value of $R(T)$ also increases. Therefore, this increase in resistance can be observed for all four types of FSRs (Figure 5.13). It can be seen that the smallest variation of resistance with changing temperature demonstrated the first and second types of FSRs which have the lower total active area, comparing with the third and the fourth design of proposed FSRs.
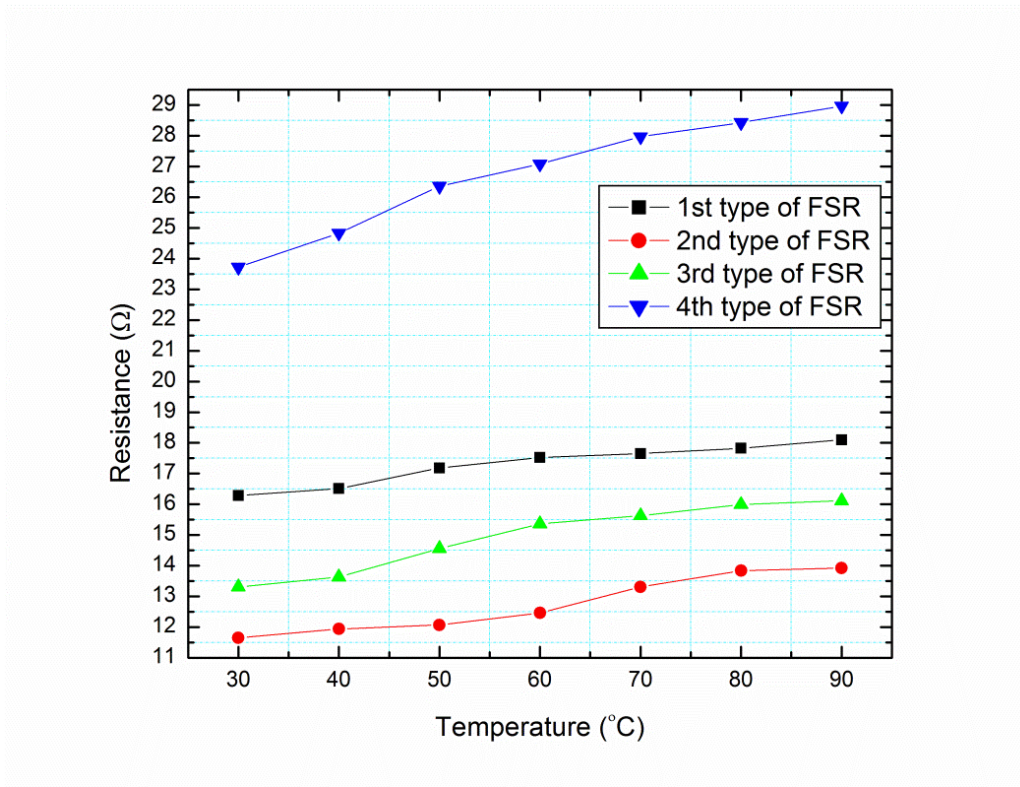
Figure 5.13- Voltage as a function of force for four types of FSRs and for $R_M = 18\,\Omega$ [115].

In addition to this, α_0 for all four fabricated FSRs has been calculated and results are presented in Table 5.2.

Table 5.2 – Temperature coefficient α_0 for characterized FSRs

	$\alpha_0(C^{-1})$
1st type of FSR	0.0019
2nd type of FRS	0.0032
3rd type of FSR	0.0035
4th type of FSR	0.0037

Our results revealed that presented cost-effective FSRs are reliable and have a good sensing property for measuring force. The proper design of FSRs, which this paper has proposed (even unconventionally), is very important when dealing with different shape of objects, in order to be able to detect adequately applied force [115].

5.2. Mechanical characterisation of used material for the fabrication of structures

Bearing in mind that humidity sensors and FSRs will be exposed to harsh environment and different mechanical stress during the practical application, their mechanical characterization was performed by means of nanoindentation. Multiple indentation (at least 10 indentations were made) tests provide measurement repeatability for the mechanical properties of analysed samples/layers. Nanoindentation tests were conducted with a *Berkovich* diamond indenter, which provide a precise control over the indentation process. Figure 5.14(a) shows load-displacement curves measured on the silver layer, whereas Figure 5.14(b) presents load-displacement curves measured on the carbon layer.
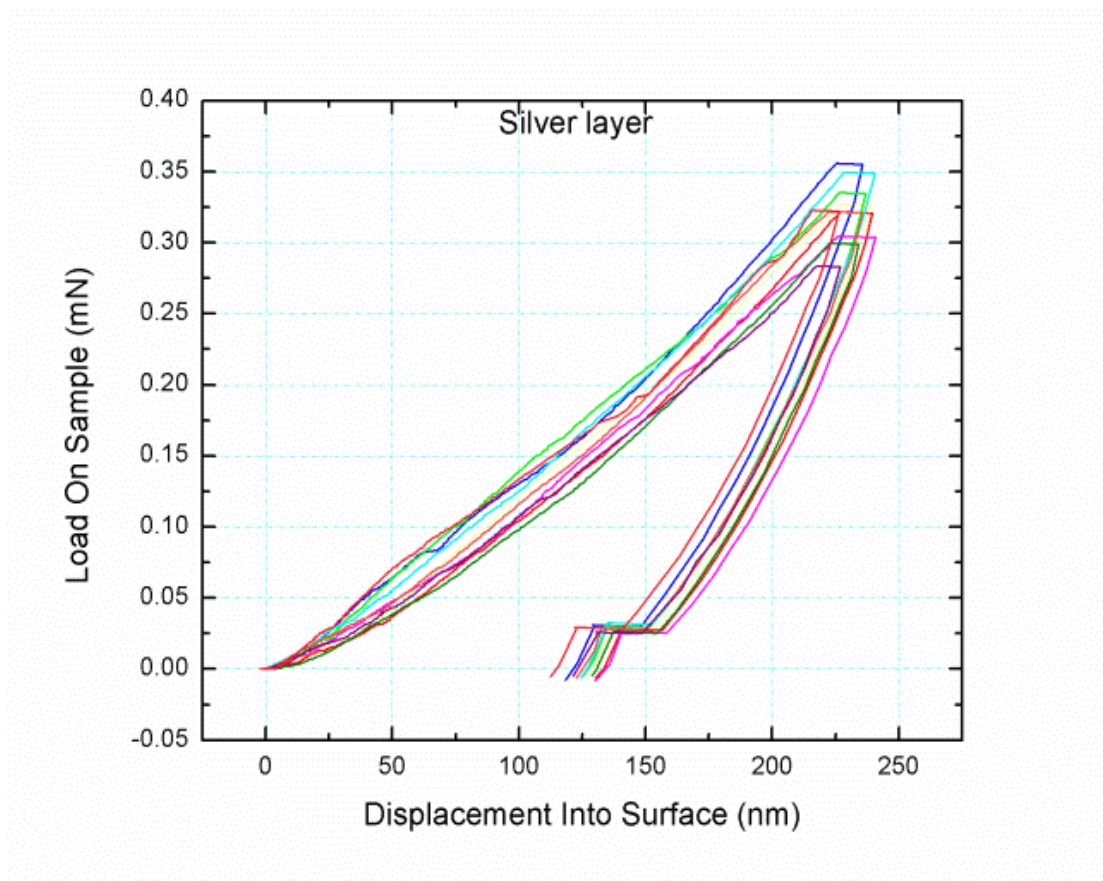
(a)
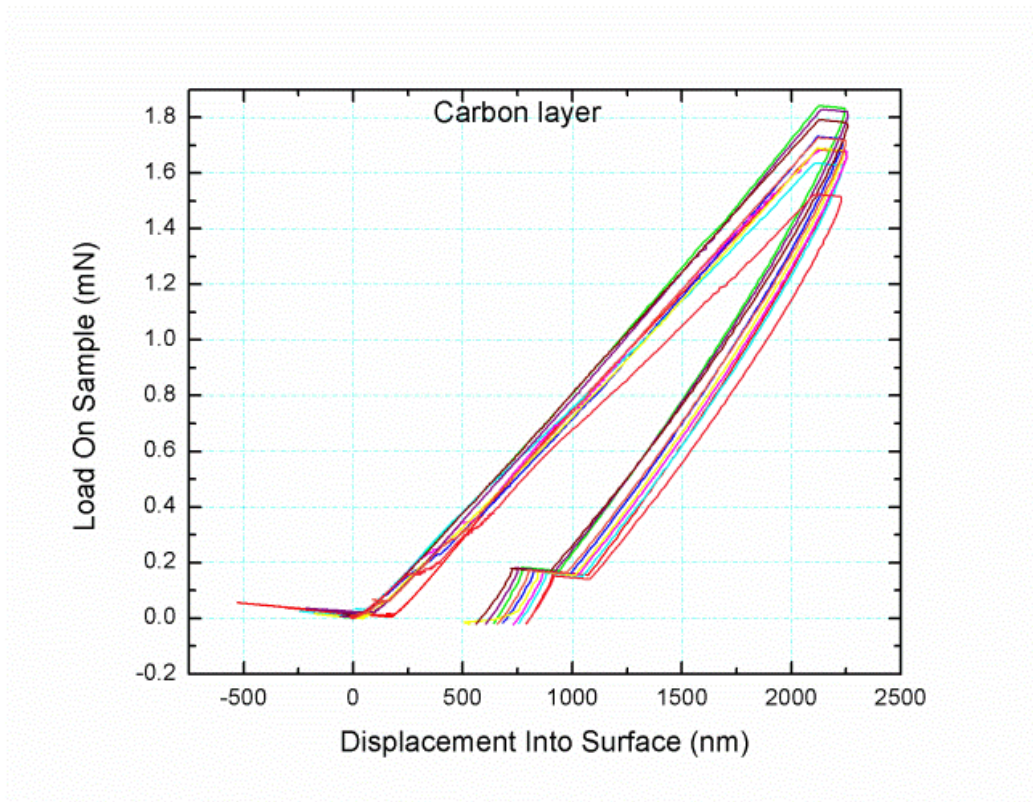
(b)

Figure 5.14 - Load-displacement curves for a) silver interdigitated electrodes, b) carbon layer [115].

It can be seen from Figure 5.14(a) that maximum load on silver layer was at 0.35 mN and corresponding maximum depth of penetration was around 240 nm, which confirm that we did not reach the substrate (the thickness of this layer is around 250 nm). Figure 5.14(b) presents load-displacement response for carbon layer for a maximum load of about 1.8 mN and the penetration depth was about 2.25 μm (which is around one third of the thickness of this layer). These force-displacement curves confirm repeatability of obtained results.

6. Conclusion

The capacitive interdigitated GO based humidity sensors and force sensing resistors were manufactured on flexible substrate by combining ink-jet printing and spin coating for humidity sensors, and ink-jet printing and flexography for force sensing resistors. The electrodes of both types of sensors, humidity and force, were fabricated using ink-jet printing of Ag nanoparticle ink. The sensing layer of humidity sensor was deposited by spin coating of GO ink, while the sensing layer of force sensing resistors was made from carbon ink using flexography method. Additive ink-jet printing process causes costs reduction and good mechanical performances. Flexible substrate, graphene oxide and carbon based ink used in the fabricated sensors enable simple monitoring of humidity and forces in different environments. The humidity sensing features of the fabricated GO based sensors were studied by exposing the sensors to humidity in the range 55–95 %RH at room temperature. Three different designs of electrodes were fabricated: interdigitated, serpentine and toothed design. All three designs of sensors showed excellent sensitivity in the considered range of humidity, changing the capacitance by almost 4 orders of magnitude. The highest sensitivity was obtained by serpentine design of electrodes (~ 60 nF/%RH).

Each of four FSRs showed that measured resistance of FSR decreases with an increase in applied force, that voltage increases with an increase in force and that resistance increases with an increase in temperature. Measured values of resistance were in the range of 8.81 - 24.81 Ω and voltage was in range from 0.79 V to 3.73 V, while applied force from around 1 N up to maximum of 65 N. Obtained results showed that sensor with largest active area has lowest resistance when applying maximal force, while sensor with smallest active area has largest value of resistance at the same applied force. The novelty of this dissertation can be summarized as follows: (1) innovative design of second type of FSRs which showed the best linearity and the smallest resistance variation at elevated temperature comparing to other designs which can be usually found off-the-shelf; (2) together with flexibility and thin structure of the sensor this brings a very wide possibilities of sensors applications in many delicate and important fields such as prosthetic medicine, dentistry, rehabilitation, robotics, etc.; (3) comparison of the complete set of performances of four different types of FSRs performed for the first time; (4) presented FSRs can be exposed to a wide range of applied forces up to 65 N; and (5) completely novel in-house developed system for experimental testing of FSRs has been presented.

Mechanical properties of ink-jet silver and carbon layers were tested, in order to check its suitability for electronic component production. Sample preparation and mechanical test setup were briefly described. Nanoindentation tests were conducted to determine Young's modulus and hardness of printed silver and carbon layers. This analysis provides very useful information about mechanical characterization of the silver and carbon layers on flexible substrates for numerous industrial applications on plastic/organic electronics.

Published scientific papers closely related to the topic of the doctoral dissertation are:

1. **D. Vasiljevic**, A. Mansouri, L. Anzi. R. Sordan, G. Stojanovic, "Performance Analysis of Flexible Ink-Jet Printed Humidity Sensors Based on Graphene Oxide", *IEEE Sensors Journal* (IF 2.617), vol. 18, no. 11, pp. 4378 - 4383, 2018, doi: 10.1109/JSEN.2018.2823696.
2. **D. Vasiljevic**, D. Brajkovic, D. Krkljes, B. Obrenovic, G. Stojanovic, "Testing and Characterization of Multilayer Force Sensing Resistors Fabricated on Flexible Substrate", *Informacije MIDEM - Journal of microelectronics, electronic components and materials* (IF 0.476), vol. 47, no. 1, pp. 40-48, 2017 (ISSN 0352-9045).
3. **Vasiljević D.**, Žlebič Č., Stojanović G., Simić M., Manjakkal L., Stamenković Z.: Cost-effective sensors and sensor nodes for monitoring environmental parameters, *Facta universitatis - series: Electronics and Energetics*, vol. 31, no. 1, pp. 11-23, 2018 (ISSN 0353-3670).
4. **D. Vasiljevic**, A. Menicanin, Lj. Zivanov: „Mechanical Characterization of Ink-Jet Printed Ag Samples on Different Substrates", *4th IFIP WG 5.5/SOCOLNET Doctoral Conference on Computing, Electrical* and Industrial Systems - DoCEIS, Lisbon, April 14-18 2013, pp. 131-141 (ISSN 1868-4238).

Other candidate's published papers:

1. M. Radovanovic, S. Kojic, **D. Vasiljevic**, G. Stojanovic: "Characterization of LC sensor structures realized in PCB and LTCC technology for determining moisture in building materials", *Processing and Application of Ceramics*, Vol. 12, No. 1, pp. 13-20, 2018 (ISSN 1820-6131).

2. Nikola Jeranče, **Dragana Vasiljević**, Nataša Samardžić, Goran Stojanović: "A Compact Inductive Position Sensor Made by Inkjet Printing Technology on a Flexible Substrate", *Sensors* (IF 1.953), vol. 12, no.2, pp. 1288-1298, 2012 (ISSN 1424-8220).

3. S.M. Savić, G. Stojanović, **D. Vasiljević**, K. Vojisavljević, A. Dapčević, A. Radojković, S. Pršić, G. Branković: "Nanoindentation study of nickel manganite ceramics obtained by a complex polymerization method", *Ceramics International* (IF 2.605), vol. 42, no. 10, pp. 12276–12282, 2016 (ISSN 0272-8842).

4. G. Stojanović, V. Mandić, M. Ćurčić, **D. Vasiljević**, M. Kisić, N. Radosavljević: "Combining rapid prototyping techniques in mechanical engineering and electronics for realization of a variable capacitor", *Rapid Prototyping Journal* (IF 1.156), vol. 20, no. 2, pp. 115-120, 2014 (ISSN 1355-2546).

5. D. Krklješ, **D. Vasiljević**, G. Stojanović: "A capacitive angular sensor with flexible digitated electrodes", *Sensor Review* (IF 0.616), vol. 34, no. 4, pp. 382-388, 2014 (ISSN 0260-2288).

6. S. Kojić, S. Ajkalo, M. Gužvica, **D. Vasiljević**, M. Radovanović, G. Stojanović: "A Counter of Number of Products on the Shelf Influences on Capacitance of Interdigitated Capacitor with Application in Intelligent Packaging", *Journal of Microelectronics, Electronic Components and Materials (MIDEM)* (IF 0.369), vol. 44, no. 4, pp. 321-329, 2014, ISSN 0352-9045.

7. Nikola Jeranče, Nataša Samardžić, **Dragana Vasiljević**: "Modeling and design of passive components for flexible electronics*", Electronics*, 2012, Vol. 16, no. 1, pp. 57-61, 2012 (ISSN: 1450-5843).

8. V. Napijalo, **D. Vasiljević**, A. Marić, G. Stojanović: "Consideration for Use of an Inkjet Technology for Fabrication of Microwave Circuits", *Microwave review*, vol. 19, no. 1, pp. 20-25, 2013 (ISSN 14505835).

9. N. Jeranče, N. Samardžić, **D. Vasiljević**, G. Stojanović: "Modeling and design of passive components for flexible electronics", *Electronics*, 2012, vol. 16, no. 1, pp. 57-61, 2012 (ISSN 1450-5843).

10. N. Jeranče, N. Samardžić, **D. Vasiljević**, G. Stojanović: "Modelling and design of passive components for flexible electronics", *Ee'2011*, Novi Sad, Republic Serbia, 26–28. October 2011, pp. 1-5, Paper No. SpS-2.1, (ISBN 978-86-7892-355-5).

11. N. Jeranče, N. Samardžić, **D. Vasiljević**, G. Stojanović: "An efficient computational technique for performance prediction of inductors on flexible substrates", *Advanced Electromagnetics Symposium – AES*, Paris, April 16-19, pp. 80-86, 2012.

12. N. Samardžić, **D. Vasiljević**, N. Jeranče, G. Stojanović: "Design and fabrication of flexible ink-jet printed resonant circuit sensor", *ISSE, Bad Aussee*, Austria, May 9-13 2012, (ISSN 2161-2528).

13. N. Blaž, B. Pantelić, A. Marić, **D. Vasiljević**, G. Stojanović, Lj. Živanov: "Influence of various parameters on capacitance of interdigital capacitor realized in flexible technology," *The 48th International Conference on Microelectronics, Devices and Materials MIDEM 2012*, 19-21 September 2012, Otočec, Slovenija, pp. 291-294, (ISBN 978-961-92933-2-4).

14. S. Kojić, S. Ajkalo, M. Gužvica, **D. Vasiljević**, M. Radovanović, G. Stojanović: "Influence of the Position of Electrodes on Capacitance of Interdigitated Capacitor Fabricated on Flexible Foil", *INDEL*, Banja Luka, 1-3. November 2012, pp. 308-312, (ISBN 978-99955-46-14-4).

15. D. Krklješ, G. Stojanović, **D. Vasiljević**, K. Babković: "Analysis of the mechanical inaccuracies in capacitive encoder with flexible electrodes", *INDEL*, Banja Luka, 1-3. November 2012, pp. 295-298 (ISBN 978-99955-46-14-4).

16. **D. Vasiljevic**, S. Kojic, M. Radovanovic, D. Medic, B. Pivas, A. Tadic, S. Mirkovic: "Cost-effective interdigitated capacitive sensors for efficient bacteria detection" *INFOTEH-Jahorina*, vol. 15, pp. 11-14, March 2016 (ISBN 978-99955-763-9-4).

17. Ž. Mihajlović, V. Milosavljević, **D. Vasiljević**, A. Joža, V. Rajs, M. Živanov: "Implementation of Wearable Energy Harvesting Wireless Sensor Node using Ink-Jet Printing on Flexible Substrate", *5. Mediterranean Conference on Embedded Computing - MECO*, Bar: University of Montenegro, 12-16 Jun, 2016, pp. 100- 103, ISBN 978-9940-9436-6-0.

18. Radovanović M., Kojić S., **Vasiljević D**., Samardžić N., Crespo F., Cargou S., Velve Casquillas G., Chirasatitsin S., Stojanović G.: Performances comparison of microfludic passive mixer fabricated in low-cost and PDMS technologies, *8. PSU-UNS International Conference on Engineering and Technology - ICET*, Novi Sad, 8-10 Jun, 2017

19. **Vasiljević D**., Stojanović G., Radovanović M., Kojić S., Medić D., Pivaš B., Šorđan R.: PCB sensor for bacteria detection in saline , *1. IEEE MTT-S International Microwave Workshop Series on Advanced Materials and Processes (IMWS-AMP)*, Pavia, 20-22 Septembar, 2017

20. N. Jeranče, N. Samardžić, **D. Vasiljević**, G. Stojanović: "Design and fabrication of printed flexible capacitors and inductors", *Swiss e-Print*, Basel, pp. 13, 2011.

21. S. M. Savić, S. Stojanović, K. Vojisavljević, S. Pršić, **D. Vasiljević**, Z. Branković, G. Branković: "Mechanical properties of nickel manganite ceramics investigated with

nanoindentation", *The Book of Abstracts CD / 11th International Conference on Nanostructured Materials, NANO 2012*, , Rhodes, pp. 224, 2012.

22. S. Savic, G. Stojanovic, K. Vojisavljevic, S. Prsic, **D. Vasiljevic**, G. Brankovic: "Nanoindentation of nickel manganite ceramics obtained by complex polymerization method", *2nd Conference of the Serbian Ceramic Society*, 5-7 June 2013, The Book of Abstracts, pp. 97.

23. S. Kojić, G. Stojanović, **D. Vasiljević**, N. Samardžić: „Mogućnosti ink-jet štampane elektronike", *International Scientific Conference "Metrology and Quality in Production Engineering and Environmental Protection" – ETIKUM 2013*, pp. 35-38, 2013 (ISBN 978-86-7892-512-2).

24. V. Napijalo, **D. Vasiljević**, A. Marić and G. Stojanović: „Characterization of Microwave Structures Fabricated Using Inkjet Technology", *Proceedings of 57th ETRAN Conference*, Zlatibor, Serbia, June 3-6, pp. MT 2.1.1-6, 2013 (ISBN 978-86-80509-68-6).

25. S. Kojić, N. Bednar, **D. Vasiljević**, M. Radovanović, N. Samardžić: „Merenje i kontrola materijala u nanotehnologijama", *International Scientific Conference "Metrology and Quality in Production Engineering and Environmental Protection" – ETIKUM 2013*, pp. 27-30, 2013 (ISBN 978-86-7892-512-2).

26. T. Puškar, **D. Vasiljević**, M. Šokac, M. Radovanović, B. Pivaš, S. Kojić, S. Mirković: "Analiza mogućnosti za unapređenje i razvoj savremenih dijagnostičkih metoda za detekciju okluzalnih opterećenja", *International Scientific Conference "Metrology and Quality in Production Engineering and Environmental Protection" – ETIKUM 2016*, pp. 69-69, 2016 (ISBN 978-86-7892-826-0).

27. **D. Vasiljevic**, S. Kojic, D. Medic, B. Pivas, A. Tadic, S. Mirkovic, M. Radovanovic: "Cost-effective interdigitated capacitive sensor for measurement of staphylococcus aureus concentration in saline", *International Scientific Conference "Metrology and Quality in Production Engineering and Environmental Protection" – ETIKUM 2016*, pp. 109-112, 2016 (ISBN 978-86-7892-826-0).

28. Radovanović M., **Vasiljević D**., Kojić S., Tadić A., Pivaš B., Medić D., Mirković S.: Određivanje tipa bakterija u fiziološkom rastvoru korišćenjem interdigitalnog kapacitivnog senzora, 2016.

Accepted patent:

1. S. Kojić, S. Ajkalo, G. Stojanović, M. Gužvica, **D. Vasiljević**, M. Radovanović: "Metod i sistem za senzorski podržano inteligentno praćenje stanja objekata na polici", Beograd, Glasnik intelektualne svojine, 2014, str.18-19 (ISBN 2217-9143).

References:

[1]   "The development of new-generation sensors driven by research and leading-edge SMEs in Montreal | Innovation Development MTL | ID MTL | English." [Online]. Available: https://ville.montreal.qc.ca/idmtl/en/the-development-of-new-generation-sensors-driven-by-research-and-leading-edge-smes-in-montreal/. [Accessed: 24-May-2018].

[2]   L. Gu, Q. A. Huang, and M. Qin, "A novel capacitive-type humidity sensor using CMOS fabrication technology," *Sensors Actuators, B Chem.*, vol. 99, no. 2–3, pp. 491–498, 2004.

[3]   M. Maksimović *et al.*, "Application of a LTCC sensor for measuring moisture content of building materials," *Constr. Build. Mater.*, vol. 26, no. 1, pp. 327–333, 2012.

[4]   A. Oprea, J. Courbat, N. Bârsan, D. Briand, N. F. de Rooij, and U. Weimar, "Temperature, humidity and gas sensors integrated on plastic foil for low power applications," *Sensors Actuators, B Chem.*, vol. 140, no. 1, pp. 227–232, 2009.

[5]   M. Z. Yang, C. L. Dai, and C. C. Wu, "Sol-Gel zinc oxide humidity sensors integrated with a ring oscillator circuit On-a-Chip," *Sensors (Switzerland)*, vol. 14, no. 11, pp. 20360–20371, 2014.

[6]   X. Li, X. Chen, X. Chen, X. Ding, and X. Zhao, "High-sensitive humidity sensor based on graphene oxide with evenly dispersed multiwalled carbon nanotubes," *Mater. Chem. Phys.*, vol. 207, pp. 135–140, 2018.

[7]   H. Farahani, R. Wagiran, and M. N. Hamidon, "Humidity sensors principle, mechanism, and fabrication technologies: A comprehensive review," *Sensors (Switzerland)*, vol. 14, no. 5, pp. 7881–7939, 2014.

[8]   D. Zhang, J. Liu, and B. Xia, "Layer-by-Layer Self-Assembly of Zinc Oxide/Graphene Oxide Hybrid Toward Ultrasensitive Humidity Sensing," *IEEE Electron Device Lett.*, vol. 37, no. 7, pp. 916–919, 2016.

[9]   T. Yang, T. Zhang, and G. Lu, "Humidity-Sensing Properties of Urchinlike CuO Nanostructures Modi fi ed by Reduced Graphene Oxide," *ACS Appl. Mater. Interfaces*, vol. 6, pp. 3888–3895, 2014.

[10]   H. Bi *et al.*, "Ultrahigh humidity sensitivity of graphene oxide," *Sci. Rep.*, vol. 3, no. 5 V, pp. 1–7, 2013.

[11]   H. Chi, Y. J. Liu, F. Wang, and C. He, "Highly sensitive and fast response colorimetric humidity sensors based on graphene oxides film," *ACS Appl. Mater. Interfaces*, vol. 7, no. 36, pp. 19882–19886, 2015.

[12]   Y. Yao, X. Chen, H. Guo, Z. Wu, and X. Li, "Humidity sensing behaviors of graphene oxide-silicon bi-layer flexible structure," *Sensors Actuators, B Chem.*, vol. 161, no. 1, pp. 1053–1058, 2012.

[13]   L. Guo *et al.*, "Two-beam-laser interference mediated reduction, patterning and nanostructuring of graphene oxide for the production of a flexible humidity sensing device," *Carbon N. Y.*, vol. 50, no. 4, pp. 1667–1673, 2012.

[14]   P. G. Su and Z. M. Lu, "Flexibility and electrical and humidity-sensing properties of diamine-functionalized graphene oxide films," *Sensors Actuators, B Chem.*, vol. 211, pp. 157–163, 2015.

[15]   D. Zhang, J. Tong, and B. Xia, "Humidity-sensing properties of chemically reduced

graphene oxide/polymer nanocomposite film sensor based on layer-by-layer nano self-assembly," *Sensors Actuators, B Chem.*, vol. 197, pp. 66–72, 2014.

[16] R. Gao, D. F. Lu, J. Cheng, Y. Jiang, L. Jiang, and Z. M. Qi, "Humidity sensor based on power leakage at resonance wavelengths of a hollow core fiber coated with reduced graphene oxide," *Sensors Actuators, B Chem.*, vol. 222, pp. 618–624, 2016.

[17] D. Zhang, H. Chang, P. Li, R. Liu, and Q. Xue, "Fabrication and characterization of an ultrasensitive humidity sensor based on metal oxide/graphene hybrid nanocomposite," *Sensors Actuators, B Chem.*, vol. 225, pp. 233–240, 2016.

[18] D. Zhang, J. Tong, B. Xia, and Q. Xue, "Ultrahigh performance humidity sensor based on layer-by-layer self-assembly of graphene oxide/polyelectrolyte nanocomposite film," *Sensors Actuators, B Chem.*, vol. 203, pp. 263–270, 2014.

[19] R. Guo, W. Tang, C. Shen, and X. Wang, "High sensitivity and fast response graphene oxide capacitive humidity sensor with computer-aided design," *Comput. Mater. Sci.*, vol. 111, pp. 289–293, 2016.

[20] D. Vasiljevic, A. Mansouri, L. Anzi, R. Sordan, and G. Stojanovic, "Performance Analysis of Flexible Ink-jet Printed Humidity Sensors Based on Graphene Oxide," *IEEE Sens. J.*, vol. 18, no. 11, pp. 4378–4382, 2018.

[21] Q.-A. Z. Cheng-Long, Q. Ming, L. Wei-Hua, and Huang, "Enhanced performance of a CMOS interdigital capacitive humidity sensor by graphene oxide," in *2011 16th International Solid-State Sensors, Actuators and Microsystems Conference*, 2011, pp. 1954–1957.

[22] P. G. Su, W. L. Shiu, and M. S. Tsai, "Flexible humidity sensor based on Au nanoparticles/graphene oxide/thiolated silica sol-gel film," *Sensors Actuators, B Chem.*, vol. 216, pp. 467–475, 2015.

[23] Y. Yao, X. Chen, H. Guo, and Z. Wu, "Graphene oxide thin film coated quartz crystal microbalance for humidity detection," *Appl. Surf. Sci.*, vol. 257, no. 17, pp. 7778–7782, 2011.

[24] T. D'Alessio, "Improving the use of force sensing resistors arrays for the measure of hand grasp," *Proc. 8th Mediterr. Electrotech. Conf. Ind. Appl. Power Syst. Comput. Sci. Telecommun. (MELECON 96)*, vol. 3, pp. 1383–1386, 1996.

[25] A. A. Gopalai and S. M. N. A. Senanayake, "Force sensing resistors for monitoring proprioception response in rehabilitation routines," *Int. Conf. Intell. Syst. Des. Appl. ISDA*, pp. 941–946, 2012.

[26] N. K. Rana, "Application of Force Sensing Resistor (FSR) in design of pressure scanning system for plantar pressure measurement," *2009 Int. Conf. Comput. Electr. Eng. ICCEE 2009*, vol. 2, pp. 678–685, 2009.

[27] Interlink Electronics, "Interlink Electronics FSR ® Force Sensing Resistors ®," pp. 1–33, 2016.

[28] Tekscan, "Comparison of Interface Pressure Measurement Options," *J. Infect. Dis.*, vol. 207, no. 11, p. 18, 2012.

[29] D. K. Kim, J. H. Kim, Y. T. Kim, M. S. Kim, Y. K. Park, and Y. H. Kwon, "Robot fingertip tactile sensing module with a 3D-curved shape using molding technique," *Sensors Actuators, A Phys.*, vol. 203, pp. 421–429, 2013.

[30] J. R. Stetter, P. J. Hesketh, and G. W. Hunter, "Sensors : Engineering Structures and Materials from Micro to Nano," *Elecrochemical Soc. Interface*, p. 66, 2006.

[31] W. B.Ribbens, *Understanding Automotive Electronics,Chapter 6 - Sensors and Actuators*, 7th ed. Elsevier, 2013.

[32] "The Future of Sensors Protecting Worker Health Through Sensor Technologies," 2016. [Online]. Available: http://www.aiha.org. [Accessed: 29-May-2018].

[33] K. Kalantar-Zadeh, *Sensors: An Introductory Course, Chapter 2 - Sensors Characteristics*, 1st ed. Springer, 2013.

[34] K. M. Willett, "Creation and Analysis of HadCRUH: a New Global Surface Humidity Dataset, Introduction : Humidity and Climate Change," University of East Anglia, Norwich, 2007.

[35] C.-Y. Lee and G.-B. Lee, "Humidity Sensors: A Review," *Sens. Lett.*, vol. 3, no. 1, pp. 1–15, 2005.

[36] A. Gall, "Relative humidity - Definitions - Physical laws." [Online]. Available: https://www.galltec-mela.de/footage/begriffe_en.pdf. [Accessed: 29-May-2018].

[37] L. A. Spomer and T. W. Tibbitts, "Chapter 3 Humidity," in *Plant Growth Chamber Handbook*, Iowa State University of Science and Technology, 1997, pp. 43–64.

[38] F. W. Dunmore, "An electric hygrometer and its application to radio meteorography," *J. Res. Natl. Bur. Stand.*, vol. 20, no. 6, pp. 723–744, 1938.

[39] Z. Chen and C. Lu, "Humidity Sensors: A Review of Materials and Mechanisms," *Sens. Lett.*, vol. 3, no. 4, pp. 274–295, 2005.

[40] D. Zhang, Y. Sun, P. Li, and Y. Zhang, "Facile Fabrication of MoS$_2$ -Modified SnO$_2$ Hybrid Nanocomposite for Ultrasensitive Humidity Sensing," *ACS Appl. Mater. Interfaces*, vol. 8, no. 22, pp. 14142–14149, 2016.

[41] M. A. Squillaci, L. Ferlauto, Y. Zagranyarski, S. Milita, K. Müllen, and P. Samorì, "Self-assembly of an amphiphilic π-conjugated dyad into fibers: Ultrafast and ultrasensitive humidity sensor," *Adv. Mater.*, vol. 27, no. 20, pp. 3170–3174, 2015.

[42] S.-H. Song, H.-H. Yang, C.-H. Han, S.-D. Ko, S.-H. Lee, and J.-B. Yoon, "Metal-oxide-semiconductor field effect transistor humidity sensor using surface conductance," *Appl. Phys. Lett.*, vol. 100, no. 10, p. 101603(1-3), 2012.

[43] X. Wang, B. Ding, J. Yu, M. Wang, and F. Pan, "A highly sensitive humidity sensor based on a nanofibrous membrane coated quartz crystal microbalance," *Nanotechnology*, vol. 21, no. 5, 2010.

[44] Y. Yao and Y. Xue, "Impedance analysis of quartz crystal microbalance humidity sensors based on nanodiamond/graphene oxide nanocomposite film," *Sensors Actuators, B Chem.*, vol. 211, pp. 52–58, 2015.

[45] M. M. Hawkeye and M. J. Brett, "Optimized colorimetric photonic-crystal humidity sensor fabricated using glancing angle deposition," *Adv. Funct. Mater.*, vol. 21, no. 19, pp. 3652–3658, 2011.

[46] D. Lopez-Torres *et al.*, "Photonic crystal fiber interferometer coated with a PAH/PAA nanolayer as humidity sensor," *Sensors Actuators, B Chem.*, vol. 242, pp. 1065–1072, 2017.

[47] Y. Zilberman, R. Ionescu, X. Feng, K. Müllen, and H. Haick, "Nanoarray of polycyclic aromatic hydrocarbons and carbon nanotubes for accurate and predictive detection in real-world environmental humidity," *ACS Nano*, vol. 5, no. 8, pp. 6743–6753, 2011.

[48] Q. Kuang, C. Lao, Z. L. Wang, Z. Xie, and L. Zheng, "High-Sensitivity Humidity

Sensor Based on a Single SnO2 Nanowire," *J. Am. Chem. Soc.*, vol. 129, no. 19, pp. 6070–6071, 2007.

[49] C. L. Hsu, J. Y. Tsai, and T. J. Hsueh, "Ethanol gas and humidity sensors of CuO/Cu2O composite nanowires based on a Cu through-silicon via approach," *Sensors Actuators, B Chem.*, vol. 224, pp. 95–102, 2016.

[50] H. Li *et al.*, "High-temperature humidity sensors based on WO3 –SnO2 composite hollow nanospheres," *J. Mater. Chem. A*, vol. 2, no. 19, pp. 6854–6862, 2014.

[51] S. Ali, A. Hassan, G. Hassan, J. Bae, and C. H. Lee, "All-printed humidity sensor based on graphene/methyl-red composite with high sensitivity," *Carbon N. Y.*, vol. 105, pp. 23–32, 2016.

[52] M. Izzat Azmer, Z. Ahmad, K. Sulaiman, and F. Touati, "Morphological and structural properties of VoPcPhO:P3HT composite thin films," *Mater. Lett.*, vol. 164, pp. 605–608, 2016.

[53] R. Fenner and E. Zdankiewicz, "Micromachined Water Vapor Sensors: A Review of Sensing Technologies," *IEEE Sens. J.*, vol. 1, no. 4, pp. 309–317, 2001.

[54] G. Sberveglieri, R. Anchisini, R. Murri, C. Ercoli, and N. Pinto, "An Al2O3 sensor for low humidity content: Characterization by impedance spectroscopy," *Sensors Actuators, B Chem.*, vol. 32, no. 1, pp. 1–5, 1996.

[55] A. Salehi, D. J. Kalantari, and A. Goshtasbi, "Rapid response of Au/Porous-GaAs humidity sensor at room temperature," *Conf. Optoelectron. Microelectron. Mater. Devices, Proceedings, COMMAD*, vol. 79, pp. 125–128, 2006.

[56] J. M. Tulliani, C. Baroni, L. Zavattaro, and C. Grignani, "Strontium-doped hematite as a possible humidity sensing material for soil water content determination," *Sensors (Switzerland)*, vol. 13, no. 9, pp. 12070–12092, 2013.

[57] H. Shimizu, Y Arai and T. Seiyama, "Theoretical studies on the impedance-humidity characteristics of ceramic humidity sensors," *Sens. Actuators*, vol. 7, pp. 11–22, 1985.

[58] X. Shi, Q. Chen, J. Fang, K. Varahramyan, and H. F. Ji, "Al2O3-coated microcantilevers for detection of moisture at ppm level," *Sensors Actuators, B Chem.*, vol. 129, no. 1, pp. 241–245, 2008.

[59] Z. Chen, M. C. Jin, and C. Zhen, "Humidity sensors with reactively evaporated Al2O3 films as porous dielectrics," *Sensors Actuators B. Chem.*, vol. 2, no. 3, pp. 167–171, 1990.

[60] W. Qu, W. Wlodarski, and J.-U. Meyer, "Comparative study on micromorphology and humidity sensitive properties of thin-film and thick-film humidity sensors based on semiconducting MnWO4," *Sensors Actuators B Chem.*, vol. 64, no. 1–3, pp. 76–82, 2000.

[61] P. M. Harrey, B. J. Ramsey, P. S. A. Evans, and D. J. Harrison, "Capacitive-type humidity sensors fabricated using the offset lithographic printing process," *Sensors Actuators, B Chem.*, vol. 87, no. 2, pp. 226–232, 2002.

[62] H. Grange, C. Bieth, H. Boucher, and G. Delapiere, "A capacitive humidity sensor with every fast response time and very low hysteresis," *Sensors and Actuators*, vol. 12, no. 3, pp. 291–296, 1987.

[63] A. R. K. Ralston, C. F. Klein, P. E. Thomas, and D. D. Denton, "A Model For The Relative Environmental Stability Of A Series Of Polyimide Capacitance Humidity Sensors," *Solid-State Sensors Actuators, 1995 Eurosensors IX.. Transducers '95. 8th Int. Conf.*, vol. 2, pp. 821–824, 1995.

[64] P. E. Thoma, J. O. Colla, and R. Stewart, "A Capacitance Humidity-Sensing Transducer," *IEEE Trans. Components, Hybrids, Manuf. Technol.*, vol. 2, no. 3, pp. 321–323, 1979.

[65] C. Roman, O. Bodea, N. Prodan, A. Levi, E. Cordos, and I. Manoviciu, "A capacitive-type humidity sensor using crosslinked poly(methyl methacrylate-co-(2 hydroxypropyl)-methacrylate)," *Sensors Actuators B. Chem.*, vol. 25, no. 1–3, pp. 710–713, 1995.

[66] J. M. Meanna Pérez and C. Freyre, "A poly(ethyleneterephthalate)-based humidity sensor," *Sensors Actuators, B Chem.*, vol. 42, no. 1, pp. 27–30, 1997.

[67] Y. Li, M. J. Yang, and Y. She, "Humidity sensors using in situ synthesized sodium polystyrenesulfonate/ZnO nanocomposites," *Talanta*, vol. 62, no. 4, pp. 707–712, 2004.

[68] P. G. Su and L. N. Huang, "Humidity sensors based on TiO2 nanoparticles/polypyrrole composite thin films," *Sensors Actuators, B Chem.*, vol. 123, no. 1, pp. 501–507, 2007.

[69] V. Correia *et al.*, "Design and fabrication of multilayer inkjet-printed passive components for printed electronics circuit development," *J. Manuf. Process.*, vol. 31, pp. 364–371, 2018.

[70] F. Varela, E. Armendáriz, and C. Wolluschek, "Inkjet printed electronics: The wet on wet approach," *Chem. Eng. Process. Process Intensif.*, vol. 50, no. 5–6, pp. 589–591, 2011.

[71] E. Halonen *et al.*, "Environmental protection of inkjet-printed Ag conductors," *Microelectron. Eng.*, vol. 88, no. 9, pp. 2970–2976, 2011.

[72] B. J. Kang, C. K. Lee, and J. H. Oh, "All-inkjet-printed electrical components and circuit fabrication on a plastic substrate," *Microelectron. Eng.*, vol. 97, pp. 251–254, 2012.

[73] P. Alpuim, V. Correia, E. S. Marins, J. G. Rocha, I. G. Trindade, and S. Lanceros-mendez, "Piezoresistive silicon thin fi lm sensor array for biomedical applications," *Thin Solid Films*, vol. 519, no. 14, pp. 4574–4577, 2011.

[74] R. H. Reuss *et al.*, "Macroelectronics : Perspectives on Technology and Applications," *Proc. IEEE*, vol. 93, no. 7, pp. 1239–1256, 2005.

[75] J. Jang, "Displays develop a new flexibility," *Mater. Today*, vol. 9, no. 4, pp. 46–52, 2006.

[76] F. C. Krebs, "Solar Energy Materials & Solar Cells Fabrication and processing of polymer solar cells : A review of printing and coating techniques," *Sol. Energy Mater. Sol. Cells*, vol. 93, pp. 394–412, 2009.

[77] A. C. Mayer, S. R. Scully, B. E. Hardin, M. W. Rowell, and M. D. Mcgehee, "Polymer-based solar cells A significant fraction of the cost of solar panels comes from the," *Mater. Today*, vol. 10, no. 11, pp. 28–33, 2007.

[78] T. Someya *et al.*, "Conformable , flexible , large-area networks of pressure and thermal sensors with organic transistor active matrixes," vol. 102, no. 35, pp. 1–5, 2005.

[79] U. S. Bhansali, M. A. Khan, and H. N. Alshareef, "Microelectronic Engineering Organic ferroelectric memory devices with inkjet-printed polymer electrodes on flexible substrates," *Microelectron. Eng.*, vol. 105, pp. 68–73, 2013.

[80] R. Zichner, E. Sowade, and R. R. Baumann, "Inkjet printed WLAN antenna for an application in smartphones," *Jpn. J. Appl. Phys.*, vol. 53, p. 05HB06(1-4), 2014.

[81]   H. Sillanpää, E. Halonen, T. Liimatta, and M. Mäntysalo, "Inkjet Printed Wireless Biosensors on Stretchable Substrate," in *2014 International Conference on Electronics Packaging (ICEP)*, 2014, pp. 322–325.

[82]   R. J. Kim D, Ahn J, Won M, Kim H, Kim T, Song J, Huang Y, Liu Z, Lu C, "Stretchable and Foldable Silicon Integrated Circuits," *Science (80-.).*, vol. 320, no. 5875, pp. 507–511, 2008.

[83]   P. V. Raje and N. C. Murmu, "A Review on Electrohydrodynamic-inkjet Printing Technology," *Int. J. Emerg. Technol. Adv. Eng.*, vol. 4, no. 5, pp. 174–183, 2014.

[84]   S. Khan, L. Lorenzelli, and R. S. Dahiya, "Technologies for printing sensors and electronics over large flexible substrates: A review," *IEEE Sens. J.*, vol. 15, no. 6, pp. 3164–3185, 2015.

[85]   S. H. Ko, H. Pan, and C. P. Grigoropoulos, "All-inkjet-printed flexible electronics fabrication on a polymer substrate by low-temperature high-resolution selective laser sintering of metal nanoparticles," *Nanotechnology*, vol. 18, no. 34, p. 8pp, 2007.

[86]   D. Tobjörk and R. Österbacka, "Paper Electronics," *Adv. Mater.*, vol. 23, pp. 1935–1961, 2011.

[87]   P. F. Moonen, I. Yakimets, and J. Huskens, "Fabrication of transistors on flexible substrates: From mass-printing to high-resolution alternative lithography strategies," *Adv. Mater.*, vol. 24, no. 41, pp. 5526–5541, 2012.

[88]   D. Sung, A. De, F. Vornbrock, and V. Subramanian, "Scaling and Optimization of Gravure-Printed Silver Nanoparticle Lines for Printed Electronics," *IEEE Trans. Components Packag. Technol.*, vol. 33, no. 1, pp. 105–114, 2010.

[89]   R. G. Sweet and R. C. Cumming, "Fluid droplet recorder with a plurality of jets," United States Patent No. 3373437, 1968.

[90]   J. Li, F. Rossignol, and J. Macdonald, "Inkjet printing for biosensor fabrication: combining chemistry and technology for advanced manufacturing," *Lab Chip*, vol. 15, no. 12, pp. 2538–2558, 2015.

[91]   M. Jović, F. Cortés-Salazar, A. Lesch, V. Amstutz, H. Bi, and H. H. Girault, "Electrochemical detection of free chlorine at inkjet printed silver electrodes," *J. Electroanal. Chem.*, vol. 756, pp. 171–178, 2015.

[92]   A. Moya *et al.*, "All-inkjet-printed dissolved oxygen sensors on flexible plastic substrates," *Org. Electron. physics, Mater. Appl.*, vol. 39, pp. 168–176, 2016.

[93]   T. H. da Costa, E. Song, R. P. Tortorich, and J.-W. Choi, "A Paper-Based Electrochemical Sensor Using Inkjet-Printed Carbon Nanotube Electrodes," *ECS J. Solid State Sci. Technol.*, vol. 4, no. 10, pp. S3044–S3047, 2015.

[94]   S. R. Das *et al.*, "3D nanostructured inkjet printed graphene via UV-pulsed laser irradiation enables paper-based electronics and electrochemical devices," *Nanoscale*, vol. 8, no. 35, pp. 15870–15879, 2016.

[95]   P. Ihalainen *et al.*, "Paper-supported nanostructured ultrathin gold film electrodes - Characterization and functionalization," *Appl. Surf. Sci.*, vol. 329, pp. 321–329, 2015.

[96]   Z. Xu *et al.*, "Real-time in situ sensing of multiple water quality related parameters using micro-electrode array (MEA) fabricated by inkjet-printing technology (IPT)," *Sensors Actuators, B Chem.*, vol. 237, pp. 1108–1119, 2016.

[97]   P. Macleod, "A Review of Flexible Circuit Technology and its Applications Flexible," in *Technology Watch*, PRIME Faraday Partnership, Wolfson School of Mechanical

and Manufacturing Engineering, 2002, p. 54.

[98] M. D. Dankoco, G. Y. Tesfay, E. Benevent, and M. Bendahan, "Temperature sensor realized by inkjet printing process on flexible substrate," *Mater. Sci. Eng. B Solid-State Mater. Adv. Technol.*, vol. 205, pp. 1–5, 2016.

[99] Z. P. Yin, Y. A. Huang, N. B. Bu, X. M. Wang, and Y. L. Xiong, "Inkjet printing for flexible electronics: Materials, processes and equipments," *Chinese Sci. Bull.*, vol. 55, no. 30, pp. 3383–3407, 2010.

[100] D. Jariwala, V. K. Sangwan, L. J. Lauhon, T. J. Marks, and M. C. Hersam, "Carbon nanomaterials for electronics, optoelectronics, photovoltaics, and sensing," *Chem. Soc. Rev.*, vol. 42, no. 7, pp. 2824–2860, 2013.

[101] K. N. Andre Geim, "The Rise of Graphene," *Nat. Mater*, vol. 6, no. 183, pp. 1–14, 2007.

[102] K. S. Novoselov *et al.*, "Electric filed effect in atomically thin carbon films," *Science (80-.).*, vol. 306, no. 5696, pp. 666–669, 2004.

[103] D. C. Marcano *et al.*, "Improved Synthesis of Graphene Oxide," *ACS Nano*, vol. 4, no. 8, pp. 4806–4814, 2010.

[104] F. Perrozzi, S. Prezioso, and L. Ottaviano, "Graphene oxide: From fundamentals to applications," *J. Phys. Condens. Matter*, vol. 27, no. 1, p. 21p., 2015.

[105] D. Sharma, S. Kanchi, M. I. Sabela, and K. Bisetty, "Insight into the biosensing of graphene oxide: Present and future prospects," *Arab. J. Chem.*, vol. 9, no. 2, pp. 238–261, 2016.

[106] J. P. Metters, R. O. Kadara, and C. E. Banks, "New directions in screen printed electroanalytical sensors: an overview of recent developments," *Analyst*, vol. 136, no. 6, p. 1067, 2011.

[107] C. Lee, B. J. Kang, and J. H. Oh, "High-resolution conductive patterns fabricated by inkjet printing and spin coating on wettability-controlled surfaces," *Thin Solid Films*, vol. 616, pp. 238–246, 2016.

[108] "Flexography." [Online]. Available: http://onlineprintfile.com/knowledge/PrintProcesses.pdf. [Accessed: 05-Jun-2018].

[109] A. De Luca *et al.*, "Temperature-modulated graphene oxide resistive humidity sensor for indoor air quality monitoring," *Nanoscale*, vol. 8, no. 8, pp. 4565–4572, 2016.

[110] R. Balzarotti, C. Cristiani, and L. F. Francis, "Spin coating deposition on complex geometry substrates: Influence of operative parameters," *Surf. Coatings Technol.*, vol. 330, no. August, pp. 1–9, 2017.

[111] A. G. Emslie, F. T. Bonner, and L. G. Peck, "Flow of a viscous liquid on a rotating disk," *J. Appl. Phys.*, vol. 29, no. 5, pp. 858–862, 1958.

[112] N. Sahu, B. Parija, and S. Panigrahi, "Fundamental understanding and modeling of spin coating process: A review," *Indian J. Phys.*, vol. 83, no. 4, pp. 493–502, 2009.

[113] R. S. Dahiya and M. Valle, "Chapter 15 - Tactile Sensing for Robotic Applications," in *Sensors: Focus on Tactile Force and Stress Sensors*, J. G. Rocha and S. Lanceros-Mendez, Eds. IntechOpen, 2008, pp. 289–304.

[114] M. G. King, A. J. Baragwanath, M. C. Rosamond, D. Wood, and A. J. Gallant, "Porous PDMS force sensitive resistors," *Procedia Chem.*, vol. 1, no. 1, pp. 568–571, 2009.

[115] D. Vasiljević, D. Brajković, D. Krklješ, B. Obrenović, and G. M. Stojanović, "Testing

and characterization of multilayer force sensing resistors fabricated on flexible substrate," *Inf. MIDEM*, vol. 47, no. 1, 2017.

[116] S. Billimoria, N. Mukherjee, A. Petrovskaya, and O. Khatib, "Tactile Sensors," Computer Science Department, Stanford University, 2008.

[117] "Datasheet: Standard versions Specifications for rectilinear and rotary standard versions." [Online]. Available: www.spectrasymbol.com. [Accessed: 11-Jun-2018].

[118] A. Hollinger and M. M. Wanderley, "Evaluation of Commercial Force-Sensing Resistors," in *NIME06, Paris, France*, 2006, pp. 1–4.

[119] D. Z. Vasiljevic, A. B. Menicanin, and L. D. Zivanov, "Mechanical Characterization of Ink-Jet Printed Ag Samples on Different Substrates," *Technol. Innov. Internet Things*, vol. 394, pp. 133–141, 2013.

[120] "Industrial Inkjet Printheads | Fujifilm USA." [Online]. Available: http://www.fujifilmusa.com/products/industrial_inkjet_printheads/. [Accessed: 03-Jun-2018].

[121] "Film," 2015. [Online]. Available: http://www.gts-flexible.com/home/know-how/film/. [Accessed: 03-Jun-2018].

[122] "Sun Chemical - Sun Chemical." [Online]. Available: http://www.sunchemical.com/. [Accessed: 03-Jun-2018].

[123] Č. Žlebič *et al.*, "Ink-jet printed strain sensor on polyimide substrate," *Proc. Int. Spring Semin. Electron. Technol.*, pp. 409–414, 2013.

[124] "Relative humidity sensor | OMEGA Engineering." [Online]. Available: https://www.omega.com/kwbld/relativehumiditysensor.html. [Accessed: 03-Jun-2018].

[125] "Chemical Analysis, Life Sciences, and Diagnostics | Agilent." [Online]. Available: https://www.agilent.com/. [Accessed: 05-Jun-2018].

[126] Q. Wang, Y. Z. Pan, S. S. Huang, S. T. Ren, P. Li, and J. J. Li, "Resistive and capacitive response of nitrogen-doped TiO2nanotubes film humidity sensor," *Nanotechnology*, vol. 22, no. 2, 2011.

[127] G. Naik and S. Krishnaswamy, "Room-Temperature Humidity Sensing Using Graphene Oxide Thin Films," *Graphene*, vol. 05, no. 01, pp. 1–13, 2016.

[128] F. Molina-Lopez, D. Briand, and N. F. De Rooij, "All additive inkjet printed humidity sensors on plastic substrate," *Sensors Actuators, B Chem.*, vol. 166–167, pp. 212–222, 2012.

[129] D. Krklješ, L. Nagy, and K. Babković, "Force-dependent contact area excitation of FSR force sensor utilizing dome-shaped rubber element," in *Proceedings of 28th International Conference on Microelectronics - MIEL*, 2012, pp. 181–184.

[130] K. B. Damir Krklješ, László Nagy, "Evaluation of the possibility of using a different excitation of FSR force sensor," in *Proceedings of 16th INTERNATIONAL SYMPOSIUM on POWER ELECTRONICS - Ee 2011*, 2011.

[131] A. Scorzoni, M. Baroncini, and P. Placidi, "On the relationship between the temperature coefficient of resistance and the thermal conductance of integrated metal resistors," *Sensors Actuators A Phys.*, vol. 116, pp. 137–144, 2004.